Università degli Studi di Napoli "Federico II"

Thesis submitted for the Degree of Doctor of Philosophy on

Novel Technologies for Materials, Sensors and Imaging – XXVII Cycle

High sensitive sensing by effective immobilization of UV photo-activated antibodies

Riccardo Funari

Coordinator

Prof. Antonio Cassinese

Tutor

Prof. Raffaele Velotta

Abstract

Nowadays there is a strong interest in precise and reliable measurement tools suitable for quantifying physical, chemical, and biological properties. Biosensors face this problem by exploiting the intrinsic specificity provided by biological sensitive molecules to reveal the presence of the compound of interest. In particular, proteins like antibodies have a dominant role in biosensor development since they are selected by host immune system to efficiently bind foreign species including bacteria, viruses and toxins. Biomolecules involved in biosensing are usually characterized by a recognition site responsible for the selective detection of the analyte. This portion of the macromolecule has to be accessible when the sensitive element is coupled with the inorganic transducer, thus making surface functionalization a crucial phase of biosensor development. This issue strongly motivates the research of new immobilization and functionalization techniques allowing the control on both amount and orientation of the biomolecules thus resulting in better sensitivity and lower limit of detection. Conventional functionalization strategies are based on covalent and non-covalent interactions between the biological element and the surface of the transducer. Even if covalent approaches provide an effective immobilization of the biomolecules, these methods are laborious and time-consuming since several chemical treatments and purification steps are needed. In addition, the high toxicity of some chemicals and the complexity of the procedure require trained operators. On the other side, non-covalent immobilization is much easier to realize since it involves the spontaneous adsorption of the biomolecules onto the substrate. It is worth mentioning that in this case uncontrolled adsorption usually results in irregular layers and compromised recognition of the analyte due to steric hindrance of the binding sites. In addition, weak connections like van der Waals and hydrogen bonding interactions sometimes do not provide a stable immobilization onto the sensor surface.

To face this issue, at the Physics Department of University of Naples "Federico II", an all optical technique (PIT, Photonic Immobilization Technique) based on the interaction of ultrashort UV pulses with antibodies has been proposed as a simple and rapid approach capable to effectively functionalize the sensitive surface of a quartz crystal microbalance. In this thesis, PIT has been used to realize immunosensors for the detection of a group of analytes of practical interest. This functionalization technology provides an effective immobilization of antibodies onto the gold sensor surface upon activation of the protein sample through the selective photoreduction of the disulphide bridge in the triad cysteine-cysteine/tryptophan, a typical

structural feature of the immunoglobulins. The absorption of ultrashort UV laser pulses required for this activation process does not affect the recognition properties of the antibodies. On the other side, the free thiol groups so produced interact with gold surface thus leading to the effective exposure of the sensitive portions of the protein, the so-called antigen binding sites, thus greatly improving the detection efficiency. The effects of this unconventional functionalization approach on immunoglobulins have been investigated by means of optical techniques, atomic force microscopy and the so-called Ellman's assay, a chemical method used to quantify the thiol groups in a protein sample. PIT based immunosensors have proven to be effective in the detection of small toxic molecules like parathion (pesticide) and patulin (micotoxin). The issue of revealing these light molecules using a microgravimetric transducer like a quartz crystal microbalance have been overcome by ballasting the analytes using two labelling procedures involving either bovine serum albumin or an antibody in a sandwich-type configuration. PIT has been used also to realize an immunosensor for the detection of gliadin, the principal responsible for the coeliac disease. In all these cases, both sensitivity and limit of detection (usually in nanomolar concentration range) result to be in line with the limits set by current regulations and comparable or even better than other techniques used to quantify these harmful molecules. These promising results make PIT a valuable functionalization method for technologies involving gold surfaces for sensing and detection purposes.

Acknowledgements

Firstly, I would like to thank my supervisor Prof. Raffaele Velotta for his support and suggestions provided during the last years. He gave me the opportunity to apply my skills and creativity in a novel and interdisciplinary field like biosensing. He was always available for clarifying my doubts about scientific issues quite far from my background. A special thank goes to Dr. Bartolomeo Della Ventura who strongly assisted me in practical aspects of biosensing and laboratory activities. Working in an interdisciplinary and open-minded group like the biophotonic group at the department of physics (UNINA) was a great opportunity to challenge myself and approaching scientific topic from a completely different point of view. Therefore, I want to kindly thank Prof. Carlo Altucci, Dr. Felice Gesuele and Dr. Mohammadhassan Valadan for their moral support, scientific tips and encouragements.

During the PhD activity there was the chance to establish a wide network of collaborations and friendships mainly thanks to Fondazione con il Sud who supported the project "*Biosensori piezoelettrici a risposta in tempo reale per applicazioni ambientali e agroalimentari*" thereby providing an exciting context for the thesis' project. Thus, I wish to thank Dr. Ernesto Lahoz, Dr. Luigi Morra, Dr. Raffaele Carrieri (CRA-FRC), Dr. Nunzio D'Agostino and Dr. Irma Terracciano (CRA-CAT) for their stimulating discussions. I would like to thank also Dr. Maddalena Autiero (IVM) and Dr. Nicola Ciancia (Strago) for their support in the project "*Dottorati in Azienda*". Their contributions were crucial to achieve these results. Furthermore, I want to thank Dr. Dirk Mayer and all members of the Bioelectronics group of the Jülich Forschungszentrum (PGI-8/ICS-8) for their support during my internship in their institute.

I thank all my friends for their encouragements and patience. Even if I am not completely sure that they understood what I was dealing with in the lab, their help was invaluable.

Finally, I would like to thank my parents, my aunt, my grandmother and my dog, Yuma, for constant encouragements, support and, moreover, their endless love. Thank you, I could not have done it without you.

Table of contents

1   Principles of Biosensing

1.1   Sensors and Biosensors

A sensor is a device providing an output signal in response to a certain input quantity. The nature of the input signal can vary significantly, ranging from physical (e.g. mechanical properties of thin films) to chemical and biological quantities (e.g. concentration of analytes and pollutants in liquid or gaseous environment), whereas the output signal is usually electrical. Thus, in a typical sensor, a transduction process leads to the conversion of the input event into an electrical output which is eventually amplified and then sent outside the sensor itself for displaying, storage or analysis. Such a devices are commonly characterized by considering three fundamental parameters: sensitivity, limit of detection (LOD) and selectivity. The sensitivity is the measure of the intensity of the output signal due to a corresponding input event; the LOD is the lowest measurable input signal and the selectivity is the capability of the device to discriminate between different inputs. Even if it is possible developing and realizing extremely sensitive sensors for both gas and liquid analysis, it is challenging achieving a selective response. On the other side, biosensor based detection provides high selective detection as a results of the intrinsic properties of biological sensitive elements like proteins or nucleic acids[1].

In the first book dedicated to biosensing (Biosensors: fundamentals and applications, 1987[2]), A. P. F. Turner defined a biosensor as "a device incorporating a biological sensing element either intimately connected to or integrated within a transducer. The usual aim is to produce a digital electronic signal which is proportional to the concentration of a specific chemical or set of chemicals. The apparently alien marriage of two contrasting disciplines combines the specificity and sensitivity of biological systems with the computing power of the microprocessor". This definition, still valid, highlights the need to connect different research areas (biology, chemistry, physics and engineering) to realize an analytical device capable to quantify the presence of a specific substance in a complex sample. The main difference between sensors and biosensors are sketched in Figure 1.1.

While a sensor involves the direct transduction of the input signal (Figure 1.1a), biosensor based devices incorporate a biomolecular recognition element reacting with only one specific type of molecule (Figure 1.1b). Biosensors are usually classified according to the sensitive molecule and the transduction principle. Some examples are reported in Table 1.1.
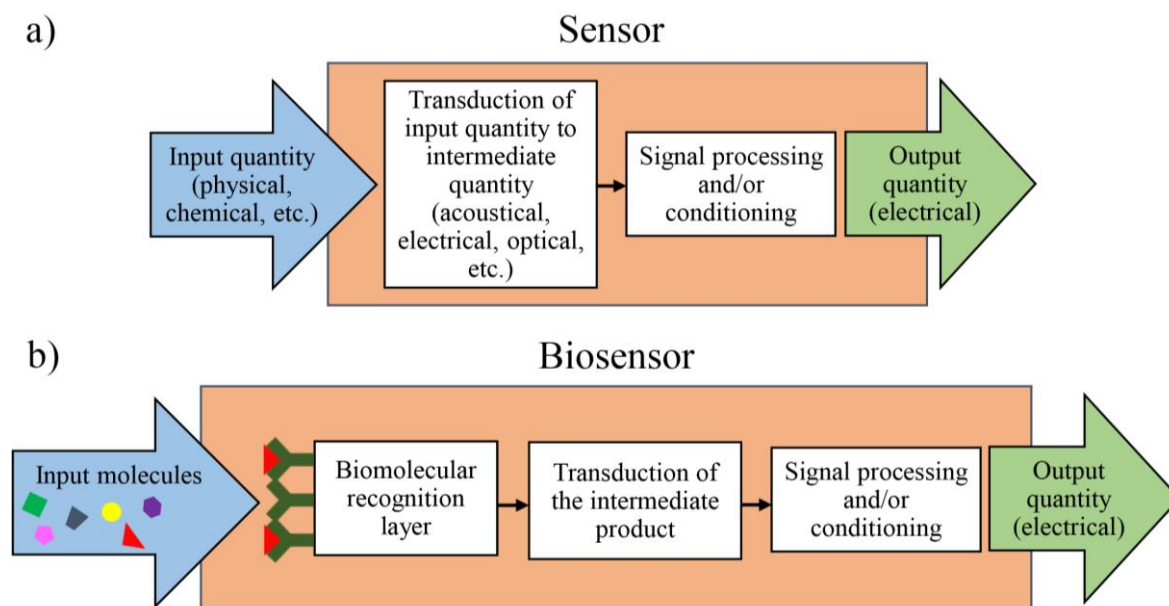
***Figure 1.1.** Sensing principles. a) sketch of a conventional sensor producing an electrical output in response to the presence of an input quantity. b) biosensor based detection. The generic device shown in a) is coupled with biomolecular recognition layer providing highly selective response.*

Biological sensitive element	Transducers
Tissues	Potentiometric
Cells	Amperometric
Organelles	Conductimetric
Membranes	Impedimetric
Enzymes	Optical
Receptors	Calorimetric
Antibodies	Acoustic
Nucleic acids	Mechanical
Synthetic molecules	"Molecular" electronics

***Table 1.1.** Usual elements used in biosensor development.*

Beyond biomolecules already available in nature, high selectivity can be achieved also by using chemical synthesis (e.g. aptamers, peptidomimetics) or protein engineering products (e.g. recombinant antibodies, fusion proteins, protein fragments, etc.).

Concerning transducers, electrochemical devices provide the non-negligible advantage that the biorecognition event is directly converted to an electronic signal[3]. Traditional

techniques like cyclic voltammetry, amperometry and potentiometry are commonly exploited to measure the concentration of dissolved ions and gases[4]. The coupling of this approach with biological sensitive elements allows to improve the specificity of the device, however these methodologies can be severely affected by other electroactive species eventually present in the sample.

Optical devices are commonly based on changes in the optical properties of a sensitive layer or medium[5]. This effect is usually related to the biorecognition of the analyte. For instance, in fluorescence-based detection, changes in the intensity of the fluorescence indicates the presence of the target molecules, providing that the compound is intrinsically fluorescent. Alternatively, either target or biorecognition molecules can be labeled with fluorescent tags. Even if this procedure is extremely sensitive, the labelling procedure is usually laborious and it may interfere with the recognition event. On the other side, label-free detection is much easier to design. Such an approach is used for some optical transducers including Surface Plasmon Resonance (SPR) devices[6].

Mechanical phenomena due to chemical and biochemical events rule motility, adhesion, transport and affinity effects on cellular and molecular scale. It is possible exploit such a properties to investigate biorecognition events (e.g. antibody-antigen interaction) thus obtaining valuable transducers for biosensor development[7]. To this aim, in view of their cost-effectiveness and reliability, mechanical and acoustic devices like Quartz Crystal Microbalances (QCM) achieved an important role in this research field.

A wide range of practical problems requiring portable and low-cost detection tools motivates the research on biosensing. For instance, real-time and in situ analysis of clinical samples is a valuable target in biomedical field. Even more interesting is achieving a continuous in vivo monitoring of drugs and metabolites level using miniaturized devices. In this topic, the classic example is the glucose sensor for diabetes[8]. Glucose biosensing has been the starting point of the modern idea of biosensor. This concept started from the scientific activity of Clark and Lyons[9], who proposed that enzymes can be immobilized onto electrochemical detectors to realize the so-called 'enzyme electrodes'. Another interesting application area for biosensing concerns food quality, which requires rapid methods for estimating deteriorations and contaminations. This issue is of paramount importance for people affected by allergies and food related pathologies like the coeliac disease. In addition, concerns for natural environment highlight the importance of sensors for pollutants like industrial products, pesticides and

polycyclic aromatic hydrocarbons (PAH). More in general, the strong need of analytical tools suitable for revealing the presence of toxic and harmful compounds strongly supports the research of novel detection devices, like biosensors, providing cheap, fast and easy analysis of the matrix of interest.

1.2 Quartz Crystal Microbalance (QCM)

In recent years Thickness Shear Mode (TSM) resonators, widely referred to as Quartz Crystal Microbalances (QCM), are receiving an increasing interest from scientific community mainly due to their wide range of application including surface characterization, material science, sensing, environmental monitoring and protein studying[1,10–14]. QCMs were originally used for studying material deposition phenomena in vacuum and air. Then, since this device have been proven to work also in liquid environment, quartz microbalances were employed in developing sensors and biosensors for water samples analysis. The physical principle which rules this kind of technology is the reverse piezoelectric effect discovered by Pierre and Paul-Jacques Curie in quartz. They found that for certain crystalline materials a mechanical stress produces an electrical polarization (direct piezoelectric effect). On the other side, if an electric field is applied to the same material this results in a mechanical deformation (reverse effect). For QCM application AT-cut quartz are commonly used. AT-cut refers to crystals cut at an angle of 35° 15' from the optical axis. A quartz crystal resonator consists of a thin disk of quartz with circular gold electrodes on both sides as shown in Figure 1.2.
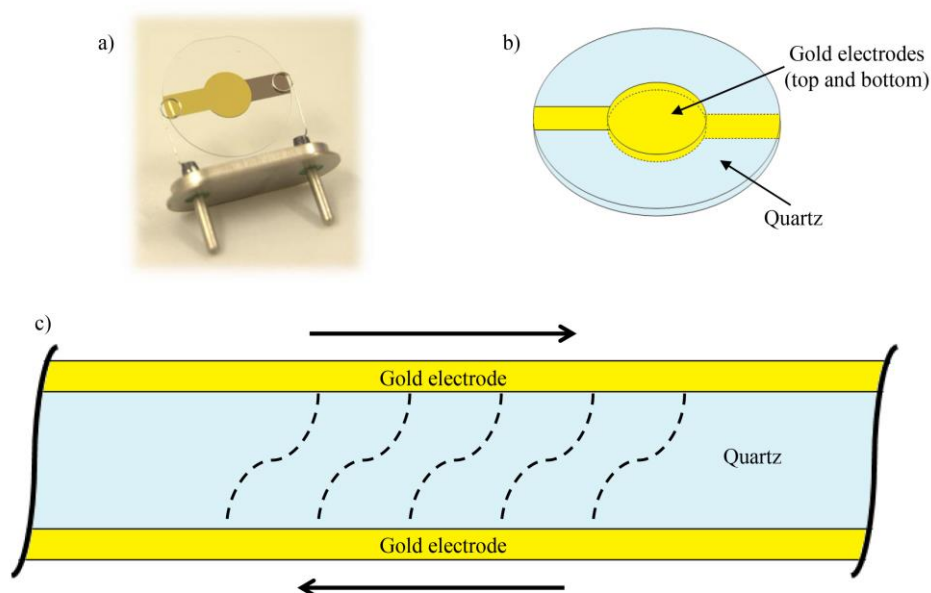
Figure 1.2. a) QCM electrode. b) Sketch (not to scale) of the structure of the electrode and c) shear deformation at the fundamental frequency. Both sides (i.e. electrodes) can be used.

In view of its piezoelectric properties, the application of an alternating voltage across the electrodes results in the generation of shear waves in the crystal. The overlap of these two waves is the displacement in the quartz.

A shear wave propagates through the crystal and is reflected on its faces. If the total phase shift is an integer multiple of 2π constructive interference will lead to crystal resonance. For a TSM resonator the following resonance conditions are valid:

$$h_s = N\left(\frac{\lambda}{2}\right) \tag{1.1}$$

$$f_N = \frac{Nv_s}{2h_s} \tag{1.2}$$

where h_s is the thickness of the crystal, N is the mode number (odd integer), λ is the acoustic wavelength, f_N the resonance frequency and v_s is the shear wave velocity which is defined as:

$$v_s = \sqrt{\frac{\mu_q}{\rho_q}} \tag{1.3}$$

where μ_q (2.947×10^{11} g cm^{-1} s^{-2}) and ρ_q (2.648 g cm^{-3}) are quartz shear modulus (stiffness) and density, respectively.

Since the displacement maximum occurs at the quartz disk faces, the device results to be extremely sensitive to surface perturbations and mass deposition thus affecting QCM resonance frequency. The gold-quartz wafer is commonly integrated in an oscillator circuit, where the oscillation frequency tracks the quartz resonance allowing to monitor material adsorption onto the gold surface. Resonance in a mechanical system is achieved only at specific frequencies where kinetic (U_k) and potential (U_p) peak energies are perfectly balanced. When mass accumulates on the gold electrode, the kinetic energy of the system rises (the material moves synchronously with the crystal surface) and resonant frequency must change to rebalance U_k and U_p. Analytical formulation for U_k and U_p are obtained summing the contributions from infinitesimal crystal slices across h_s:

$$U_k = \frac{\omega^2 u_{x0}^2}{2}\left(\rho_s + \frac{\rho_q h_s}{2}\right) \tag{1.4}$$

$$U_p = \frac{\mu_q k^2 u_{x0}^2 h_s}{4} \tag{1.5}$$

where u_{x0} is the surface displacement amplitude, ρ_s is the surface density (mass/area) of the adsorbed material and k is the wavenumber. Since U_k and U_p are supposed to be equivalent, the following relationship turns out:

$$\left(\frac{\omega_0}{\omega}\right)^2 = 1 + \frac{2\rho_s}{h_s\rho_q} \tag{1.6}$$

where ω_0 and ω are the basal and the final angular resonance frequencies, respectively. In particular ω_0 is obtained when $\rho_s = 0$:

$$\omega_0 = 2\pi f_0 = \frac{\pi}{h_s}\sqrt{\frac{\mu_q}{\rho_q}} \tag{1.7}$$

For $\rho_s \ll h_s\rho_q$ Equation 1.6 can be linearly approximated as follow:

$$\frac{\Delta f}{f_0} = -\frac{\rho_s}{h_s\rho_q} \tag{1.8}$$

This relationship shows that the fractional shift in the oscillation frequency of the oscillator is equal to the fractional shift in mass due to the adsorbed material. This approximation is valid for mass fractions up to a few percent of the mass of the wafer.

Combining equations 1.1, 1.2, 1.3 and 1.8 leads to the so called Sauerbrey's equation which is used to estimate the amount of material deposited onto the QCM gold electrode[15]:

$$\Delta f = -\frac{2f_0^2\rho_s}{\sqrt{\mu_q\rho_q}} = -\frac{2f_0^2\Delta m}{A\sqrt{\mu_q\rho_q}} \tag{1.9}$$

where A is the piezoelectrically active area (the surface of the electrode) and Δm is the deposited mass. To apply this relationship the layer on the electrode must be rigid and thin. QCM can be used also to measure the accumulation of soft molecules from liquid phase or properties of the contacting fluid (e.g. density, viscosity, etc.). In that case the electrical properties of the oscillating circuit and dissipation phenomena have to be considered thus leading to a more complex model. For example Kanazawa and Gordon[16] showed that the liquid in contact with the electrode damps the crystal oscillation and Sauerbrey's equation has to be modified:

$$\Delta f = -\sqrt{f_0^3\frac{\rho_l\eta_l}{\pi\mu_q\rho_q}} \tag{1.10}$$

being ρ_l and η_l the density and the viscosity of the liquid, respectively.

More in general, a variety of papers show that the combined effect of hydration water, liquid trapped in the absorbed molecules, and the flexibility of many polymers/biomolecules, induce frictional (viscous) losses and thus a dampening of the QCM oscillation frequency[10–12,17,18]. An accurate estimation of the amount of mass adsorbed on the electrode will require the measurement of the dissipation using expensive and up-to-date QCM devices like the QCM-D. However, since the quartz microbalances are extremely sensitive to mass deposition onto the electrode surface, it is possible use them as transducers to convert biomolecular recognition events in frequency shifts. Biomolecules can be used to functionalize the gold sensor surface thus exploiting the intrinsic specificity and sensitivity of proteins and nucleic acids to bind and detect the desired compound. The biorecognition leads to an increase of the mass onto the electrode thus decreasing the resonance frequency of the QCM. After a proper calibration and specificity tests (e.g. analysis of a real sample) it is possible using the QCM technology to develop sensors and biosensors.

1.3   Surface functionalization

Coupling a biomolecule with an inorganic transducer is one of the main issues in developing biosensors. The topic of surface functionalization has been widely explored in various research areas including diagnostics, affinity chromatography, ELISA assays and microarrays.

Generally, a biological molecule (e.g. proteins, nucleic acids) moves into aqueous environment and its functions are characterized by biochemical parameters, which can be severely affected by the immobilization process. A biomolecule suitable for biosensing usually has a sensitive site responsible for the selective recognition of the compound of interest. Since this portion has to be available and well exposed to the environment to achieve the effective detection of the analyte, the orientation of the biological sensitive element is crucial. In view on the importance of this issue, there is a strong interest in the research of new immobilization and functionalization techniques providing better sensitivity and lower LOD as highlighted by the vast literature on this topic[19,20]. In particular, Trilling et al.[21] have recently investigated the relationship between analyte characteristics and capture molecule anchoring, showing that the uniform orientation of the recognition elements provides a huge systematic improvement in sensitivity when the binding involves weak interactions. They observed that the smaller the molecule and the lower the epitope number per analyte, the more important is the orientation of the sensitive biomolecule.

The easiest way to immobilize biomolecules onto a hydrophobic substrate is via spontaneous adsorption based on weak and non-covalent connections like van der Waals and hydrogen bonding interactions. The main advantage of this method is that it avoids chemical treatments but, on the other side, uncontrolled adsorption usually results in irregular layers and compromised recognition of the analyte due to steric hindrance of the binding sites. Other non-covalent approaches involve well-known strong biomolecular interactions. For instance, biotinylated and His-tagged proteins (i.e. proteins having a poly-histidine sequence) can be easily immobilized onto streptavidin-coated and Ni^{2+} chelating supports, respectively[22]. Even if these strategies allow a more efficient orientation of the immobilized biomolecules, they require recombinant proteins in which amino- or carboxy-terminal tags have to be introduced.

It is also possible take advantage of existing functional groups on the biomolecule. Concerning covalent based immobilization, the most common methods involve the random conjugation of the amino groups exposed by the biomolecule (mainly due to the lysine residues in proteins) to amine-reactive surfaces. These kind of strategies are usually laborious since the chemicals used during the activation process need to be removed at the end of each step. In some cases, more strategies are coupled to obtain uniform protein layers. For example, antibodies can be oriented onto the substrate through binding to immobilized protein A or G[23]. These biomolecule recognize the Fc region of most immunoglobulins, but this interaction sometimes is not stable enough for some applications.

Another covalent approach involves a photochemical reaction between the biomolecule and a compound activated by absorbing photons in the visible or UV range. Several light-induced immobilization techniques have been developed[24] showing that the treatments required can severely affect structure, activity and orientation of the target protein.

A particular category of functionalization involves the deposition of self-assembled monolayers (SAM), widely used for metallic substrates[25,26]. This technique provides uniform and homogeneous layers, which are crucial for optical sensors.

The functionalization of gold surfaces entices many efforts in view of their role in many sensors including Quartz Crystal Microbalances[27–30] and Surface Plasmon Resonance (SPR)[31–33] based devices. Gold is a noble metal having a low tendency to oxidize and easily cleanable by chemical treatments such as piranha solution (a mixture of sulfuric acid and hydrogen peroxide). The stability of gold-sulfur interaction is usually exploited to immobilize molecules on gold supports, since the only requirement is the availability of a free thiol group (-SH). This

chemical function is the main characteristic of the cysteine, one of the amino acids normally present in proteins and peptides. If the biomolecule has not intrinsic thiol groups, it possible introducing them by chemical reaction. For instance, the so-called Traut's reagent (2-iminothiolane hydrochloride) is used to modify amine groups on proteins thus obtaining new sulfhydryl groups for further applications.

The majority of these immobilization methods require one or more time-consuming chemical and thermal treatment, sometimes involving hazardous reactants, which can potentially affect both structure and activity of the biological sensitive element. Therefore, there is the need of less invasive procedures preserving the functional properties of the biomolecule.

To this aim, Neves-Petersen et al.[34,35] developed the so-called LAMI (Light Assisted Molecular Immobilization), a photonic method for protein functionalization of thiol-reactive substrates which preserves the native structural and functional properties of the biomolecule. This strategy allows to achieve spatially oriented and localized immobilization of biomolecules by exploiting an intrinsic natural property of some proteins and peptides, whereby a disulphide bridge, located in close proximity to an aromatic residue (i.e. tryptophan, tyrosine and phenylalanine), is reduced as a consequence of the UV irradiation of the sample. Since, the triad of residues cys-cys/aromatic (typically cys-cys/trp) is present in many proteins including enzymes and immunoglobulins[36], LAMI has been used to realize several biosensors and protein microarrays[34,35,37,38]. The main drawback of this technique is that, using conventional UV lamps, an effective protein activation requires several hours of irradiation. Therefore, there is the opportunity to improve significantly the photonic activation process by using UV sources (i.e. lasers) capable to deliver the amount of energy required by the photoreduction process in much shorter time.

1.4   Immunoglobulins: antibody structure and immune response

Antibodies or immunoglobulins are big Y-shaped proteins, which play a key role in the immune response since they are involved in catching and possibly neutralizing foreign targets (named antigens) like bacteria, viruses and toxins[39]. The presence of an extraneous object into an organism causes the activation of a complex metabolic pathway which leads to several immune effects including the production and releasing of antibodies by B lymphocytes (a kind of white blood cell). These cells expose a membrane immunoglobulin named B cell receptor (BCR). The antigen binding by these membrane proteins and the eventual stimulation from other elements of the immune system lead to B lymphocytes activation and differentiation in

either "antibody factories" (plasma cells) or memory cells, which will survive in the organism providing a faster immune response upon future exposure to the same antigen.

The majority of immunoglobulins has a common basic architecture consisting of three globular domain of similar size connected by a flexible portion named "hinge region". This big tetrameric structure, weighing about 150 kDa, is made of two kinds of polypeptide chains, the so-called heavy chains (of about 50 kDa) and light chains (of about 25 kDa), which are folded in constant (C) and variable (V) immunoglobulin domains. This fold (of about 110 amino acids) is typical of immunoglobulins and consists of two antiparallel β-sheets, which are assembled through a disulphide bonds and non-covalent interactions (i.e. salt bridges, hydrophobic interactions and hydrogen bonds). The two sheets are placed opposite to each other to form the so-called "β barrel". The four polypeptidic chains are connected into the Y-shaped structure through inter-chain disulphide bridges and non-covalent bonds. The antibodies have two distinct functions. The former is the antigen binding which allows to label and eventually neutralize the antigen. The latter is the recruitment of other components of the immune system to destroy and degrade the flagged object. These activities involve two distinct globular domains of the macromolecule: the two antigen binding fragments (Fab) and the crystallizable fragment region (Fc) which correspond to the arms and the legs of the "Y", respectively. Each Fab contains the variable domains of heavy and light chains (V_H and V_L) which form the antigen-binding site, or paratope, which is specific for a portion of the antigen, the epitope. The paratope, which includes the so-called complementary determining regions (CDR), is generated by random arrangements of a specific gene cluster. After the activation of the lymphocyte, this DNA region is slightly modified through random mutation to improve the immunoglobulin binding affinity. This pathway provides an enormous variability in antibody specificity thus allowing the immune system to recognize a wide range of antigens. The typical structure of a type G immunoglobulin (IgG)[40] and its classification in domains are shown in Figure 1.3.

Depending on the constant region, antibodies are classified in isotypes with different functional locations and immunological properties. For instance, mammalian immunoglobulins are divided in five classes: IgA, IgD, IgE, IgM, and IgG. IgA is dimeric and localized in mucosal areas. IgD acts as membrane immunoglobulin on B cells and participate in immune system stimulation. IgE is involved in allergic responses. IgM is expresses as either monomer on B cells surface or as pentamer in the early stages of the antibody production. Finally, IgG, which represents about the 75% of human adult serum antibodies, is the main effector molecule of the

a)

b)
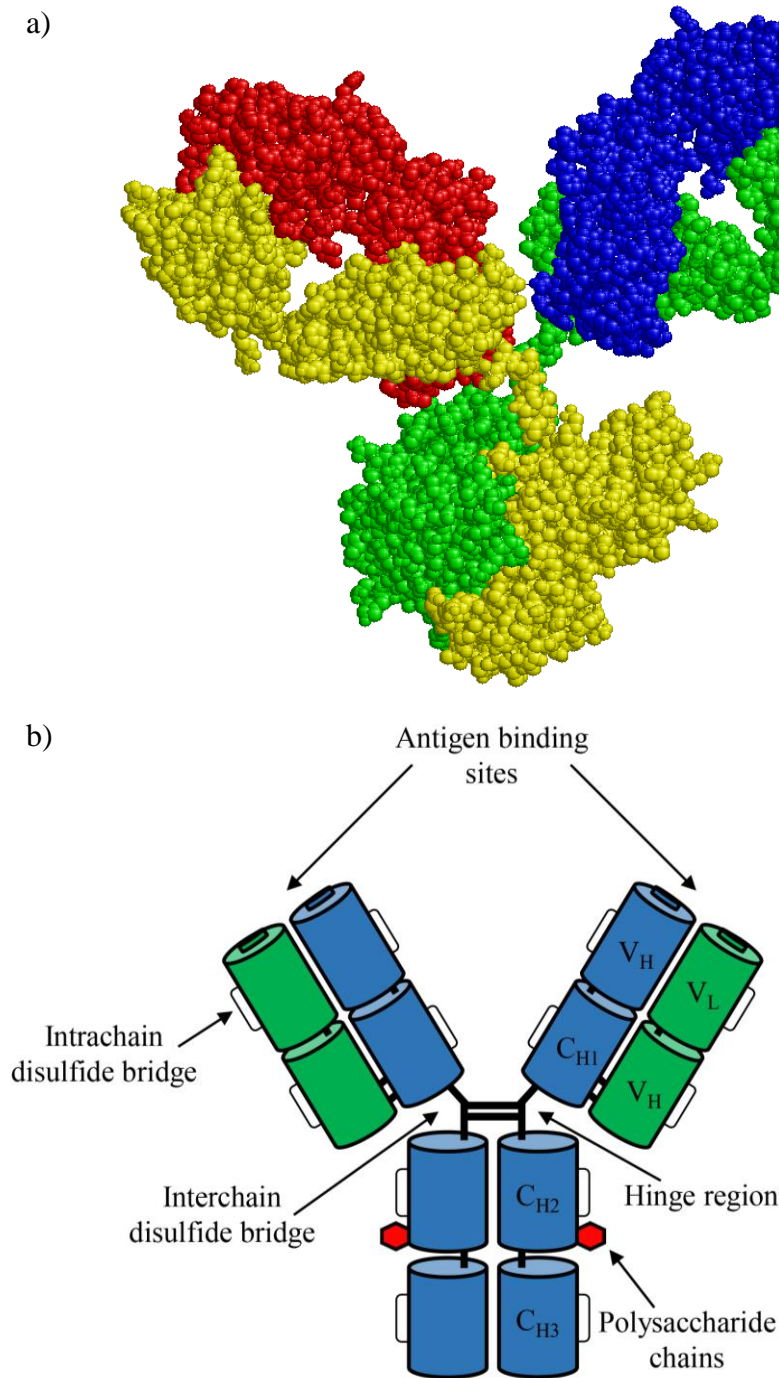
Figure 1.3. a) Crystallographic structure of a type G immunoglobulin (1IGY). The four polypeptide chains are highlighted in different colors. b) Schematic representation of the antibody where the different portions are labelled. Key: light chain – green; heavy chain – blue; V_H – variable domain heavy chain; V_L – variable domain light chain; C_H – constant domain heavy chain; C_L – constant domain light chain.

B cell activity against invading pathogens. In view of their properties (e.g. high specificity and avidity), immunoglobulins are commonly used as biological sensitive element in biosensors development[31].

1.4.1 Polyclonal, monoclonal and recombinant antibodies

There are different ways to produce antibodies for practical applications like immunosensing and diagnostics. The easiest is the immunization of a mammal (the most common are rabbit and mouse). The host immune system will respond to the injection of a foreign antigen producing big amounts of immunoglobulins, which will be purified from the blood through chromatographic procedures (for more details see paragraph 2.2). Since different B-lymphocytes clones produce antibodies against the injected antigen, these immunoglobulins are known as polyclonal antibodies (pAb). pAbs bind different epitopes on the antigen thus providing an effective neutralization of the targets. On the other side, this property can lead to false positive events in detection techniques since pAbs can catch antigens showing similar sets of epitopes (this risk is mostly negligible in small molecule detection since in that case the epitope corresponds to the whole antigen). In addition, the production of pAbs is limited by the size of the host. Mice are commonly killed during the blood taking while bigger mammalians (e.g. rabbit) can be immunized several times.

The antibody production has been revolutionised by Kohler and Milstein in 1975[41] who developed a procedure to get monoclonal antibody (mAb) producing cells winning the Nobel Prize for physiology and medicine in 1984. Since mAbs are produced by a cell line deriving from a single differentiated B-lymphocyte, they are able to recognize only a specific epitope on the antigen. B-cells cannot artificially survive for long time, therefore, after the extraction from the host, they are fused to cancer cells (i.e. myeloma cells) to get immortal cell lines. The fusion is performed using polyethylene glycol (PEG) or, more recently, electric pulses (electrofusion). The new immortalized cells are known as hybridoma cells. They are diluted and screened for the ability to produce antibodies against the desired target using enzyme-linked immunosorbent assays (ELISA). This selection procedure is performed several times (three at least) until a stable cell line is achieved. Finally, these hybridoma cells are amplified for large scale antibody production. In view of the more advanced techniques required for their production, mAbs are usually more expensive than pAbs. The sketch in Figure 1.4 shows the differences between the production processes of pAbs and mAbs.

Recent advances in protein engineering and molecular biotechnology allow in vitro modifications of natural antibodies. The so-called recombinant antibodies (rAb) were initially developed to face the issue of "humanise" natural mammalian mAbs for clinical applications[42].
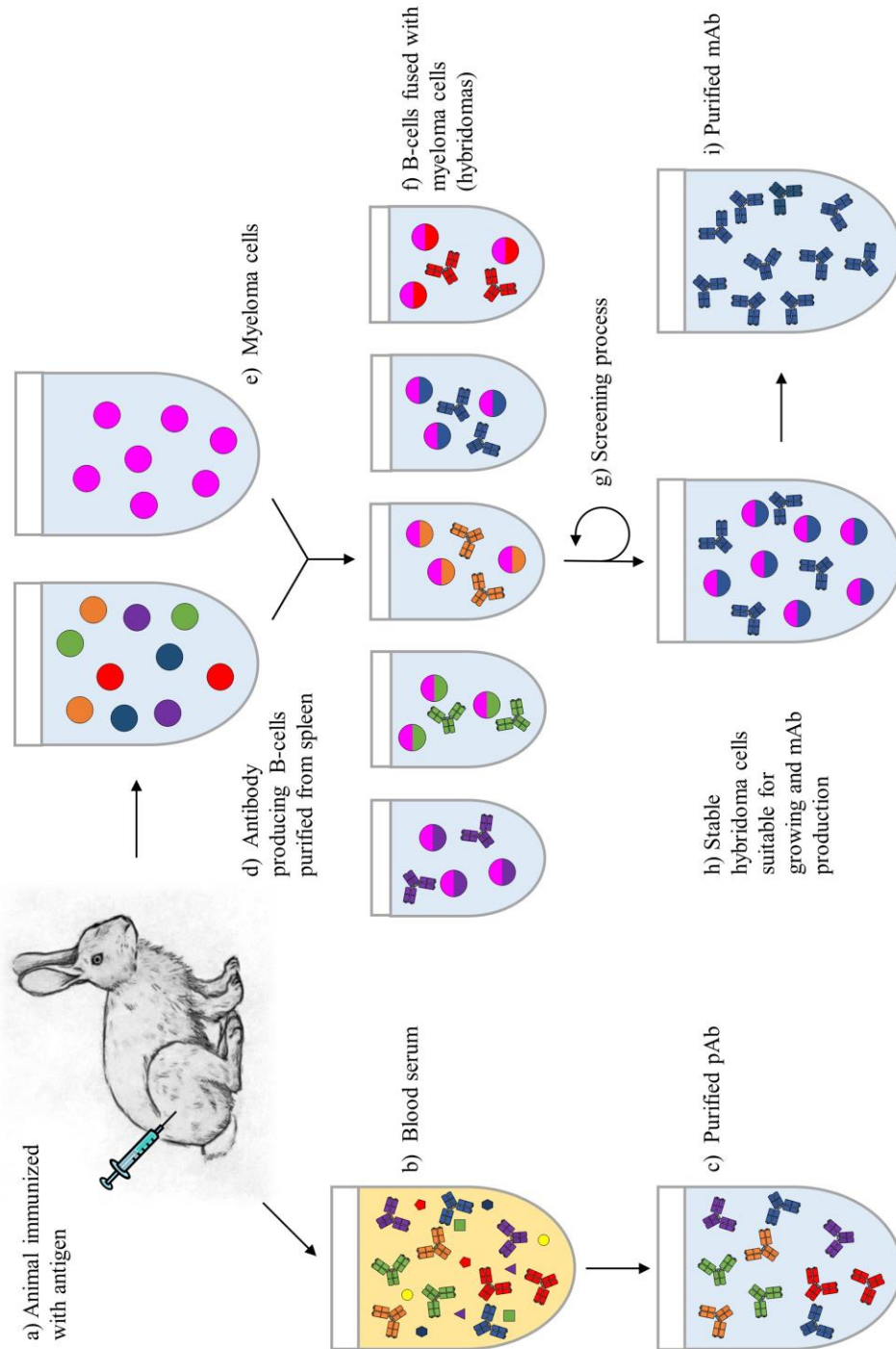
Figure 1.4. *Overview of pAb and mAb production, see text for detailed description. The immunization of the animal a) is required in both procedures. b) and c) are related to pAb extraction and purification. d) to i) describe mAb production.*

Further development of these techniques lead to "smaller" antibodies, improved binding affinity and conjugation with specific molecules for imaging and cell-target therapies. It is worth highlight that it is very hard producing antibodies against highly toxic molecules in conventional ways. Mammalian hosts/cells usually do not survive for enough time to produce antibodies against the harmful compound. On the other side, novel techniques like phage display allow to overcome this issue exploiting CDR codifying DNA segments resulting from random in vitro synthesis (i.e. polymerase chain reaction, PCR) and B-cells from immunized and unimmunized (i.e. naïve B-cells) donors. Two examples of rAbs are the single-chain variable fragment (scFv) and the Fab. The scFv consists of the V_H and V_L domains, which form the paratope, connected by a short flexible peptide while the Fab is the macroglobular domain of the immunoglobulin involved in the antigen recognition. rAbs have several advantages compared to "classic" antibodies but the procedures to realize these novel immunoglobulins are quite expensive and time-consuming. These bottlenecks make the conventional antibodies the most valid choice for immunosensing.

1.5   A sensing challenge: detection of small molecules

The effective detection of small molecular weights analytes is of paramount importance in a wide range of scientific topics like investigating molecular recognition events and sensing of toxic molecules[10,12,43,44]. In particular, in the field of environmental monitoring it would be valuable having cost-effective and sensitive tools allowing the detection of harmful compounds like steroids, herbicides, pesticides, toxins and combustion products like PAHs. Usually, these pollutants are low soluble in aqueous environment and have a quite small molecular weight (i.e. about hundreds of Da) thus making their detection challenging. In view of their properties, parathion and patulin have been chosen as cases studies to realize efficient detection tools. These molecules have a relatively low molecular weight and high interest for environment and health safety.

1.5.1 Parathion

Parathion [IUPAC name O,O-Diethyl O-(4-nitrophenyl) phosphorothioate] is the trading name of a powerful insecticide and acaricide developed by IG Farben in the 1940s. Organophosphate pesticides, like parathion, are chemical synthesis products widely used to enhance agricultural production. This class of chemicals selectively inhibits the acetylcholinesterase, an essential enzyme for nervous function in insects and mammalians. Organophosphates act by phosphorylating the serine hydroxyl group in the active site of the

acetylcholinesterase thus resulting in the inactivation of the enzyme. Acetylcholine is a neurotransmitter produced during the nervous signal transmission and must be hydrolyzed to prevent the continuous stimulation of cholinergic receptors[45]. As a consequence of the organophosphate poisoning, the inhibition of the acetylcholinesterase leads to the accumulation of the neurotransmitter thus resulting in respiratory distress and muscular overstimulation.
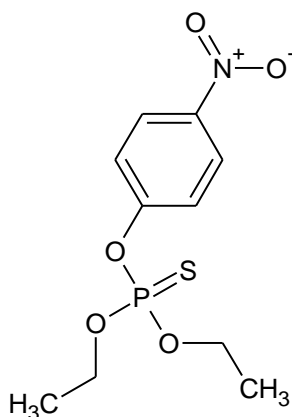
Figure 1.5. *Structure of parathion*

Parathion acts as indirect inhibitor of the acetylcholinesterase since, after the absorption, it is converted by oxidases of the organism to its more reactive derivative paraoxon, which covalently binds the enzyme[46]. The chemical difference between parathion and paraoxon (also used as pesticide) is the double bonded sulfur replaced with an oxygen atom. The phosphate ester (paraoxon) is more reactive than the phosphorothiolate ester (parathion) because the phosphorus atoms are much more electropositive in the first case. In view of its high toxicity, the use of this chemical is strictly limited or even banned in many countries including European Union, which sets the limit of parathion in food between 50 and 100 μg/kg (Commission Regulation (EC) no. 839/2008).

Nowadays the usual treatment of organophosphate poisoning in humans consists of a combination of an antimuscarinic agent (e.g. atropine), an acetylcholinesterase reactivator (e.g. pyridinium oximes) and diazepam[47]. In addition, since the organophosphates are naturally degraded by enzymes of the organism, the level of the phosphate in urine is usually controlled.

Atropine is a deadly poison extracted from nightshade (*atropa belladonna*) and other plants of the family Solanaceae. This alkaloid is an antagonist of the acetylcholine which acts on the muscarinic cholinergic receptors thus relieving some of the symptoms of organophosphates poisoning. In view of its properties, atropine is given frequently in small

doses. The usual therapy consists in giving 2 mg (0.02 mg/kg in a child) intravenously every 5-10 minutes. The effect of atropine should be kept for the whole treatment.

In view of their high nucleophilicity, pyridinium oximes are able to reactivate phosphorylated acetylcholinesterase by displacing the phosphoric group from the active site of the enzyme thus releasing phosphorylated oximes. The efficiency of this treatment depends on the organophosphate compound and on the rate of dealkylation of the phosphoric residue bounded to the enzyme. This phenomenon, known as aging, stabilizes the enzyme-inhibitor complex thus making the acetylcholinesterase resistant to both spontaneous and oxime-induced reactivation. Pralidoxime (also known as 2-PAM) is commonly used in combination with atropine for organophosphate poisoning[48]. The usual therapy consists in a PAM-2 intravenous infusion (30 mg/kg for adults and 20-50 mg/kg for children) for the first 15-30 minutes. Depending on the severity of the poisoning, additional oxime is given.

Diazepam is a benzodiazepine frequently used for treating and preventing convulsions and muscle fasciculation due to organophosphate poisoning. It is given intravenously in both absence (5-10 mg) and presence (10-20 mg) of convulsions.

The details of the treatment of organophosphate poisoning have been pointed out in several publications[49–51].

Organophosphate pesticides are usually quantified exploiting chromatographic based strategies which requires sample pre-treatment and highly sensitive detection systems like mass spectrometry[52–54]. On the other side sensor and biosensor based detection allows in situ and real-time analysis for both environmental monitoring and food quality control[32].

In this research field the lowest LOD for organophosphates in aqueous environment has been achieved by Walker et al.[55] using a Polymerized Crystalline Colloidal Array (PCCA) photonic crystal sensing material. The crystals were coupled with acetylcholinesterase which, once covalently modified by the pesticide, changes the optical properties of the device thus reaching a detection limit of 4.26 fM. Since this PCCA based biosensor requires low ionic strength solution, its application in analysing real aqueous samples is strictly limited. In addition, it is worth to highlight that inhibition-based strategies involving acetylcholinesterase are intrinsically not selective.

Another widely explored organophosphate detection method involve amperometric devices[56]. This technique allows cheap, rapid and effective analysis of aqueous samples

providing that the molecules to be detected are electroactive. For example, Chough et al. realized a sensitive procedure for the detection of parathion using an enzyme electrode containing organophosphorus hydrolase and albumin immobilized on a nylon net attached to a carbon paste electrode. Exploiting this strategy, they were able to detect parathion with a LOD of 15 nM. Even if this kind of devices offers several advantages for water analysis, electrochemical detection can be easily influenced by other oxidizable molecules eventually present in a real sample.

Among all the physical transducers, QCM technology has attracted research interest as valid alternative to conventional strategies (e.g. immunoassays) for detecting pesticides. While laboratory techniques require trained operators and expensive (and eventually dangerous) chemicals, QCM based sensors and biosensors provide real-time output, high sensitivity, simplicity of use, and cost-effectiveness[57]. For instance, Bi and Yang[58] detected pesticides in aqueous environment using a QCM based method. They used molecular imprinted monolayers (MIMs), obtained from hexadecanethiol self-assembling on the QCM gold electrode, to detect imidacloprid and thiacloprid pesticides in celery juice reaching a LOD of 1 μM by using an extremely sensitive QCM apparatus. Concerning immunosensing, March et al.[59] quantified carbaryl insecticide and 3,5,6-trichloro-2-pyridinol (a derivative of both the chlorpyrifos and triclopyr pesticides) using a QCM based detection. They developed a competitive immunoassay method based on the covalent immobilization of hapten conjugated via thioctic acid self-assembled monolayer on the gold sensor surface. The sample to test is mixed with a mAb solution and then conveyed into the QCM camber. This strategy allows to achieve a LOD of 55 and 35 μM for carbaryl and 3,5,6-trichloro-2-pyridinol, respectively. Another kind of immunosensor has been developed by Jia et al.[60] who used patterned QCM electrodes prepared via electron beam evaporation. Different patterned areas are functionalized by either anti-carbofuran or anti-atrazine antibodies by using thiol chemistry. This methodology provides the sequential detection of the antigens reaching a limit of detection of 4.5 and 4.6 μM for carbofuran and atrazine, respectively.

1.5.2 Patulin

Mycotoxins are a wide class of secondary metabolites produced by filamentous fungi, or molds[61,62]. Even if they are not necessary for growth or development, some of them involved in weakening the infested host thus favouring fungal proliferation. They severely affect humans and animals in different ways including mutagenesis and immune system deficiencies.

Mycotoxins are usually found in crops as a result fungal infestation. Since they are highly resistant to degradation, some of them even to thermal treatments, it is valuable have a detection tool for monitoring food chains and analysing agricultural products.

Patulin is an example of this class of molecules produced by several species of fungi belonging to the genera *Aspergillus*, *Penicillium* and *Byssochlamys*. It is most likely to be found in apples and apple-derived products such as juice, cider, compotes and baby food. Since it has strong affinity for sulfhydryl groups it acts as inhibitor of many enzymes. Patulin exposure is associated with immunological, neurological and gastrointestinal diseases. In addition, it shows mutagenic activity and high embriotoxicity[63]. Patulin level in food is strictly regulated in European countries (Commission Regulation (EC) no. 1881/2006) which set a maximum level of 50 μg/kg for fruit juices and derived products, 25 μg/kg for solid apple products and 10 μg/kg for baby foods.
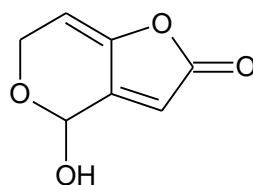
Figure 1.6. *Structure of patulin*

Mycotoxins are conventionally revealed by using expensive, time-consuming and complex techniques like High-Performance Liquid Chromatography (HPLC) and/or mass spectroscopy[64,65]. The lack of any commercial and standard efficient immunochemical method underpins the research for biosensor based detection allowing in situ and real-time analysis for crop monitoring and food quality control.

Electrochemical[66], optical[65] and piezoelectric[67,68], sensors and biosensors for the detection of mycotoxins are reported in literature, but only few papers concerned patulin detection. A fluorescence assay was proposed by De Champdoré et al.[69] with a LOD of 10 μg/L (less than 0.1 μM), but no test on a real sample was carried out. Damián Chanique et al.[70] realized a detection method based on the electrochemical reduction of patulin using glassy carbon electrodes. With this strategy, they reached a LOD of 300 nM quantifying patulin in commercial apple juices. Starodub and Slishek[71] proposed a nano-porosus silicon based immunosensor for measuring the level of patulin and T2 mycotoxinin real samples reaching a sensitivity of about 10 ng/mL for both pollutants. They tried several immobilization strategies for the anti-patulin antibodies and found that the transducer functionalization can easily affect the detection signal. More recently, Pennacchio et al.[72] proposed a competitive SPR based

bioassay for the detection of patulin. Exploiting the competition between free and immobilized mycotoxin for anti-patulin antibodies they achieved a LOD of 0.1 nM. It is worth noticing that the accuracy of SPR measurements can be influenced by interfering effects like temperature and sample composition which produce a change in the refractive index not related to the analyte binding.

1.6   Biosensors in food analysis

The risks associated with the presence of allergens, contaminants and harmful pathogens in food and water raised the need for fast and sensitive procedures to detect these species in complex matrixes. In particular, food industries seek rapid and reliable methods to assure the quality of products and process control, where the use of conventional analytical techniques (e.g. HPLC) is usually expensive and laborious. In view of their extremely high specificity, the application of biosensor-based approaches in this field is promising[73–75]. For instance, the availability of such a detection tool to analyse food for people affected by the coeliac disease would be valuable.

1.6.1 Gliadin

Gliadins are a class of prolamin (plant storage proteins having high proline content) mostly present in wheat and other cereals. Gliadins and glutenins are the main constituents of gluten, a protein composite found in wheat and related grains. These proteins are the primary responsible for celiac disease, a genetically determined autoimmune pathology characterized by stimulation of helper T-cells resulting in a chronic inflammation of the mucosal tissue of the small intestine[76,77]. This immunological disease is the most common food intolerance in the Western population showing an incidence of about 1%[78]. In view of the lack of effective medical treatments, celiac patients have to strictly follow a gluten-free diet to avoid intestinal mucosal inflammation and other complications.

Concerning current regulation, the international Codex Alimentarius defines as "gluten-free" a food having a gluten content which does not exceed 20 mg/kg or ppm (CODEX STAN 118 – 1979 and ALINORM08/31/26, Appendix III – 2008). According to Codex Alimentarius, the prolamin fraction (i.e. gliadin content) is generally taken as 50% of gluten so that the gluten content is estimated by doubling the prolamin concentration. In addition, food products labelled as "very low gluten" can have a gluten level ranging between 20 and 100 ppm. These limitations

are consistent with those set by other countries and international bodies like the European Union and the American Food and Drug Administration (FDA).

Conventional detection procedures used to quantify gliadin in real samples involve techniques like gluten-specific polymerase chain reaction (PCR)[79], enzyme-linked immunosorbent assay (ELISA)[80] and HPLC[81]. The validated standard method for gluten determination (according to the Codex Alimentarius) is an ELISA which uses the R5 monoclonal antibody[82]. This approach is exploited in several commercial immmunoassays (RIDASCREEN®) which provide a LOD of about 1.5 ppm (3 ppm of gluten). However, these gliadin detection procedures are time-consuming, expensive and require extensively trained operators to be performed.

Both people affected by coeliac disease and industries processing raw materials for gluten-free food could benefit from in situ and easy-to-use gluten detection tools for food analysis and monitoring the production process. Biosensor based detection could provide a rapid and low-cost alternative to conventional analytical methods for revealing the presence of the analyte (e.g. gliadin) in various application fields including food safety. For instance, De Stefano et al.[83] exploited a glutamine-binding protein (GlnBP) from *Escherichia coli* which recognizes an amino acid sequence typical of the prolamins. This bioreceptor has been immobilized onto a nanostructured porous silicon (PSi) surface thus achieving a linear response between 2.0 and 8.0 μM of gliadin. The main drawback of this procedure is that the sample requires several complex and time consuming manipulation steps to make the amino acid sequence detected by the GlnBP available. Nassef et al.[84] realized amperometric and impedimetric immunosensors for the detection of gliadin using Fab fragments. These immunoglobulin fragments have been immobilized onto the gold electrodes using a self-assembled monolayer (SAM) approach thus achieving a LOD of 3.29 ng/mL and 0.42 μg/mL for amperometric and impedimetric devices, respectively. Anyway, these immunosensors have not been tested against a real complex sample like a wheat extract, which can in principle contain species affecting the gliadin detection. More recently, Chu et al.[85] developed a QCM based immunosensor incorporating gold nanoparticles to increase the effective surface area of the electrode. They functionalized the gold sensor surface by immobilizing chicken anti-gliadin antibodies (IgY) using a cross-link procedure thus claiming a LOD of 8 ppb by using an extremely sensitive QCM device.

2   Experimental section

2.1   Chemicals

Parathion (45607), patulin (P1639), and gliadin from wheat (G3375) were from Sigma-Aldrich. Anti-parathion (ABIN113883) and anti-patulin (AS11-1699) polyclonal antibodies were purchased as rabbit sera from antibodies-online.com and Agrisera, respectively. The type G immunoglobulins were purified using the Protein A Antibody Purification Kit (PURE1A) from Sigma-Aldrich. Purified anti-gliadin polyclonal antibody from rabbit (G9144), anti-mouse polyclonal antibody from goat (M8642), IgG from mouse (I5381), 5,5′-dithiobis-(2-nitrobenzoic acid) also known as Ellman's reagent (D8130), bovine serum albumin (A2153) and the compounds used for the specificity tests, bisphenol A (239658), p-nonylphenol (46018), dichlorvos (45441), diazinon (45428) and paraoxon (36186), were from Sigma-Aldrich.

Bisphenol A or BPA (IUPAC name 4,4'-(propane-2,2-diyl)diphenol) is an organic compound having two phenolic functions. It is used in the industrial manufacturing of certain plastics and epoxy resins. This molecule is an endocrine disruptor involved in child development and male fertility[86].

Nonylphenol (p-nonylphenol) is a synthetic organic compound used as precursor in the production of detergents, emulsifiers and solubilizers. Since it mimics the molecular structure of the estradiol, this molecule acts as endocrine disruptor[87].

Dichlorvos (IUPAC name 2,2-dichlorovinyl dimethyl phosphate), diazinon (IUPAC name: O,O-Diethyl O-[4-methyl-6-(propan-2-yl)pyrimidin-2-yl] phosphorothioate) and paraoxon (IUPAC name diethyl 4-nitrophenyl phosphate) are, like parathion, powerful organophosphorus pesticides and inhibitor of the acetylcholinesterase. The exposure to these chemicals produces the same symptoms of parathion poisoning.

Patulin has been extracted from real apple puree samples by using a Polyintell Affinimip® SPE cartridge.

The pollutant samples were prepared using PBS 1x buffer, ethanol and acetonitrile solution in the fume hood. Elix water (Millipore), sulfuric acid 98% and hydrogen peroxide 40% were used for the cleaning procedure of the QCM gold surfaces.
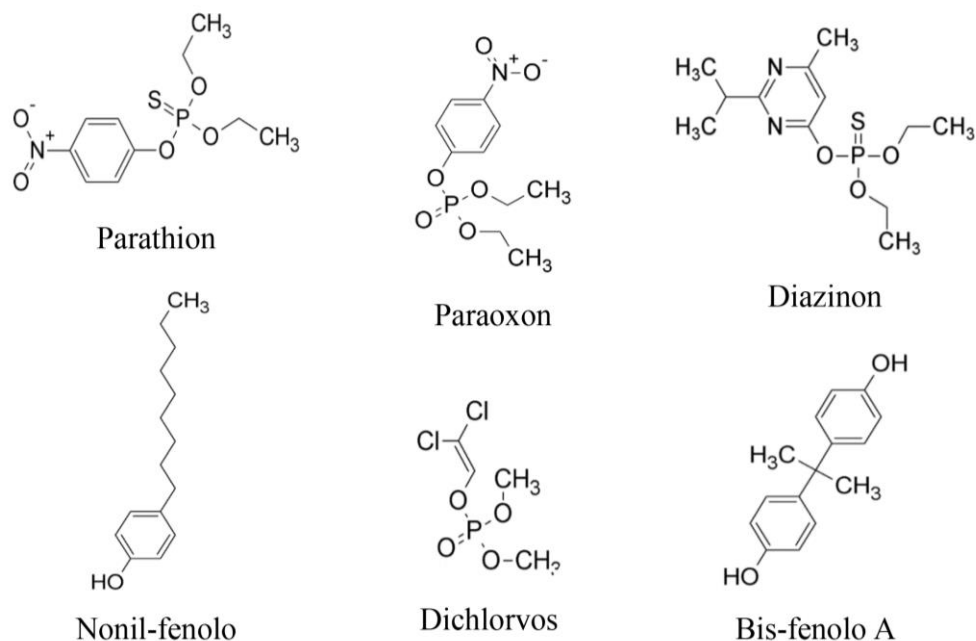
Figure 2.1. *Structures of the chemicals used for specificity tests.*

2.2 Immunoglobulin purification

A serum is the liquid phase separated from clotted blood by centrifugation. It has the same composition of blood plasma without clotting factors. Serum contains proteins (e.g. antibodies), electrolytes and various small molecules. The immunoglobulins were extracted using a Protein A Antibody Purification kit from Sigma-Aldrich. Protein A is a 42 kDa polypeptide found in the cell membrane of several strains of Staphylococcus aureus. This biomolecule has four high affinity ($K_a = 108 \ M^{-1}$) binding sites able to specifically bind the Fc portion of immunoglobulins of most mammals, such as rabbit. This Protein A-based affinity chromatography provides purified antibodies at physiological pH. The eluted fractions have been analysed by means of a UV spectrophotometer and SDS-PAGE. The purified antibody aliquots are stored at -20°C for later use.

2.3 QCM apparatus and fluidic setup

The QCM device used for this activity is a μLibra from Technobiochip, Italy. It is designed for 10 MHz quartz oscillators purchased from International Crystal Manufacturing (ICM), USA. The gold-quartz wafer, mounted in its support, is placed on the electronic console

of μLibra which is connected via USB cable to the computer. The oscillation frequency data are displayed and stored by a producer released software.

In order to analyse liquid samples, the QCM device has been integrated in a fluidic apparatus to convey the desired solution onto the sensor sensitive surface. One of the main issues in realizing microfluidic circuits for cells and biological material is the accumulation of aggregates which leads to channel obstructions causing leaks. To overcome this problem it is worth to use easily cleanable plastic materials which are treated to avoid the adhesion of biological molecules. For our experiments, platinum cured silicon pipes (070497) from Saint Gobain and Tygon tubes designed for biological samples have been used.

Since QCM devices are extremely sensitive to surface perturbation, it is worth control both density and pressure variations by using the same buffer solution for the various steps of the experiment and a peristaltic pump from Gilson to keep constant the flow rate of the circulating solution.

Another crucial issue concerns the accumulation of air bubbles in the cell containing the electrode which affects the measurement in two different ways. If the bubbles are big, they will be entrapped in the cell onto the gold plate, thus nullifying the experiment since the sensitive part of the sensor will not be exposed to the liquid sample to analyse. While big bubbles can be easily removed from the circuit by temporarily increasing the flow rate or gently hitting the cell, small bubbles result to be more problematic. These are usually blocked between the input channel and the gold electrode. Since these small bubbles are affected by peristalsis due to the pump, they start pulsating onto the sensor surface thus greatly perturbing the oscillation frequency of the QCM. The air bubble problem can be significantly reduced by placing before the cell a "bubble trap" like a syphon or a small connection pipe with inner diameter slightly bigger than the others.

Since the QCM technology is based on the quartz oscillation frequency, the device is placed on a polystyrene base to protect the oscillator from vibrations and hits from the bench.

Figure 2.2 shows the experimental setup. The tubes have 0.51 and 0.64 mm internal diameters for the input and output channel, respectively. The solution volume in contact with the electrode in the cell is about 30 μL. In view of all its components the total volume of the circuit is about 300 μL.
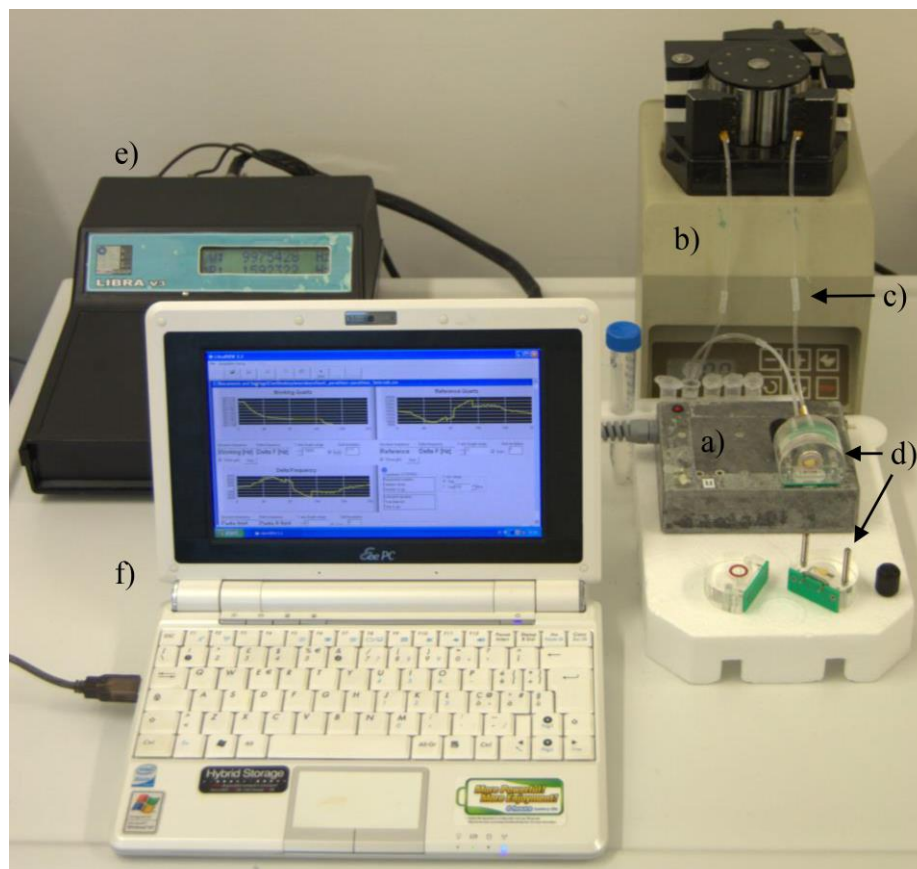
Figure 2.2. Experimental apparatus. a) electrode console; b) peristaltic pump; c) "bubble trap"; d) cell containing the electrode (a opened cell is shown under the console); e) frequency reader; f) computer for data acquisition.

2.4 Gold surface preparation

In view of its properties (i.e. high stability, low tendency to oxidize, biocompatibility) gold is the first choice for metallic sensitive surfaces of technologies like QCM or Surface Plasmon Resonance (SPR). In order to effectively immobilize biomolecules, the gold plates have to be cleaned using the so called "piranha solution". This extremely aggressive chemical treatment is commonly used in microfabrication laboratories to remove organic impurities from substrates, eliminate the photoresist in photolithographic processes and for surface hydroxylation. The traditional piranha solution is a 3:1 mixture of sulphuric acid (H_2SO_4) and 30% hydrogen peroxide (H_2O_2). Other protocols use a 4:1 or 7:1 ratio and eventually a more concentrated hydrogen peroxide solution. For our experiments the typical 3:1 ratio has been used.

Since it is both highly acidic and a strong oxidizing solution, piranha cleaning procedures have to be performed with extreme caution and using specific safety equipment (i.e. thick chemically resistant gloves, cotton based lab coat, etc.). In the fume hood, the hydrogen peroxide is slowly poured in a glass beaker containing the sulphuric acid. Since the solution is highly corrosive, plastic vessels or tweezers are avoided. The reaction is extremely exothermic and since the solution quickly reaches temperature up to 120°C it is used only after it cools down. The effectiveness of this procedure lies in two distinct processes. The first and faster is the dehydration due to sulphuric acid which leads to a cloudy solution. The second is related to the formation of atomic oxygen and radical species which oxidize and degrade the dehydrated organic compounds thus leading back the solution to its original clearness. The treated surfaces have to be quite clean and completely free of organic solvents from previous steps because a big amount of organic contaminants can cause violent bubbling or even explosion. The QCM oscillators are immerged by steel tweezers in the reactive solution for about 2 minutes, washed with Elix water and then left to dry in air. Finally, the quartz crystals are mounted on the support, being careful in avoiding contact between tweezers or gloves and gold surfaces. This chemical treatment allows to use the oscillators about 3-4 times making the quartz disks progressively more fragile to handle. It is worth highlight that each gold-quartz wafer allows to perform two QCM experiments, one for each face.

2.5   QCM experiment

A typical QCM output concerning a classic model system IgG-anti-IgG (antibodies which catch other antibodies) is shown in Figure 2.3.

The first step of the experiment is the reaching of the basal frequency stabilization by flowing 1x DPBS (Dulbecco's Phosphate Buffered Saline) solution at pH 7.4. DPBS is used as common buffer for all the phases to avoid frequency shifts due to different solution densities. Then the gold surface is functionalized using the biological sensitive element (i.e. antibodies). An immunoglobulin solution (50 µg/mL) is conveyed in the cell containing the electrode and the proteins are adsorbed onto the sensor surface thus resulting in the first frequency drop of about 300 Hz. When the oscillator reaches again the stabilization, the circuit is purged with PBS to remove the excess of immunoglobulins. Then a Bovine Serum Albumin (BSA) solution at 50 µg/mL is used to fill the remaining available space on the gold electrode thus preventing non-specific interaction between the sensor surface and the sample to analyse. It is worth highlight that the BSA blocking step results in a negligible perturbation of the resonance
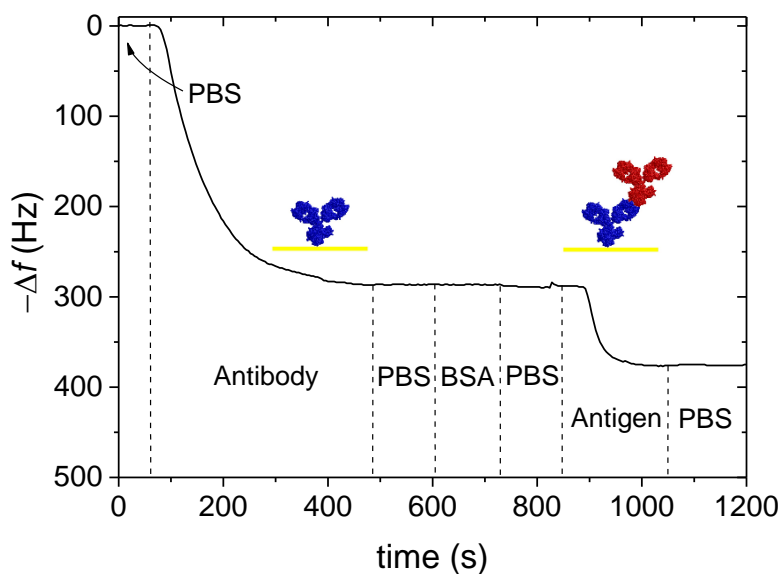
Figure 2.3. *Typical QCM output obtained using 50 µg/mL of anti-IgG and 10 µg/mL of mouse IgG. The vertical dashed lines show the steps described in the text. The antibody (anti-IgG) and the antigen (IgG) are sketched in blue and red, respectively.*

frequency of the QCM thus showing that gold surface is quite fully covered by immobilized immunoglobulins. After another washing step with PBS, the antigen solution (i.e. IgG at about 10 µg/mL) flows in the circuit. The antigen binding results in the second frequency shift of about 100 Hz. A final washing step is then used to remove weakly bonded analytes. All the QCM experiments have been performed in triplicate.

Since a QCM device is a mass sensitive tool, the bigger is the mass of the compound to be detected the larger is the frequency shift due its binding by immobilized antibodies thus resulting in a bigger sensor sensitivity. Therefore revealing small molecules using a QCM based biosensors is challenging. One of the objectives of this activity is developing strategies to detect light harmful molecules which will be shown in the next sections.

2.6   UV laser source

The QCM based immunosensors described in this thesis are realized using an effective functionalization procedure named Photonic Immobilization Technique (PIT)[88]. This strategy requires the activation of antibodies in solution through UV irradiation (the details of PIT will be explained in the next section). The UV light source used for these experiments is a PHAROS SP 1.5 laser system (Light Conversion Ltd). It is a femtosencond laser build upon the Chirped Pulse Amplification (CPA) technique using Yb:KGW (Ytterbium doped potassium gadolinium tungstate) lasing medium pumped by solid state diodes. This device provides ultrashort high

power pulses (of about 190 fs) with high tunable repetition rate, from single pulse to 200 kHz (eventually extendable to 1 MHz). Its maximum average power is about 6 W while the centre wavelength is 1028 nm ± 5 nm. The UV pulses are obtained coupling PHAROS with a harmonic generator stage (HIRO) which provides the conversion to 515 nm, 343 nm and 258 nm wavelength of the IR fundamental radiation. All the immunoglobulin samples have been irradiated in a quartz cuvette under mechanical stirring.

2.7   Atomic Force Microscopy (AFM) measurements

Goat anti-IgG antibody aliquots are irradiated by UV laser pulses delivered using the femtosecond laser described in the previous section. The UV source operates at a repetition rate of 10 kHz and 250 mW of average power at $\lambda = 258$ nm (resulting in energy per pulse of 25 μJ). Surface functionalization has been realized by incubating these samples with a metallic substrate for about 90 s.

AFM imaging is performed using a Nanoscope Multimode 8 (Bruker) microscope equipped with a 120 μm piezoelectric scanner and phosphorus doped Si cantilevers from Veeco (RTESPW). The samples for AFM analysis have been prepared by stripping a gold-Si wafer (80 nm Au) and functionalizing the metallic surfaces by using a custom glass and polydimethylsiloxane (PDMS) microfluidic apparatus. The PDMS (Sylgard® 184) has been prepared with a 1:10 w/w ratio between the curing agent and the prepolymer. The system consists of a PDMS layer (about 5 mm) attached to a glass ring covered with a PDMS thin film to confine the liquid onto the surface. The sample is loaded by using a tygon pipe connected to a 1 mL syringe. The volume of the chamber is about 40 μL while the whole circuit is about 100 μL. The fluidic apparatus is shown in Figure 2.4.

a)

b)

c)
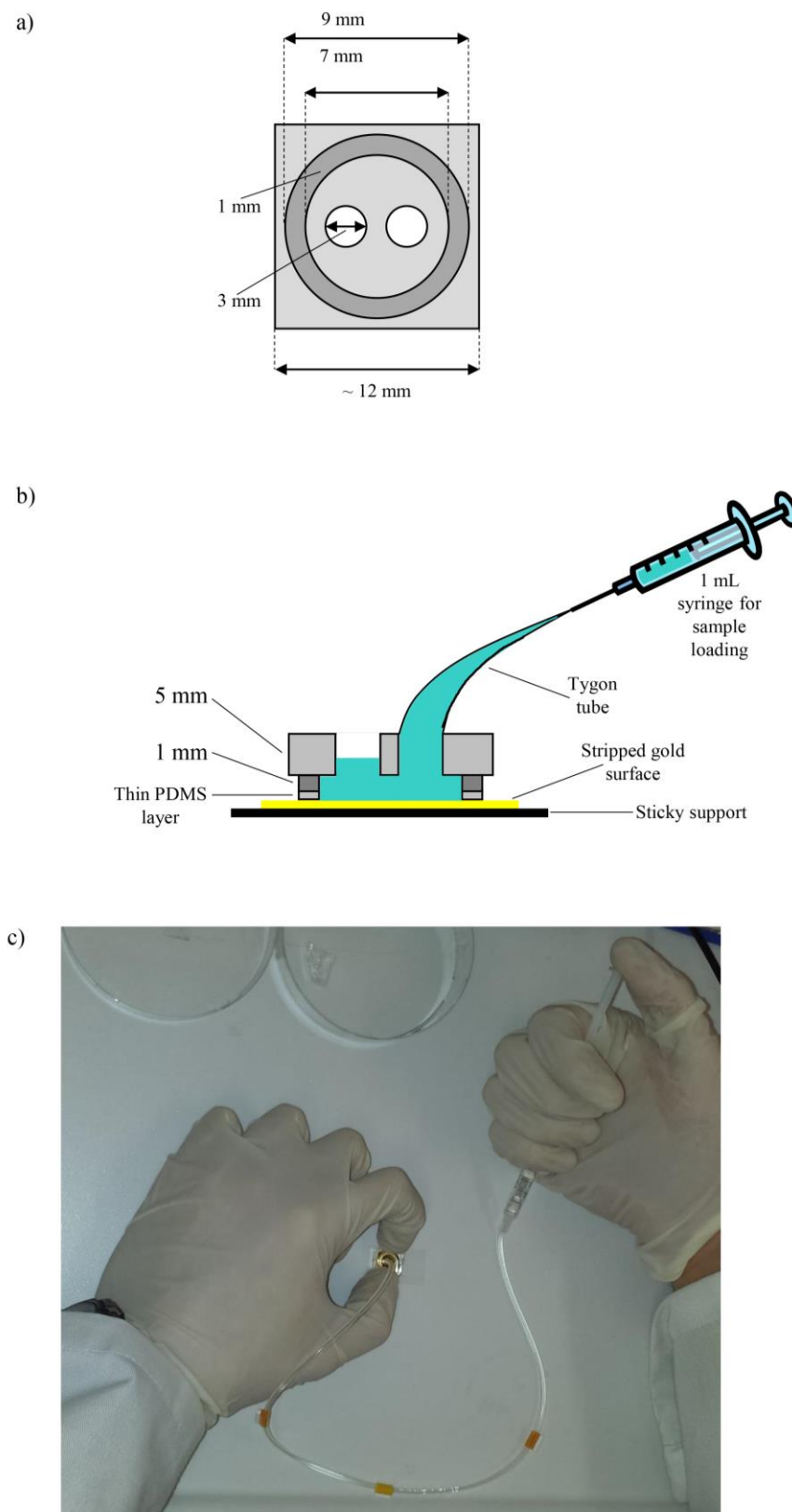
Figure 2.4. *a) Top and b) cross-section of the fluidic device used for preparing the samples for AFM analysis. In light and dark grey are highlighted the PDMS and glass elements, respectively. c) Picture showing sample preparation.*

3   Photonic Immobilization Technique (PIT)

3.1   Photonic activation of immunoglobulins: molecular mechanism

Photonic Immobilization Technique (PIT)[88] is a functionalization strategy based on the photoreduction of disulphide bridges in immunoglobulins upon UV illumination of closely spaced aromatic residues[89]. This light-induced reaction favours the proper orientation of the immobilized antibody thus improving the antigen catching. On the other side, it is well known that UV radiation affects both biomolecular structure and activity[24,45,90]. Therefore, it is of paramount importance finding the best agreement between effective antibodies immobilization and low protein damage (this issue will be discussed in the next sections).

Disulphide bonds (SS) are quite common in proteins since they have a crucial role in protein folding and stability. They are the result of the oxidation of thiol groups (-SH) of two cysteine residues thus connecting two portions of the molecule and biasing the protein folding. The analysis of the 3D structures deposited in the Protein Data Bank (PDB) shows that many proteins (e.g. immunoglobulins) have an aromatic sidechain (tryptophan, tyrosine or phenylalanine) placed nearby a disulphide bridge located in the core of the molecule[36]. The conservation of this feature suggests that the aromatic residue might play an important role in stabilizing or protecting the disulphide bond. In particular, immunoglobulin domains show highly conserved cysteine-cysteine/tryptophan (cys-cys/trp or C-C/W) triads. For instance, every type G immunoglobulin has twelve immunoglobulin domains, each of them containing a cys-cys/trp triad. The two cysteine residues are involved in the intra-chain disulphide bond which connects the two β-sheets of the domain. These amino acids are mostly constant in all the known Ig and Ig-like sequences while the tryptophan is also highly conserved in the core of the fold in proximity of the disulphide bridge. It is worth highlight that the geometric parameters of the triad (position of the atoms, angles and distances) are quite constant. The characteristics of this feature are shown in Figure 3.1.

The details of the photonic activation pathway have been recently reported[38]. The results of several papers concerning photophysics and photochemistry of tryptophan and cystine[90–93] are assembled in the scheme in Figure 3.2.
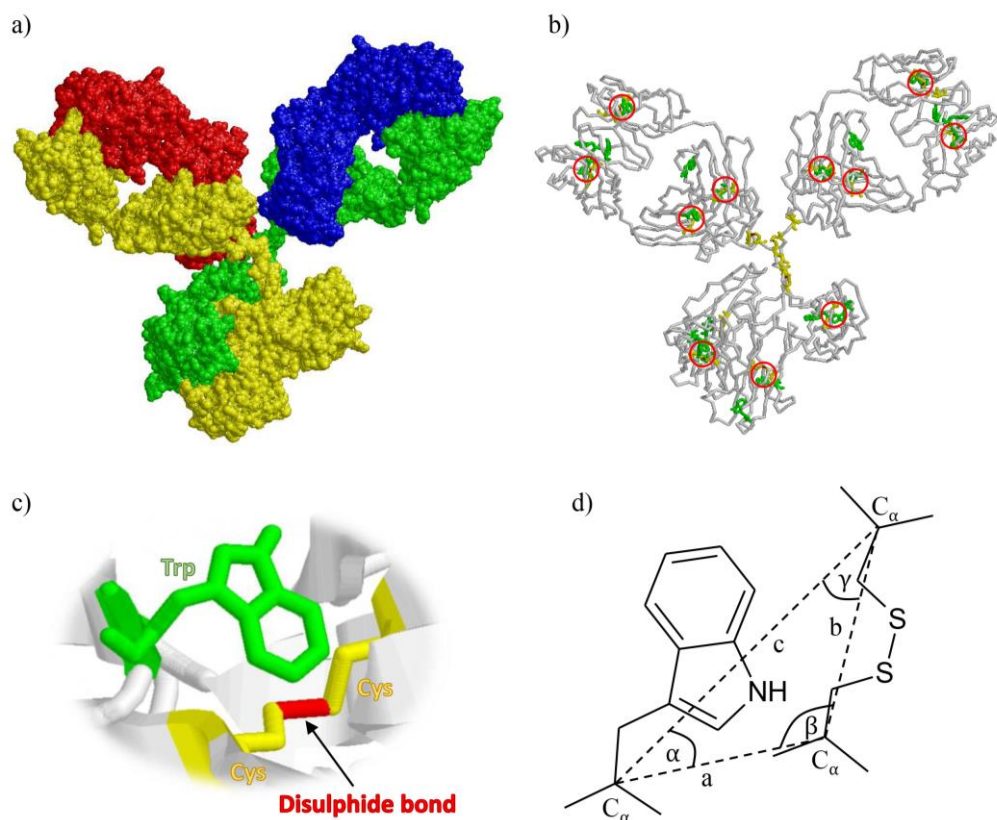
Figure 3.1. *a) 3D structure of the antibody (1IGY). b) On the same protein cysteine (yellow), tryptophan (green) and disulphide bridges (red) have been highlighted. Every immunoglobulin domain shows a closely spaced cys-cys/trp amino acidic triad (red circles). c) Magnification of one of these triads. d) Geometric characteristics of this structural feature. Both distances (a, b and c) and angles (α, β and γ) are highly conserved.*
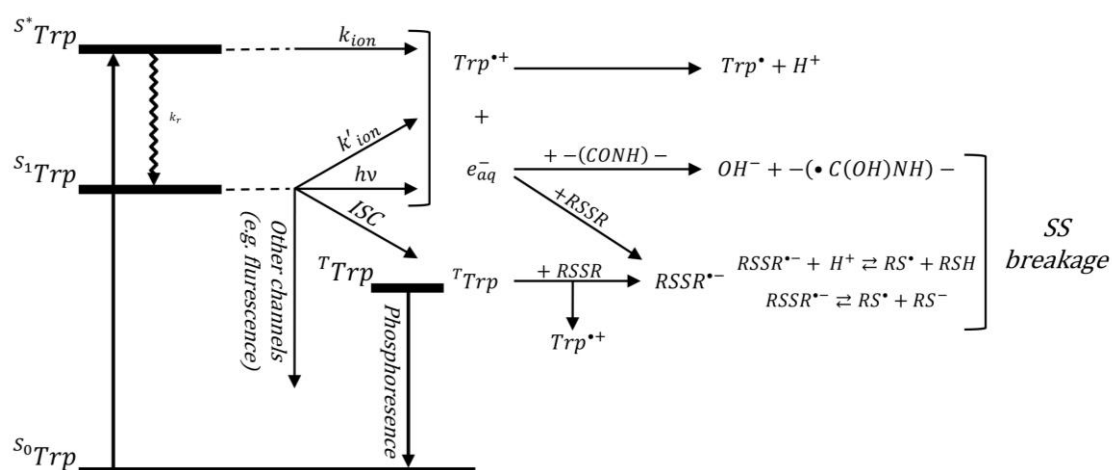
Figure 3.2. *Photophysical and photochemical pathways of tryptophan in proteins upon UV excitation.*

Bent and Hayon in 1975[91] described two non-radiative relaxation channels of the singlet excited states of tryptophan (S_1 and S^*). The first results in the formation of tryptophan radical cation ($Trp^{\bullet+}$), which rapidly deprotonates generating a neutral radical ($Trp^{\bullet}$), and solvated electrons (e^-_{aq}). These particles can easily react with electrophilic species like molecular oxygen, hydronium cations (at low pH), amidic bonds (forming ketyl radicals) or disulphide bridges ($RSSR$). The last event generates an unstable disulphide bond electron adduct ($RSSR^{\bullet-}$).

$$^{S^*}Trp \rightarrow Trp^{\bullet+} + e^-_{aq} \tag{3.1}$$

$$^{S_1}Trp \rightarrow Trp^{\bullet+} + e^-_{aq} \tag{3.2}$$

$$Trp^{\bullet+} \rightarrow Trp^{\bullet} + H^+ \tag{3.3}$$

$$RSSR + e^-_{aq} \rightarrow RSSR^{\bullet-} \tag{3.4}$$
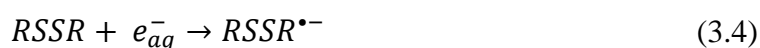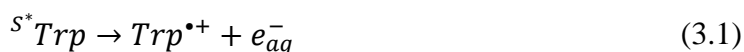
The latter channel involves the formation of a triplet-state tryptophan (^{T}Trp) from ^{S_1}Trp through intersystem crossing (ISC). ^{T}Trp can transfer an electron to nearby electrophilic species like disulphide bridges thus generating the electron adduct.

$$^{S_1}Trp \rightarrow {}^{T}Trp \tag{3.5}$$

$$^{T}Trp + RSSR \rightarrow Trp^{\bullet+} + RSSR^{\bullet-} \tag{3.6}$$

The intrinsic instability of the radical adduct can lead to the scission of the disulphide bond. This result is achieved also when the adduct is protonated.

$$RSSR^{\bullet-} \rightleftarrows RS^{\bullet} + RS^- \tag{3.7}$$

$$RSSR^{\bullet-} + H^+ \rightleftarrows RS^{\bullet} + RSH \tag{3.8}$$

The sketches in Figure 3.3 shows the steps of the photonic activation.

These free thiol radicals/groups can easily react with other thiols thus forming new disulphide bonds, or, alternatively, they can be exploited to achieve the oriented covalent protein immobilization onto thiol-reactive surfaces (e.g. gold plates) for biosensing applications[88,94,95]. Once immobilized, UV activated antibodies do not show any significant loss in the antigen binding efficiency and selectivity. On the other side, the rise of the number of the thiol groups onto the protein allows new structural conformation for the immobilized immunoglobulins, which are characterized by a proper exposure of the antigen binding sites thus greatly improving sensor sensitivity.
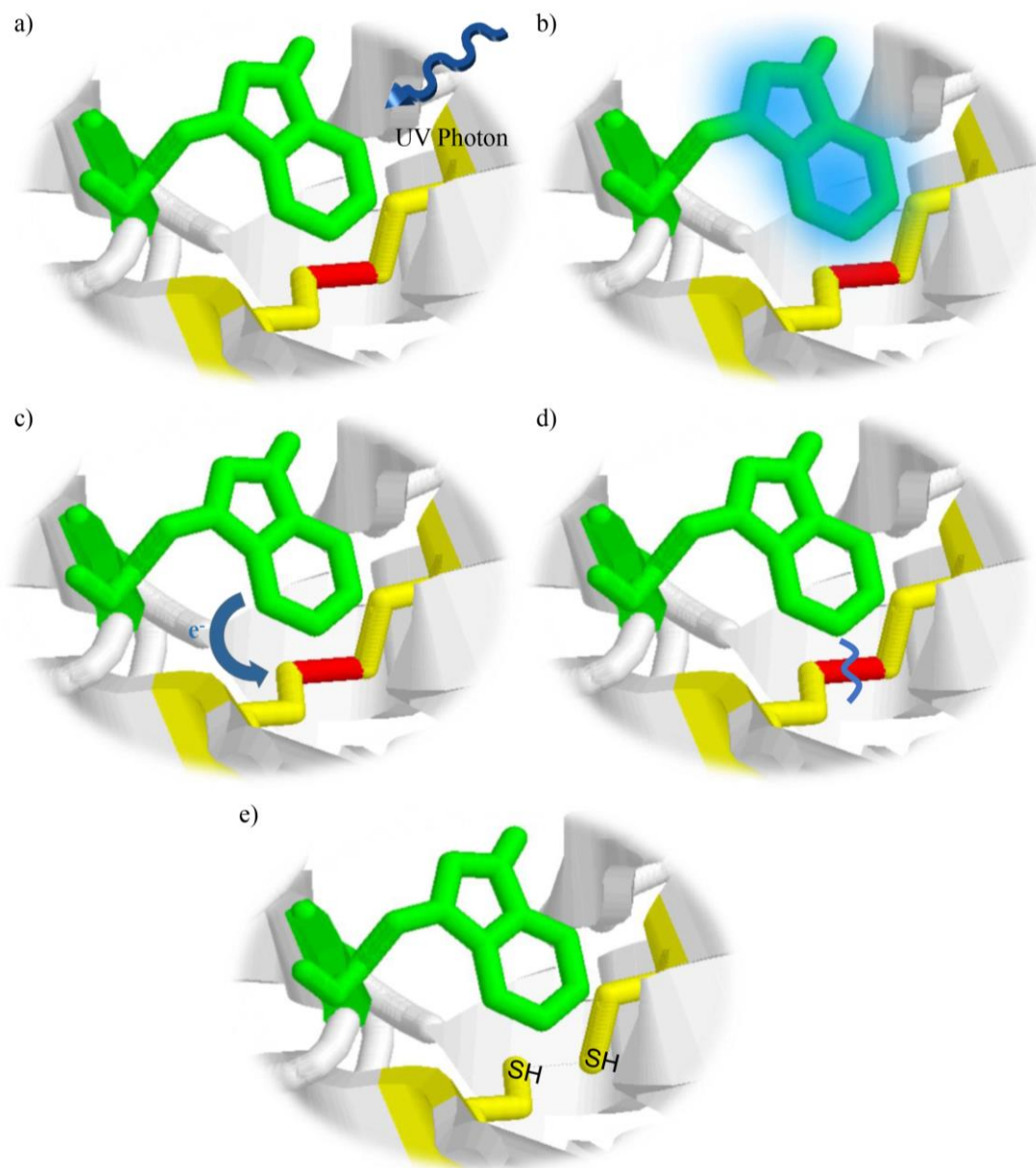
Figure 3.3. *Photoreduction mechanism. a) Protein irradiation; b) UV photon absorption; c) electron transfer; d) electron adduct formation and disulphide bond destabilization; e) breakage of the sulfur-sulfur bond.*

3.2   Revealing thiol groups in proteins: Ellman's assay

The so-called Ellman's assay is a chemical procedure first introduced in 1959 for estimating the number of thiol groups in proteins or peptides in aqueous media[96]. This strategy has been used to identify the irradiation conditions which maximize the thiol groups in immunoglobulin samples. The method is based on the reaction between the 5,5'-dithiobis-2-nitrobenzoic acid (also known as DTNB or Ellman's reagent) and a thiol group thus generating

a mixed disulphide and a 3-thio-6-nitrobenzoic acid (TNB), which rapidly deprotonates under mild basic conditions (pH 7-8) in TNB^{2-} thus giving an intense yellow colour.
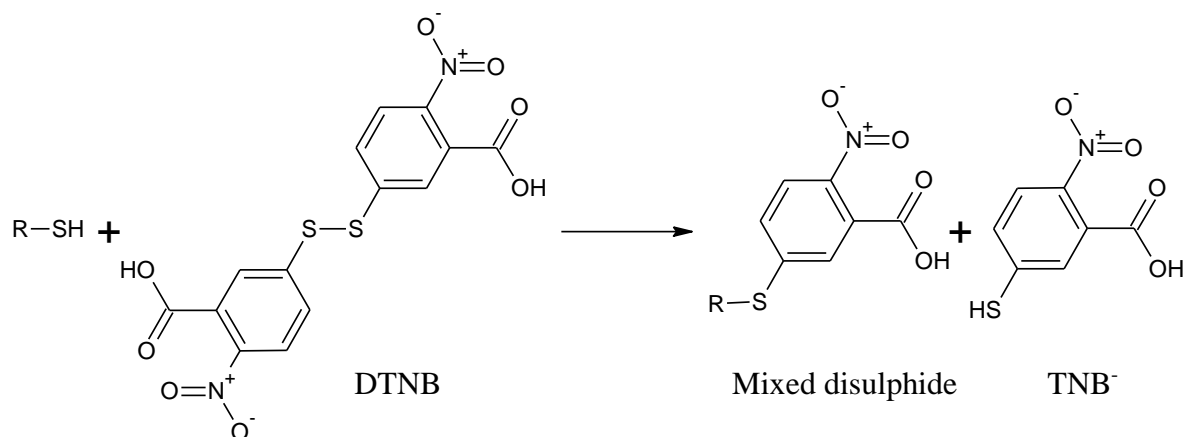
Figure 3.4. *The thiol group reacts with the Ellman's reagent (DTNB) giving a mixed disulphide and the TNB^{-} anion, which deprotonates to TNB^{2-} in water. Since TNB^{2-} absorbs at 412 nm, the measurement of the absorbance at that wavelength allows to quantify the -SH groups in the original sample.*

Since this anion has an absorption maximum at 412 nm, it is possible to quantify the reaction product (and the initial thiol groups) using a spectrophotometer. The molar extinction coefficient of the TNB^{2-} is affected by saline concentration and denaturing agents[97,98] (e.g. urea, guanidinium) ranging from 11400 to 14150 M^{-1} cm^{-1}. The latter value corresponds to assays performed in dilute saline solutions like 1x PBS. Alternatively, it is possible to compare the sample absorbance at 412 nm with a calibration curve obtained using free cysteine thus neglecting the TNB^{2-} extinction coefficient.

The experimental protocol consists of the following steps. The antibody sample (0.5 mL with a protein concentration of 50 μg/mL in 1x PBS) is irradiated with UV laser pulses at 258 nm, with a repetition rate of 10 kHz, provided by the PHAROS system. The exposure time and the average power change for each aliquot. The irradiation is performed in a q cuvette under mechanical stirring. Then the sample is recovered in a vial containing 0.5 mL of 2 mM DTNB (Sigma D8130) solution in 1x PBS buffer at pH 7.4. After 15 minutes of reaction time, the sample absorbance at 412 nm is measured.

A similar protocol has been applied by Della Ventura et al.[88] to measure the UV activation efficiency in goat IgG samples. Figure 3.5 shows the sample absorbance at 412 nm as function of irradiation time (a) and average laser power (b).
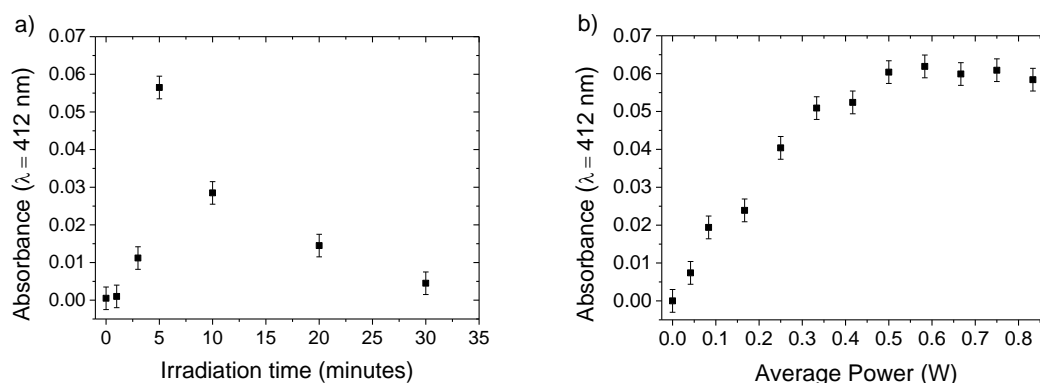
Figure 3.5. *a) Absorbance of antibody samples at 412 nm as a function of the irradiation time. The average laser power is 0.3 W. The DTNB is added immediately after the irradiation providing a quantification of the thiol groups. b) Absorbance of antibody samples at 412 nm as a function of the average laser power. The irradiation time is 5 minutes.*

The first plot shows an optimal irradiation time at about 5 minutes. The decrease in the activation efficiency can be explained by denaturation phenomena occurring after long time exposure to UV light. This issue has been studied using optical techniques[99] (i.e. absorbance and fluorescence) and will be discussed in the next section. On the other side, the increasing of the energy per pulse (i.e. the average power) leads to a saturation effect, thus suggesting that the photonic activation is a linear process (one photon process). It is worth highlighting that the Ellman's assay performed on antibodies from different species (e.g. goat, mouse, rabbit) gives similar results showing optimal irradiation times ranging from 1 to 5 minutes. These slight changes can be due to modifications in the amino acids surrounding the cys-cys/trp triad (different chemical environment).

3.3   Role of the UV source in the photonic activation

One of the main issues of technologies based on UV irradiation of biomolecules (e.g. antibodies) is that both molecular structure and biological activity can be severely affected. While protein activation can be studied using the Ellman's assay, structural changes and modifications of the biological activity have been investigated by means of optical techniques (e.g. absorbance and stationary fluorescence) and QCM based strategies[99].

The Ellman's assay performed on UV activated immunoglobulins shows that the rise of the number of thiol groups in proteins due to photonic activation results to be directly proportional to the intensity of the radiation delivered by the UV source. This linear behaviour entails that any source able to deliver the same energy dose to the sample, even conventional

UV lamps, should be equally efficient in triggering the photoreduction of the disulphide bridges.

The photonic activation of proteins was first performed using an UV lamp[89]. These light sources are quite cheap and widespread but, if compared with a laser, they provide low surface power density. In view of this property, the effective activation of a protein like the cutinase from *Fusarium solani pisi* is achieved only after about 5 hours of UV exposure (the number of thiol groups was estimated using the Ellman's assay). On the other side, laser-based photonic activation requires only a few minutes of irradiation[88]. The efficiency of the PIT-based functionalization using either nanosecond or femtosecond laser sources, delivering the same energy dose, has been studied my means of the Ellman's assay, QCM and optical techniques (i.e. absorbance and stationary fluorescence)[99]. The UV pulses are generated using the fourth harmonic of a Nd:YAG system (260 nm, 25 mJ/pulse, 5 ns, 10 Hz repetition rate) and a PHAROS system (258 nm, 25 µJ/pulse, 150 fs, 10 kHz repetition rate) for ns and fs pulses, respectively. These experiments involve antibodies against parathion, a harmful and toxic small molecule used as pesticide.

The maximum efficiency in antibody activation is achieved for both sources at about 60 s irradiation with an average power of 0.25 W. It is worth to highlight that the Ellman's assay data show that the number of free thiol groups generated by the fs activation is bigger than that for ns (see Figure 3.6).
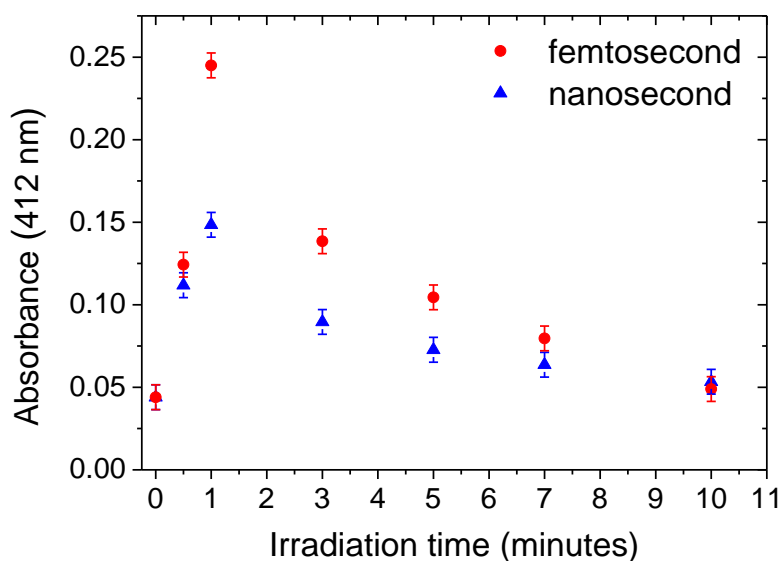
Figure 3.6. *Ellman's assay data for femtosencond (red circles) and nanosecond (blue triangles) irradiated antibody samples.*

Typical biosensor outputs for parathion detection are reported in Figure 3.7, where the QCM response using non-irradiated antibodies is compared to fs- and ns-PIT based sensors. The antibody aliquots (50 μg/mL) used for surface functionalization are irradiated for 1 minute with an average power of 0.25 W.
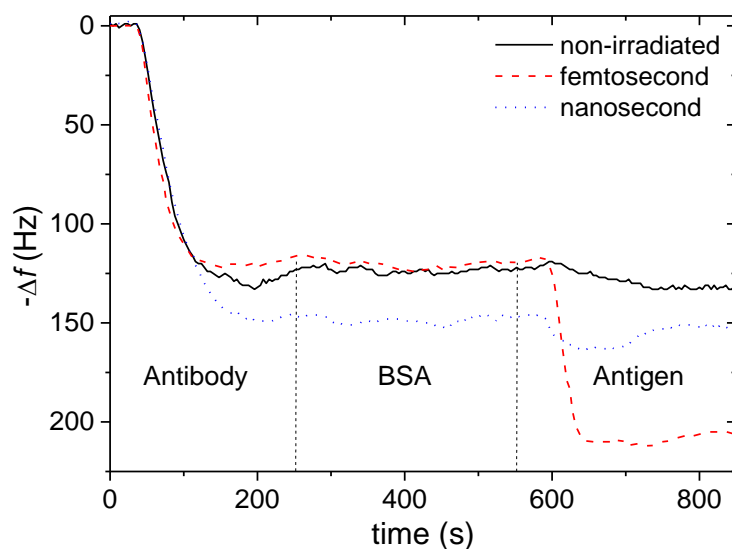
Figure 3.7. *QCM-based biosensor response for parathion detection in real time. Black solid line: no PIT is used. Red dashed line: femtosecond-based PIT is carried out. Blue dotted line: nanosecond-based PIT is used. The first drop between 0 and 150 s corresponds to the immobilization of antibodies onto the electrode and is poorly affected by PIT only with nanosecond irradiation, whereas the second drop at about 600 s is given by an antigen solution (parathion 1.5 μM) conveyed to the cell and is effective only when femtosecond-based PIT is carried on. The vertical dashed lines show the steps of the protocol described in the text.*

The issue of detecting light molecules using a microgravimetric device like a QCM has been faced by developing a one-step sandwich method. This strategy will be described in the next sections. The first drop in frequency (corresponding to the immobilization of the antibodies) is nearly the same in all conditions, being the ns irradiation shift slightly higher than the other two cases. This effect can be explained by molecular fragmentation induced by ns pulse irradiation, with the consequence of deposition of small antibody peptides with no active recognition function. The second frequency shift corresponds to the antigen biding by the immobilized immunoglobulins. This step shows that that QCM is effective in the analyte detection only when PIT is realized with fs UV pulses.

Structural modification in protein folding can be easily revealed by comparing absorption and fluorescence UV spectra of irradiated immunoglobulins with those of non-irradiated species. A typical UV absorption spectrum (recorded with a Jenway 6715 UV−visible

spectrophotometer) displays two peaks at 220 nm (ammidic bond) and about 280 nm (aromatic amino acids, particularly tryptophan). A clear peak at 280 nm usually indicates a well-folded protein. This is, indeed, the case of the curves obtained for non-irradiated samples shown in Figure 3.8, where the UV absorption spectra of the anti-parathion antibody samples are reported at several irradiation times for fs (a) and ns (b) laser irradiation. In both cases, the irradiation leads to a significant change in the protein spectrum with the consequent almost complete disappearance of the peak at 280 nm. This phenomenon requires much shorter irradiation times if the protein sample is irradiated using the ns rather than the fs laser source. It is worth noticing that after short irradiation times (18, 30 and 60 s), there is still a shoulder at 280 nm. Since antibodies are still able to bind the antigen in these conditions (as proven by the QCM experiments shown in Figure 3.7), spectral changes can be attributed to a structural modification which does not affect the recognition properties of the protein.

Stationary fluorescence is a rapid and low-cost method to investigate protein denaturation, folding and structural changes. It is based on the emissions of intrinsic protein probes (i.e. aromatic amino acids: tryptophan, phenylalanine, and tyrosine) which are strongly affected by changes in both chemical environment and protein structure[100]. Since the photonic activation of antibodies results in the breakage of the disulphide bonds placed nearby the tryptophan sidechain, the protein structure becomes less compact. This structural modification allows the penetration of water molecules in the core of the protein thus resulting in the red shifting of the fluorescence spectra. This behaviour is consistent with protein denaturation induced by either chaotropic agents or temperature rising. The emission spectra are acquired using a Perkin Elmer LS55 spectrofluorometer, the excitation wavelength being 278 nm. The fluorescence emission is mainly due to the tryptophan sidechain which strongly absorb at that wavelength. The stationary fluorescence of antibody samples as function of the irradiation time using either fs (c) or ns (d) laser source are reported in Figure 3.8.

UV irradiation leads to both protein activation and denaturation. At the optimal irradiation time for maximizing the sensor efficiency (60 s), the reduced emission can be related to a structural modification which does not entail a complete denaturation, the latter occurring only after several minutes of irradiation. These two phenomena can be easily observed in Figure 3.9 where the fluorescence signal integrated in the 320-370 nm range is reported.
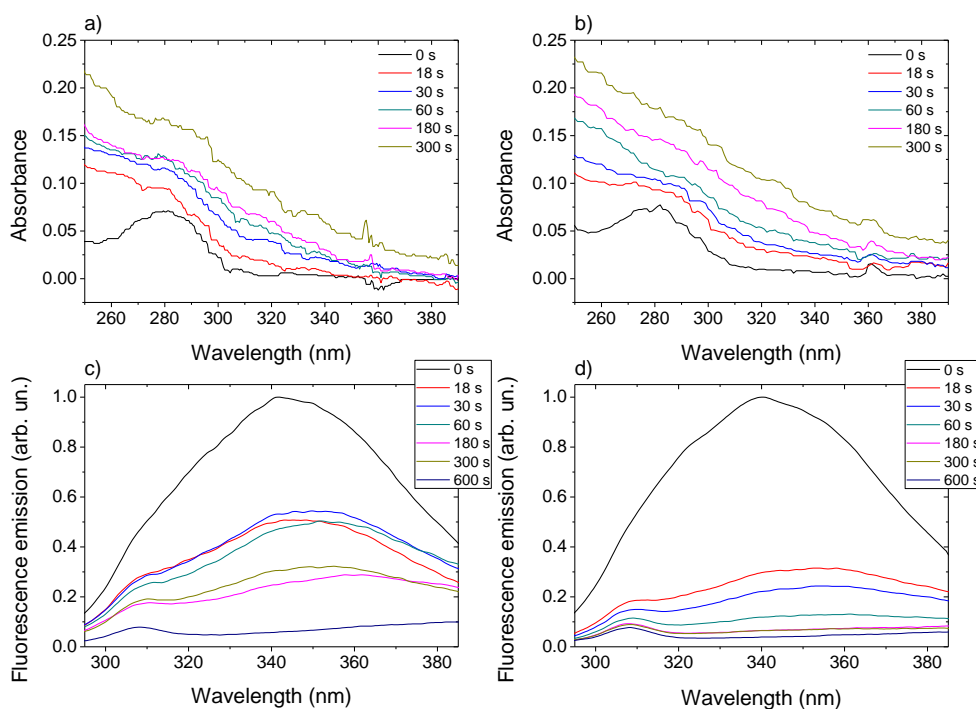
Figure 3.8. *UV Absorption spectra of anti-parathion solutions for a) fs and b) ns UV pulse treatment at various irradiation times. The antibody concentration is 50 µg/mL. The irradiation conditions are 25 µJ/pulse, 10 kHz repetition rate for the fs system and 25 mJ/pulse, 10 Hz for the ns source. In this way, the same UV dose is delivered to the target in both cases in correspondence to the same irradiation time. UV Fluorescence spectra of anti-parathion samples for c) fs and d) ns UV pulse activation at various irradiation times. The excitation wavelength is 278 nm. Experimental parameters concerning antibody concentration and laser irradiation are the same as for a) and b).*
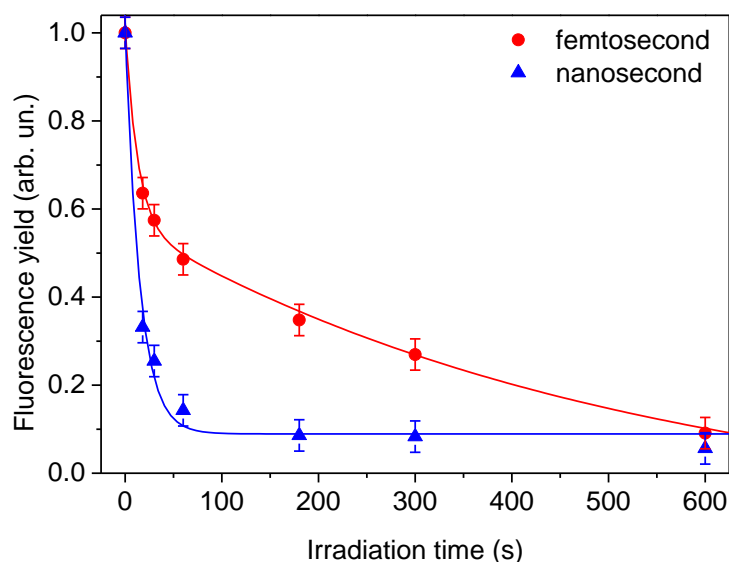
Figure 3.9. *Integrated fluorescence emission in the 320-370 nm spectral window for anti-parathion activated with fs (red circles) and ns (blue triangles) pulses versus the UV laser irradiation time. Red solid line: best fit using a double exponential model for fs ($A_1 = 0.44 \pm 0.03$; $t_1 = 13 \pm 2$; $A_2 = 0.7 \pm 0.1$; $t_2 = 512 \pm 172$; $y_0 = -0.1 \pm 0.1$). Blue solid line: best fit using a single exponential model for ns ($A = 0.91 \pm 0.04$; $t = 15 \pm 2$; $y_0 = -0.09 \pm 0.02$).*

If the protein sample is activated using femtosecond laser pulses, there is a rapid variation in fluorescence emission related to protein activation and a subsequent decrease due to denaturation. This difference is not so evident if the antibodies are irradiated using much more energetic UV pulses. Nanosecond irradiated antibodies show a more rapid drop in fluorescence emission due to denaturation phenomena and protein damage induced by thermal coupling. The solid lines in Figure 3.9 are the result of best fits of the experimental data using a biexponential decay for femtosecond and a single exponential function for nanosecond outputs. All these differences suggest that femtosecond based PIT provides the best compromise between protein activation and denaturation.

3.4   Imaging proteins on nanometric scale: Atomic Force Microscopy (AFM)

Since both the number and the orientation of the immobilized antibodies are strictly related to the sensor sensitivity, it is crucial have investigation techniques providing high-resolution information about the immunoglobulin layer. This issue is commonly faced by simply verifying the antigen capturing efficiency of the immobilized antibodies. If the biomolecules are well oriented onto the sensor surface (i.e. with their sensitive portion well exposed to the environment), the device will be able to efficiently detect the analyte. It is worth mentioning that a wide range of techniques, including optical methods and QCM[101,102], is available for this purpose. Anyway, only minimal direct information about protein orientation can be deduced with such approaches.

Trilling et al.[103] have recently reported a selection of modern approaches for characterizing the orientation of immobilized antibodies in a more direct and effective way. They focused on Atomic Force Microscopy (AFM), Time-of-Flight Secondary Ion Mass Spectrometry (ToF-SIMS), Neutron Reflectometry (NR) and Spectroscopic Ellipsometry (SE). In particular, AFM results to be one of the most promising characterization strategies since this it is very effective in analysing nano-sized objects like proteins.

Concerning photonic immobilization technique, although there is a clear evidence that UV light is able to orient antibodies on a gold surface, there is still a lack of direct demonstration based on the imaging of the functionalized surface. The tethering of antibodies on gold surface has been investigated by imaging the stripped gold surfaces using tapping mode AFM. This

activity has been realized in collaboration with the Bioelectronics group (ICS8/PGI8) of the Institute of Complex System and Peter-Grünberg-Institute (Forschungszentrum Jülich GmbH).

Tapping mode AFM has been already used to image globular Y-shaped proteins like antibodies on mica surfaces[104] finding that it is possible distinguish between different protein morphologies. Immobilized immunoglobulins can adopt four molecular orientations: side-on (one Fc and one Fab in contact with the surface), tail-on or side-up (Fc onto the surface), head-on (both Fabs attached onto the surface) and flat-on (all three portions connected to the surface). In order to achieve the best binding efficiency, antibodies should show the antigen-binding regions after immobilization. Therefore, the side-up morphology is the one which better recognizes the antigen. These four morphologies have been found in a first stripped gold sample functionalized with non-irradiated antibodies. This experimental result and the sketches of the possible orientations of the immobilized immunoglobulins are shown in Figure 3.10.

It is worth mentioning that the height of the imaged proteins is significantly different from the results obtained using X-ray crystallography[40]. In particular, the measured height of nanoscale protein features in the atomic force microscopy is often smaller than the true value (the loss in height ranges between 10 and 90%). This effect is commonly attributed to sample deformation[105], accumulation of salt deposits on support surfaces[106] or dehydration[107]. More recently, Santos et al.[108], who worked on both double strand DNA and antibodies, showed that also the geometry of the tip-surface/sample interaction area could affect the imaging of the biomolecule. As a consequence of this artefact, the height information is spread-out laterally across the tip-sample interaction area thus resulting in broader features. Anyway, as shown in Figure 4.10, the four morphologies assumed by immobilized antibodies are still recognizable.

In a preliminary attempt to image UV-activated antibodies on gold, we used tapping mode AFM on stripped gold samples functionalized using irradiated (Figure 3.11a) and non-irradiated (Figure 3.11b) protein sample. In both panels of Figure 3.11, the blue and red circles highlight "side-up" and "flat-on" antibodies, respectively.

This analysis suggests that PIT enhances the "side-up" conformation thus leading to a more effective antigen detection. Nevertheless, a careful image analysis, which would help in the recognition of all the possible antibodies orientations, coupled with a systematic study carried out as a function of surface coverage is required in order to clarify the effects of PIT.
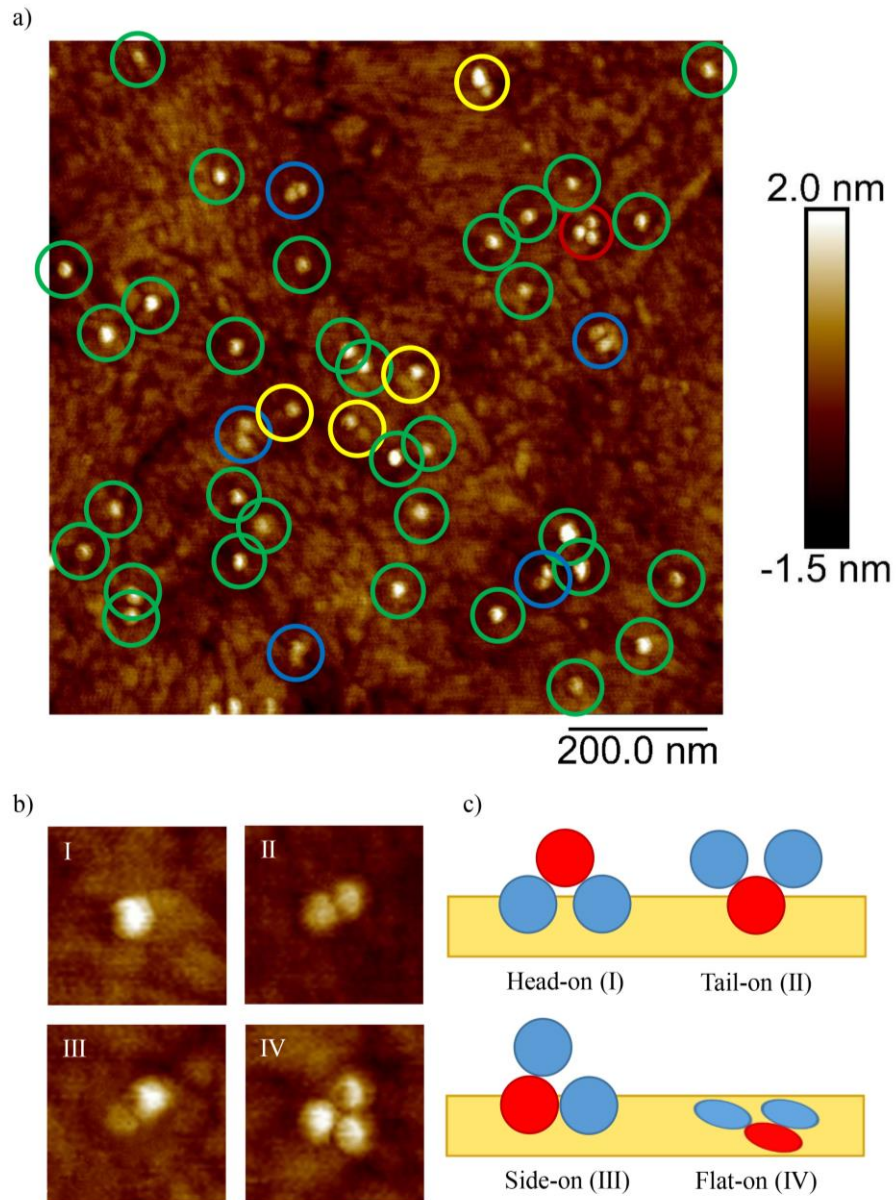
Figure 3.10 *a) Tapping-mode AFM image of antibodies on stripped gold surface. The proteins show several morphologies according to the orientation to the support. b) Characteristic morphologies of immobilized antibodies. c) Schematic representation of the four possible morphologies. Key: I – "head-on"; II – "side-up"; III – "side-on"; IV – "flat-on".*
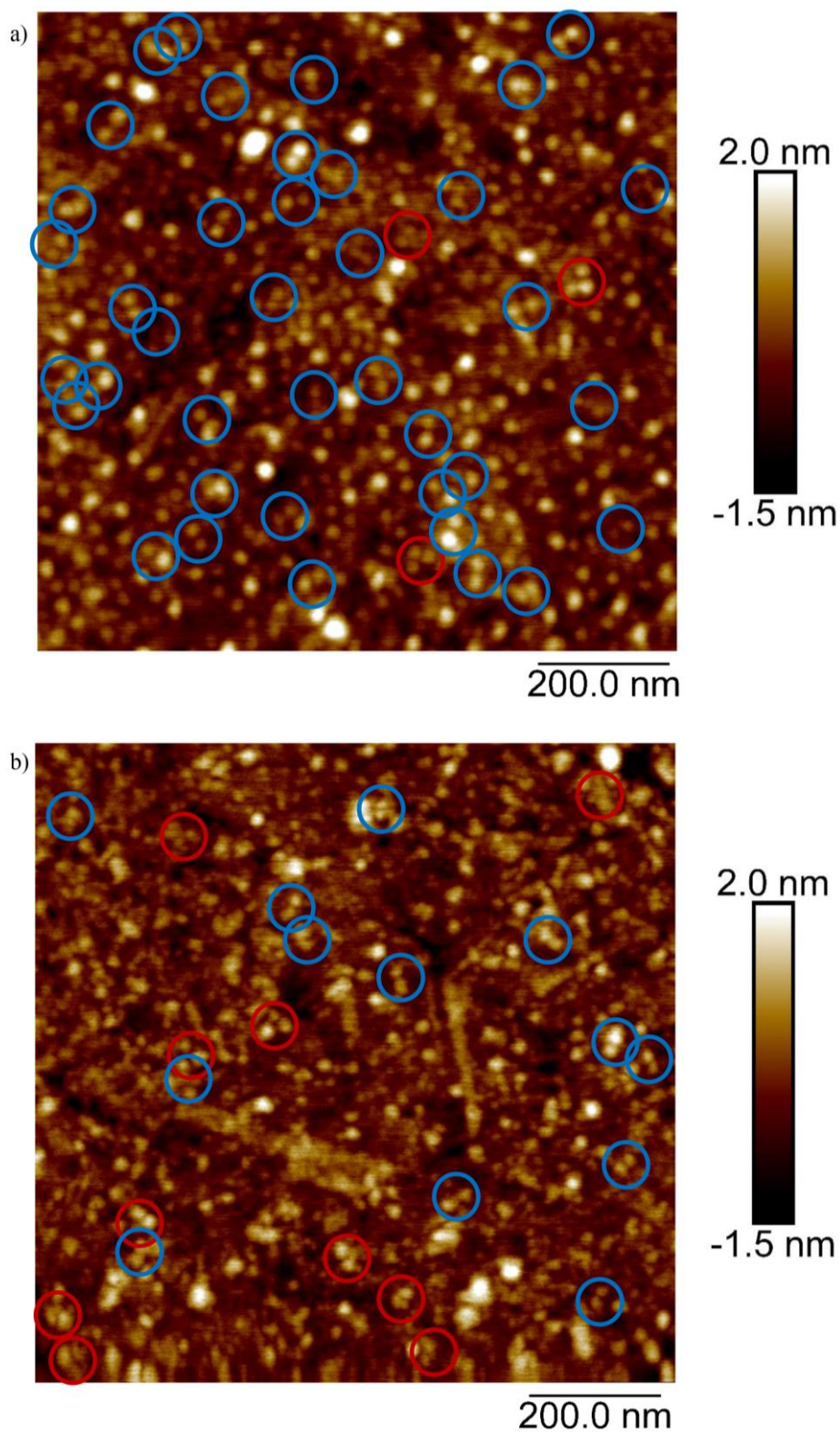
Figure 3.11 AFM images for (a) irradiated and (b) non-irradiated samples where the "side-up" and "flat-on" antibodies are highlighted (blue and red circles, respectively). The substrate is stripped gold while the protein concentration is 0.5 μg/mL.

4   Applications of PIT

4.1   A case study: IgG and anti-IgG

In order to investigate the efficiency of PIT in functionalizing surfaces, Della Ventura et al.[88] realized a QCM based biosensor on the model antigen-antibody system IgG-anti-IgG (i.e. an antibody which catches another antibody). This scheme is quite common in immunoassays since it is used to amplify the signal due to antigen binding[109]. The "antibody" is an anti-IgG produced in goat while the "antigen" is a murine IgG. The irradiation conditions ($\lambda = 258$ nm) resulting from the Ellman's assay are: 10 kHz repetition rate, 5 minutes irradiation time and 0.3 W average power (30 µJ/pulse). The protein concentration used for surface functionalization is 50 µg/mL.

The QCM responses versus time for both irradiated and non-irradiated (control) immobilized antibodies are reported in Figure 4.1.
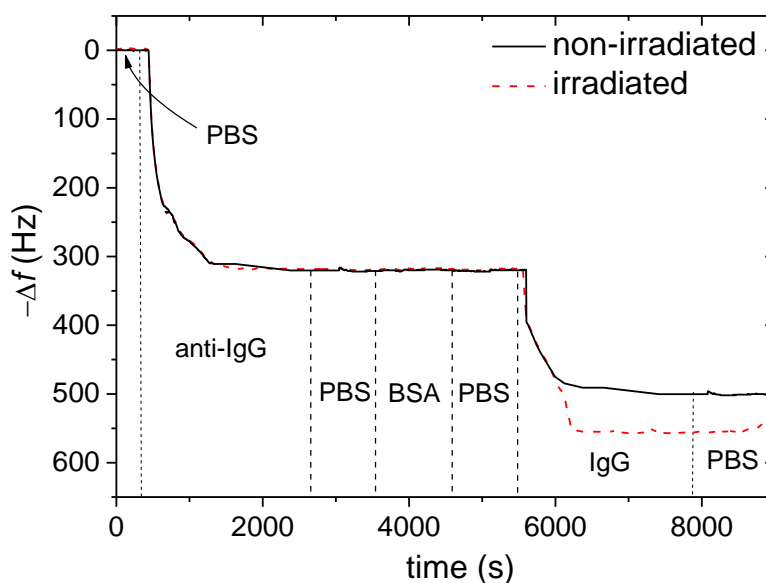
Figure 4.1. *QCM outputs obtained with 50 µg/mL of anti-IgG and 50 µg/mL of mouse IgG of non-irradiated (black solid line) and irradiated antibody (red dashed line). The vertical dashed lines show the steps described in the text.*

The comparison between the two curves (the solid and dashed lines correspond to the non-irradiated and irradiated samples, respectively) shows that the amount of tethered antibody (first drop in frequency of about 320 Hz) is mostly the same in both conditions. On the other side, since the photonic activation leads to a more effective orientation of the immobilized antibodies, the detection of the antigen results to be more efficient for irradiated

immunoglobulins (second drop in frequency). The frequency shifts due to analyte binding as function of the antigen concentration for PIT based (red circles) and control (black squares) sensors are shown in Figure 4.2.
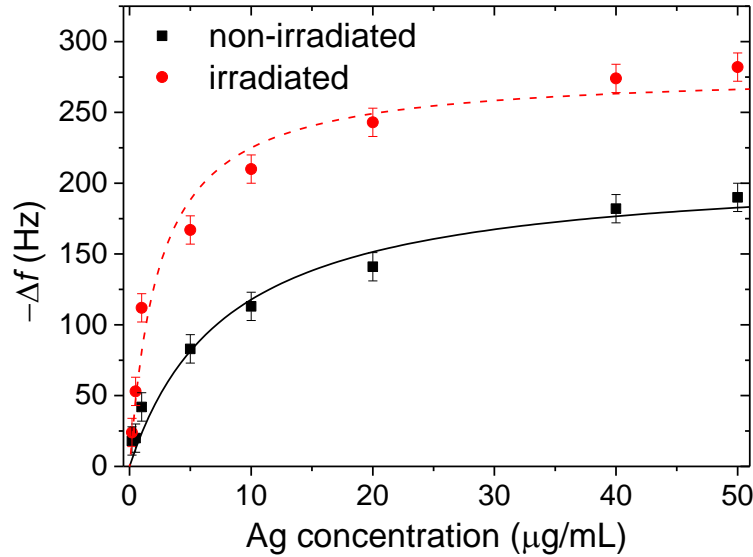
Figure 4.2. *Frequency shifts observed with irradiated (red circles) and not-irradiated (black squares) antibody solutions as function of the antigen concentration. The best fit obtained with Equation 4.1 provides $(\Delta f)_{sat} = 212 \pm 14$ Hz, $k_M = 8 \pm 2$ µg/mL and $(\Delta f)_{sat} = 279 \pm 13$ Hz, $k_M = 2.4 \pm 0.6$ µg/mL for the irradiated and non-irradiated anti-IgG samples, respectively.*

This behaviour has been fitted by using a Michaelis-Menten type equation, a mathematical model commonly used to describe a wide range of biochemical reactions, enzymatic kinetics and antigen-antibody binding events[110]:

$$\Delta f(Ag) = \frac{(\Delta f)_{sat} Ag}{K_M + Ag} \qquad (4.1)$$

where Ag is the antigen concentration, $(\Delta f)_{sat}$ contains the instrument response and K_M is the so-called Michaelis-Menten constant. $(\Delta f)_{sat}$ is the maximum frequency shift achieved by the system at saturating antigen concentration, while K_M is the antigen concentration at which the sensor response is half of its maximum. This parameter is an inverse measure of the affinity of the antibody for the antigen. The rise in both slope and saturation level observed when PIT is applied is attributed to the better exposure of the antigen binding sites. This effect increases the capture probability thus making the immobilized antibodies more efficient in binding the antigen and affecting both $(\Delta f)_{sat}$ and K_M. The decrease of K_M (i.e. the increase of the apparent affinity of the immobilized immunoglobulins) results in the rise of the slope. On the other side, a more correct orientation of the immunoglobulins increases the number of the available

binding sites thus leading to larger saturation value. These effects result in a significant improvement in sensing efficiency thus making PIT a valid alternative to conventional and time-consuming immobilization procedures.

4.2   Parathion

The high toxicity of organophosphorus pesticides and their bioaccumulation effects in human body underpins the research for fast response detection tools with high sensitivity and specificity for these harmful molecules. Parathion is an example of this class of chemicals which has been used as target analyte to develop a QCM-based immunosensor exploiting the PIT functionalization procedure. The main drawback of a mass-based transducer like QCM in detecting light molecules like parathion (291.26 Da) is the small frequency shift associated with their binding by the immobilized antibodies. This issue has been faced by increasing the mass of the analyte in two different ways. The first involves the complex formation between parathion and Bovine Serum Albumin (BSA). This big protein results to be able to absorb small molecules through nonspecific interactions[94]. The second mimics the sandwich configuration widely used in the ELISA assay where the antibody itself is used to increase the mass of the antigen[95].

4.2.1 "BSA protocol"

Antibody aliquots of 1 mL containing 5 μg of anti-parathion polyclonal antibody have been irradiated by means of the femtosecond laser system previously described. The laser source operates, in this case, at a pulse repetition rate of 10 kHz and delivers 250 mW of average power at $\lambda = 258$ nm (resulting in energy per pulse of 25 μJ) for 5 minutes. The fluidic setup is designed so that the whole replacement of the solution volume above the electrode takes about 80 s with a flow rate of 3.3 μL/s. This was tested by measuring the time required by a buffer solution to remove completely a coloured sample (flavin adenine dinucleotide) from the cell.

The experimental procedure consists of the following steps. The basal frequency stabilization is achieved by flowing 1x PBS pH 7.4. Then the sensor surface is functionalized using UV-assisted adsorption or passive adsorption of anti-parathion polyclonal antibodies. The remaining free gold areas are blocked by using a BSA solution (50 μg/mL) to avoid non-specific interactions between the antigen and the electrode. The parathion sample in then conveyed in the microfluidic circuit. The permanence of BSA above the gold surface entails that this protein is still present when the parathion reaches the cell, so that the complex between the protein and

the analyte is formed as a consequence of unspecific interactions. The immobilized antibodies recognize the parathion-BSA complexes. A final washing step with PBS 1x is then used to eliminate weakly bonded analytes. The antigen binding is sketched in Figure 4.3 where the BSA and the analyte are represented as big green and small orange spheres, respectively.
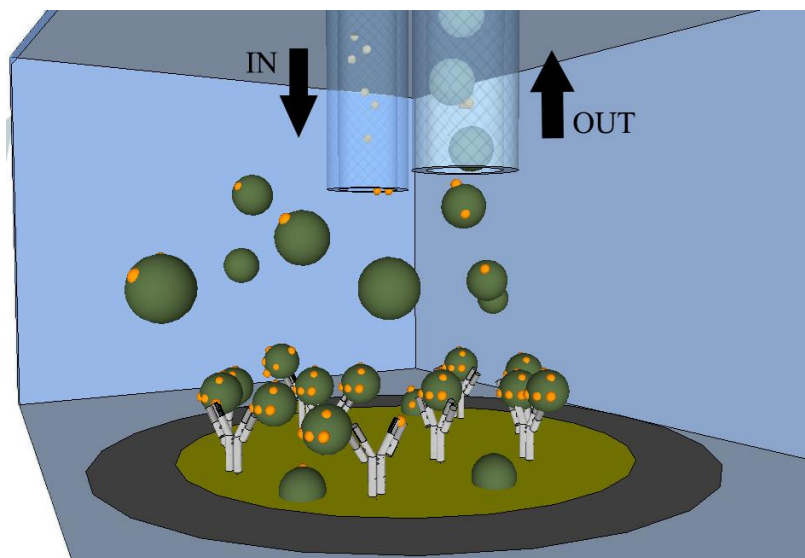
Figure 4.3. *Antigen binding on the functionalized gold electrode. The big green spheres are the BSA macromolecules which are complexed with the smaller antigens (orange spheres). The model is not in scale.*

Figure 4.4 shows typical QCM outputs obtained when the antibodies are irradiated (red dashed line) and non-irradiated (black continuous line).
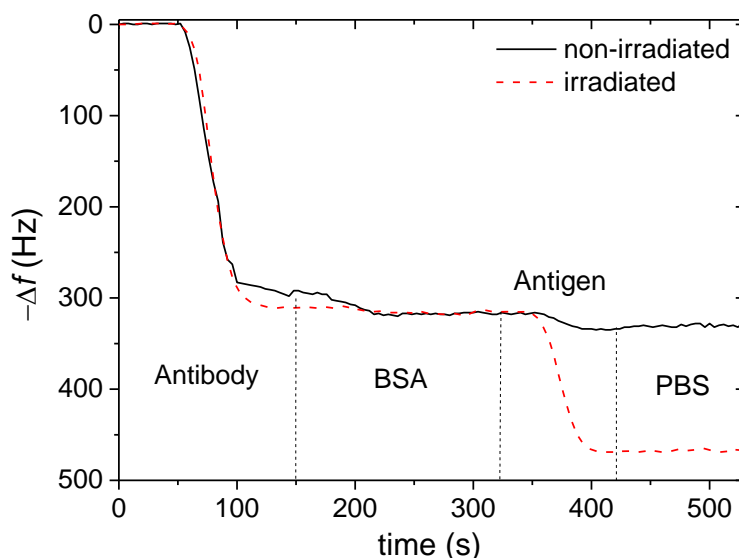
Figure 4.4. *QCM responses of irradiated (red dashed) and non-irradiated (black solid line) antibody samples having a protein concentration of 5 μg/mL. The first drop at ~50 s corresponds to the antibodies tethered to the electrode and is not affected by PIT, whereas the second drop at ~350 s is given by an antigen solution (parathion 51.5 μM) conveyed to the cell and is much larger when PIT is used. The vertical dashed lines show the steps described in the text.*

It is important noticing that the first drop in frequency ($\sim$300 Hz) is essentially the same in both conditions (irradiated and non-irradiated) so that it is reasonable assuming that PIT does not change the amount of antibody tethered to the electrode. This phenomenon is in fair agreement with the surface density measurements reported by Peluso et al.[111] who studied the effects of protein orientation on both whole immunoglobulins and Fab' fragments, finding comparable surface densities between oriented and random aligned antibodies. Then, during the blocking phase of the experiment, the crystal oscillation frequency keeps constant (see the signal in the interval 150-330 s) thus suggesting that gold surface is most completely covered by immobilized antibodies. Then, when the analyte sample is conveyed to the electrode, a much larger frequency shift due to the antigen binding is achieved when PIT is applied (second drop in frequency). Such a difference is kept even when the electrode is washed by means of PBS. The improvement in the detection of parathion is attributed to the more effective orientation of UV-activated antibodies.

When the parathion sample reaches the volume above the electrode, the BSA solution is still there thereby allowing the complex formation. The BSA molecules ($\sim$66 kDa) bind the organophosphate compound by means of unspecific interactions thus making the analyte "heavier" and detectable by a microbalance. In fact, even if all the antibodies on the electrode bound one parathion molecule (291.26 Da), the frequency shift would be only few hertz and, thus, not detectable by the QCM device. This has been verified by washing the fluidic circuit, thus removing the BSA, and checking that the parathion is not detectable any more, even if PIT is used. It is worth mentioning that the complex formation between parathion and BSA has been investigated by measuring the protein fluorescence spectrum (λ_{ex} = 278 nm) thus observing a strong reduction of the yield as a function of the parathion concentration (Figure 4.5). This quenching effect of parathion on BSA fluorescence emission shows the interaction between these two partners. A similar behaviour has been observed also for other pollutants incubated with the BSA.

Since the response of the QCM is related to the mass tethered to the electrode, the second drop in frequency $\Delta f\,(P)$, P being the concentration of parathion, is a measure of the amount of analyte caught by the immobilized antibodies. The responses of QCM devices functionalized using irradiated (PIT) and non-irradiated antibodies have been compared obtaining the results shown in Figure 4.6.
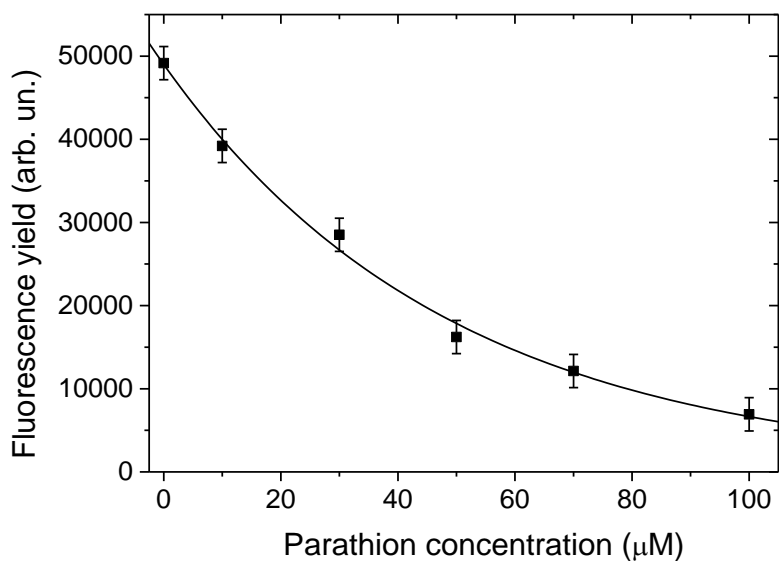
Figure 4.5. *Fluorescence yield of BSA versus parathion concentration. The area of the BSA fluorescence spectra in the range 335-350 nm is reported versus the concentration of the pollutant added to the BSA sample.*
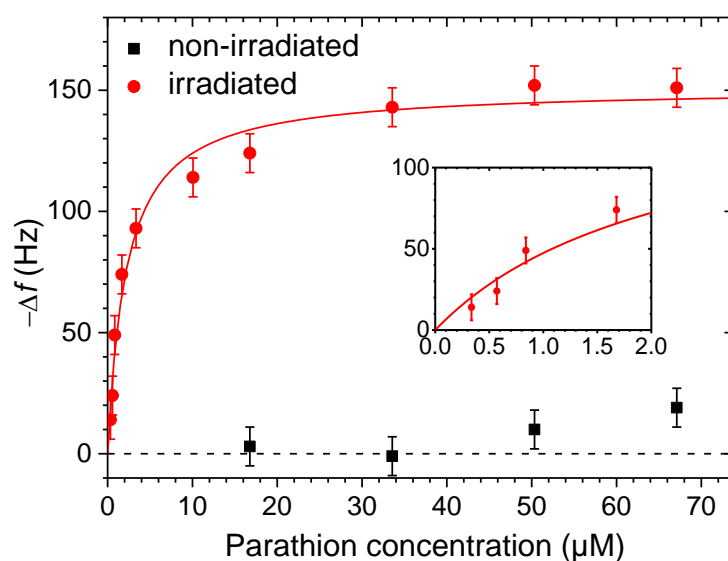
Figure 4.6. *QCM response versus the parathion concentration with irradiated (circles) and not-irradiated (squares) antibodies. The experimental points obtained with the irradiated antibody are fitted by a Michaelis−Menten type equation (black solid line). The small frequency shift achieved when the antibody is not irradiated does not allow any significant fit of the experimental data. The inset is the enlargement of the low concentration region.*

It is evident that no significant signal is measured at a parathion concentration lower than 50 μM (about 15 μg/mL) when the antibodies are not irradiated (black squares). On the other side, the signal is already in the saturation region if PIT is used (red circles).

By considering the law of mass action and given the free diffusion conditions of this experiment, the analysis of the interaction kinetic between the analyte and the antibody leads to a Michaelis-Menten type equation[110]:

$$\Delta f(P) = \frac{(\Delta f)_{sat} P}{K_M + P} \qquad (4.2)$$

The best fitting of the experimental results obtained with UV-activated antibodies by Equation 4.2 (solid line in Figure 4.6) provides $(\Delta f)_{sat} = 151 \pm 5$ Hz and $K_M = 2.2 \pm 0.7$ μM. The uncertainty in the measurements is due to instrumental limitations of the QCM device, as well as to random fluctuations in some steps of the detection procedure. In view of these restrictions, a conservative frequency error of 15 Hz has been considered. Therefore, a minimum frequency change $(\Delta f)_{min}$ of 15 Hz is required to consider a measurement different from zero. An estimation of the LOD has been obtained by inverting Equation 4.2:

$$LOD \approx \frac{(\Delta f)_{min} K_M}{(\Delta f)_{sat}} \approx 200\ nM \approx 60\ ng/mL \qquad (4.3)$$

The striking difference shown in Figure 4.6 allows to estimate an increase in the sensitivity of at least 1 order of magnitude when PIT is used. It is reasonable attributing this result to the improved orientation of the antibodies which is much more significant than that achieved with the IgG-anti-IgG model system[88]. These observations are in fair agreement the mass dependence effects described by Trilling et al.[21], who have recently reported that the smaller the analyte, the more important is the orientation of the sensitive biomolecule.

To prove sensor specificity, the same experimental procedure has been used for four compounds, progressively similar to parathion, from the chemical and structural point of view. They are bisphenol A, p-nonylphenol, dichlorvos, and paraoxon. At a concentration of approximately 1.7 μM, where parathion exhibits a significant response, all the four chemicals showed no detectable frequency shift when they were tested separately. Therefore, the sensor response has been measured while working in contact with a mixture of the four compounds at an even higher concentration (3.5 μM), thereby mimicking a real complex sample. The results of these experiments are reported in Figure 4.7, where the detection steps of the protocol are highlighted.
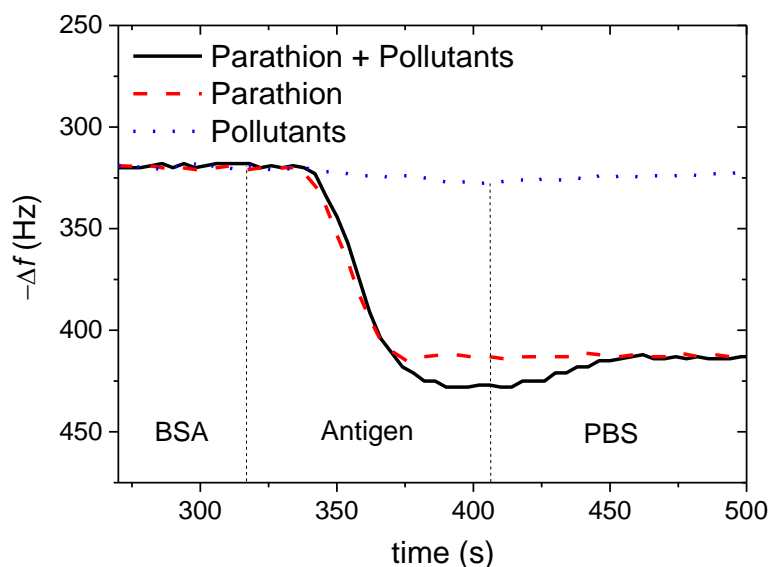
Figure 4.7. *Sensor specificity i.e. sensor responses against different pollutants similar to parathion. QCM response to parathion (red dashed line), to a mixture of bisphenol A, p-nonylphenol, dichlorvos, paraoxon (blue dotted line), and to parathion + other pollutants (black solid line). The concentration of all the compounds is 3.5 μM.*

The signal measured when only the four compounds are in solution is just few hertz, but the frequency goes back to the previous value when PBS is conveyed into the circuit (blue dotted line). The parathion alone at 3.5 μM leads to a frequency shift of approximately 90 Hz (red dashed line). The mixture containing all the pollutants (including parathion) produces a slightly larger shift (solid black line) that disappear after washing with PBS. As final test, the concentration of the pollutants were increased by two orders of magnitude (170 μM) compared to the initial experiment (1.7 μM), but despite such high concentration, the QCM responses were always lower than those provided by parathion in the saturation regime of the dose-response curve. All these results demonstrate that recognition efficiency of antibodies is not affected by photonic activation.

4.2.2 "Sandwich protocol"

Since not all the molecules are able to complex with BSA, a more general approach leading to higher sensitivity and specificity has been developed. Basically, the light analyte (i.e. parathion) is ballasted by the same antibodies used to functionalize the QCM. This procedure mimics the so-called sandwich configuration widely used in the ELISA technique[109]. It is worth mention that "sandwich" immunoassays can be performed in two different ways commonly referred to as "one-step" and "two-step". The first requires that antigen and antibody are mixed

56

before the detection step, thus significantly reducing the time required for the assay, while the latter involves the sequential incubation of analyte and antibody with the immobilized proteins.

A "one-step" sandwich method has been coupled with PIT based immunosenor to effectively detect parathion in liquid environment. In this case, the irradiation conditions are λ = 258 nm, 10 kHz repetition rate, 250 mW of average power and 1 minute irradiation time. These irradiation conditions provide the maximum efficiency in protein activation as demonstrated through the Ellman's assay. Before the QCM experiment, each pollutant sample has been incubated for 30 minutes with the same volume of immunoglobulin solution at a fixed concentration (25 μg/mL), corresponding to an initial concentration of free antibody (A_{free}) of about 0.17 μM. This mixture is then tested by the QCM based immunosensor. The experimental procedure is quite similar to "BSA protocol", but involves intermediate washing steps to purge the circuit as shown in Figure 4.8 where the phases of the experiment are highlighted.
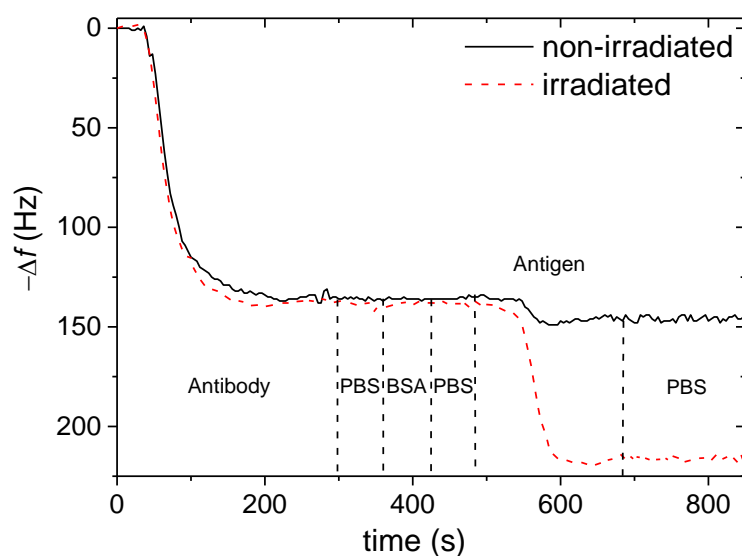
Figure 4.8. QCM-based immunosensor outputs for parathion detection using either irradiated (red dashed line) or non-irradiated (black solid line) antibodies. The first frequency shift at about 150 s corresponds to the antibody immobilization onto the sensor surface, while the second drop at about 550 s is due to the detection of analyte–antibody complex (parathion 0.85 μM). The vertical dashed lines highlight the phases of the protocol described in the text.

While the antigen-antibody mixture is flowing onto the QCM, three species can interact with the sensor surface (see sketch in Figure 4.9): A_{free}, the antigen (*B*) and the antigen-antibody complex (*C*).
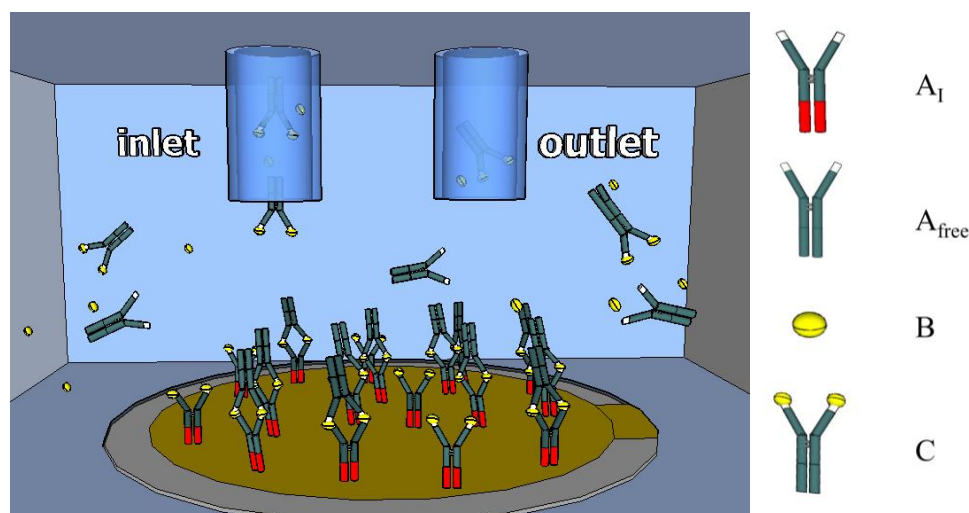
Figure 4.9. *Sketch of the cell containing the gold-quartz wafer. The antibodies activated by the PIT are shown with their lower part in red and are tethered side-up on the gold electrode. The solution flowing through the cell contains analyte (small yellow particles) bound to the Ab (green Y-shape), but also "free" Ab and "free" analytes. When a free analyte is recognized by the Ab tethered to the gold, there is no effect on the QCM frequency since the deposited mass is too small. Only when the "sandwich" configuration is realized there is a detectable response.*

One of the advantages of the conveying a mixture rather than the single B and A_{free}, as it occurs in the "two-steps" ELISA protocol[109], relies in stationary equilibrium occurring in the interaction volume above the QCM electrode which allows to efficiently analyse the original sample. In a "two-steps" procedure, when the sample is conveyed to the QCM and the antibody is injected after a necessary washing, the amount of antigen entrapped by immobilized antibodies is lower since there are no free analytes that could replace those detached from the QCM plate by washing and free antibodies.

The main drawback of a "one-step" sandwich approach relies in the need of high antibody concentration in the original solution so that virtually all the antigens are complexed and the probability of finding free analytes is negligible. At antigen concentration much higher than antibody concentration there will be free analytes that would bind the antibodies tethered to the gold surface. In this case the QCM will not provide a detectable signal because of the low antigen mass thus giving rise to the so-called "hook effect" which can be shifted to high analyte concentration by simply increasing the antibody concentration[112]. While in the proposed procedure a relatively low antibody concentration has been used (25 μg/mL), the "two-step" ELISA usually requires a much bigger amount of protein.

A "one-step" sandwich method involves the competitive binding of two types of antigens that significantly differ in size. A similar model system has been studied by Schramm and Paek[113] who compared the antibody binding efficiency of a small molecule (a progesterone

derivative) with that of an enzyme-labelled form of the same antigen. A possible strategy to characterize the competitive binding between large and small antigens is considering the equilibria between the different species which are involved. These are shown in Figure 4.10.

Figure 4.10. Scheme of equilibria. The immobilized antibody (A_I) can bind either the native (B) or labelled (C) form of parathion thus making two kind of antigen-antibody complexes (A_IB and A_IC, respectively). Also the two forms of the antigen are at the equilibrium. k_1, k_2 and k_3 are the kinetic constants characterizing the three equilibria.

In this scheme, only the formation of the A_IC complex leads to a significant change of the resonance frequency of the QCM. This is due to the huge mass of the big antigen (*C*), which weighs about 150 kDa, like the free immunoglobulin (A_{free}) used to label the organophosphate compound. On the other side, since native parathion (*B*) molecules weigh only 291.26 Da, their binding onto the antibody-functionalized surface results in a negligible frequency variation. These analytes occupy the sensitive sites of immobilized antibodies (A_I) thus acting as "inhibitors" of the immunosensor.

The model shown in Figure 4.10 can be described by three equilibrium equations:

$$k_1[A_IC] = [A_I][C] \qquad (4.4)$$

$$k_2[A_IB] = [A_I][B] \qquad (4.5)$$

$$k_3[C] = [A_{free}][B] \qquad (4.6)$$

where k_1 and k_2 are the affinity constants of the immobilized antibody for the large and small antigens, respectively, while k_3 is the affinity constant of the free antibody for the non-labelled parathion. These equations contain six variables: concentrations of both immobilized and free non-occupied antibodies (A_I and A_{free}), both small and large antigens (*B* and *C*), and two antigen-

antibody complexes (A_IB and A_IC). It is possible derive also three mass balance equations for the two type of antibodies and for parathion:

$$[A_{free}] + [C] + [A_IC] = [A_{free}]_0 \tag{4.7}$$

$$[A_I] + [A_IC] + [A_IB] = [A_I]_0 \tag{4.8}$$

$$[B] + [C] + [A_IB] + [A_IC] = [B]_0 \tag{4.9}$$

where $[A_{free}]_0$ is the initial concentration of free antibody used to label the organophosphate compound (0.17 µM), $[A_I]_0$ is the effective concentration of the immobilized antibody onto the sensor surface and $[B]_0$ is the concentration of parathion sample used to calibrate the sensor response.

Since $[A_IC]$ is directly proportional to the frequency variation of the QCM, an analytical expression for this concentration should provide a good description of the experimental results. However, the combination of the six equation results in a non-linear system which requires much more experimental data and complex numerical procedures to be solved. For instance, Schramm and Paek[113] faced this problem by detecting both large and small antigens using two different principles: fluorescence and radioactive labelling.

To overcome this issue, a different approach has been adopted. A standard Michaelis-Menten type equation (like Equation 4.1) is expected to well describe the process when $[B]_0 << [Ab_{free}]_0$:

$$\Delta f(B_0) = \frac{(\Delta f)_{sat} B_0}{B_0 + K_M} \tag{4.10}$$

being B_0 the initial concentration of the antigen. On the other side, an excess of analyte concentration in the original solution ($[B]_0 >> [A_{free}]_0$) rises the probability that immobilized antibodies bind the free antigens (B) rather than the complexed analytes (C), but due to the small mass of the molecule such a recognition does not lead to a measurable frequency shift. Therefore, when $[B]$ increases and the condition $[B]_0 \approx [A_{free}]_0$ is reached an "inhibition effect" starts and further increase of $[B]$ results in a reduction of Δf. The experimental evidence of this phenomenon is clearly shown in Figure 4.11.
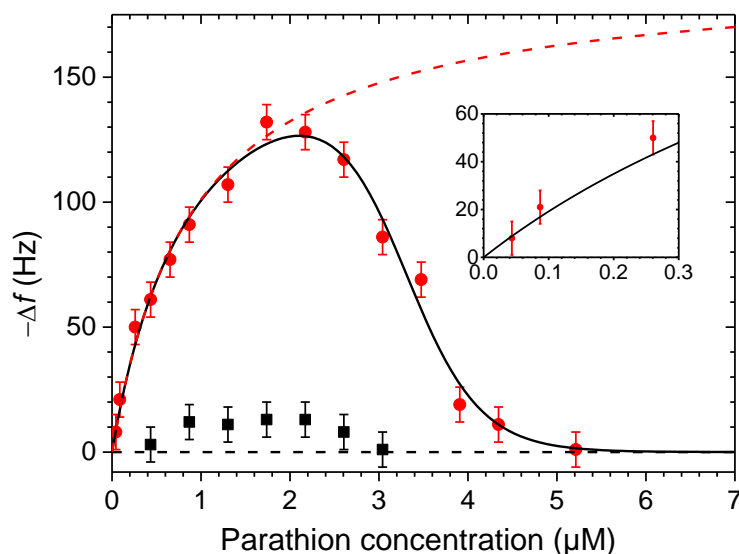
Figure 4.11. *Response of the QCM to parathion concentrations when the antibody is irradiated (circle points) and not irradiated (square points). The points achieved with the irradiated antibody are fitted by Equation 4.11 (bold line). The low frequency change achieved when the antibody is not irradiated does not allow any significant fit of the experimental data. The inset is the enlargement of the low concentration region, whereas the dashed red line is the plot of Equation 4.10, i.e. the inhibition effect of the free antigens is hampered by high Ab free concentration.*

At low $[B]_0$ the frequency shift follows Equation 4.10 (red dashed curve), whereas a reduction of the sensor response occurs at high analyte concentration. A simple way to model the inhibition role played by the free analyte is through a two parameters logistic function, in which one parameter accounts for the analyte concentration at which the inhibition becomes relevant and the other is related to the decay rate of the available recognition site. In view of these considerations, the experimental results have been fitted using the following function:

$$\Delta f(B_0) = \frac{(\Delta f)_{sat} B_0}{K_M + B_0} \frac{1}{1 + e^{a(B_0 - B_M)}} \tag{4.11}$$

where a and B_M are two free parameters accounting for the different kinetics the analytes and antibodies may have, whereas $(\Delta f)_{sat} = 192 \pm 2$ Hz has been evaluated by measuring the saturation value achieved when a layer of antibodies covers the gold sensor surface. Although such a value refers to irradiated antibodies, it is essentially the same even when the antibodies are not irradiated[88].

The fitting of the experimental data obtained with irradiated antibodies by Equation 4.11 (black solid line in Figure 4.11) provides $K_M = 0.90 \pm 0.05$ μM, $a = 2.4 \pm 0.1$ μM^{-1} and $B_M = 3.3 \pm 0.1$ μM. The black square points are the results obtained when PIT is not applied and the

antibodies are randomly adsorbed on the gold surface. In this case it is evident that no significant signal is measurable.

Assuming an overall error of 10 Hz, (see also the insets in Figure 4.11) so that a minimum frequency change $(\Delta f)_{min}$ of 10 Hz is required for a measurement to significantly differ from zero, an evaluation of the LOD can be obtained by adopting the same procedure used for the "BSA protocol". Inverting the Michaelis-Menten type equation which rules at low $[B]_0$, a LOD of 50 nM for parathion in water has been estimated.

To ascertain the sensor specificity, the same experimental procedure has been used to test the response of the QCM when compounds similar to parathion are in the sample. A mixture of bisphenol A, p-nonylphenol, dichlorvos, diazinon and paraoxon (each of them at a concentration of 2 µM) has been prepared. When this sample is conveyed into the QCM no response is provided by the device (black solid line in Figure 4.12). On the opposite, when parathion at 0.2 µM is present in this mixture, the sensor exhibits a frequency shift of approximately 35 Hz (red dashed line in Figure 4.12) in satisfactory agreement with the calibration curve shown in Figure 4.11, thereby evidencing that pollutants other than parathion do not affect the detection of the pesticide.
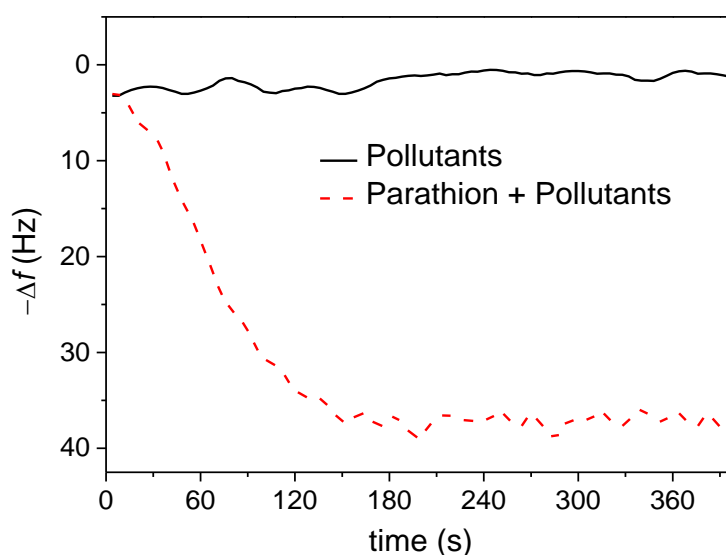
Figure 4.12. *Measure of sensor specificity. Parathion at 0.2 µM tested against bisphenol A, p-nonylphenol, dichlorvos, diazinon and paraoxon each of them at 2 µM. The detection of parathion is not affected by the other chemicals.*

4.3   Patulin

The lack of portable detection tools for an extremely harmful food contaminant like patulin makes valuable the realization of a PIT based immunosenor for revealing the presence of this mycotoxin. Since patulin is a light molecule like parathion (it weighs only 154.12 Da), its detection suffers of the same limitations of the organophosphate compound. To overcome these issues, patulin has been quantified using a "one-step" sandwich method[94]. The results achieved detecting the analyte using UV activated antibodies immobilized onto the QCM gold surface are shown in Figure 4.13. The irradiation conditions are the same used for anti-parathion antibodies. These experiments have been performed in collaboration with the Italian "Consiglio per la ricerca e la sperimentazione in agricoltura (CRA) – Unità di ricerca per le colture alternative al tabacco".
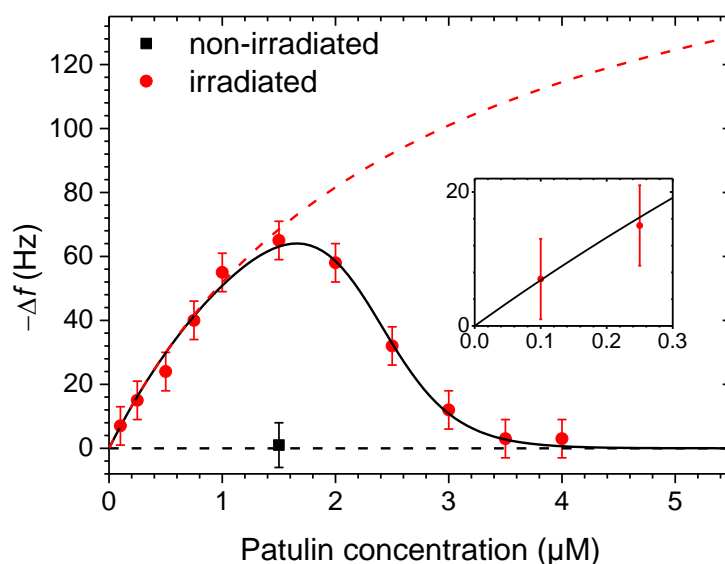
Figure 4.13. *QCM responses using irradiated (circle points) and non-irradiated (square points) antibodies. The responses obtained using PIT-based immonosensor have been fitted using Equation 4.11 (bold line).*

When PIT is not applied no significant frequency shift is measured. The experimental data have been fitted using Equation 4.11 (black solid line) which gives $K_M = 2.70 \pm 0.05$ μM, $a = 3.0 \pm 0.1$ μM^{-1} and $B_M = 2.3 \pm 0.1$ μM. This procedure allows to achieve a LOD for patulin in aqueous environment of about 140 nM.

The sensor specificity has been verified by measuring the sensor response to real samples of patulin extracted from apple puree provided by apple processing factories. To this end, a commercial kit (Polyintell Affinimip® SPE cartridge) is used. The extraction is performed by mixing 10 g of apple puree with 150 μL of a pectinase enzyme solution and 10 mL of deionized

water. The sample is left at room temperature overnight (or alternatively for 2 h at 40°C), then centrifuged at 4500 g for 5 min and filtered with a 0.2 μm filter. This solution is used as loading solution. The SPE Cartridge was conditioned with 2 mL of acetonitrile (ACN) and subsequently with 1 mL of deionised water. A volume of 5 mL of loading solution is put in the cartridge, which is then washed with 4 mL of deionized water containing 1% of acetic acid. Water is forced down into the column. The cartridge is treated with 1 mL of $CHCl_3$ and finally patulin is eluted by flowing 2 mL of ACN containing 1% acetic acid. The SPE procedure requires approximately 30 minutes. The elution fraction is then evaporated and dissolved in water containing 0.1% acetic acid. This solution is analysed by a Perkin Elmer HPLC with UV detector to estimate the concentration of patulin. The same sample is then used in QCM validation analysis.

Figure 4.14 reports the QCM response to real samples previously analyzed by HPLC. When there is no patulin in the extract from apple puree, no frequency shift is observed (black solid line). On the opposite, when extracts from apple puree containing 0.2 μM and 1.0 μM of patulin (measured by HPLC) are analysed, the response of QCM (-12 Hz and -43 Hz, for the two concentrations, respectively) results to be in very satisfactory agreement with the calibration curve reported in Figure 4.13.
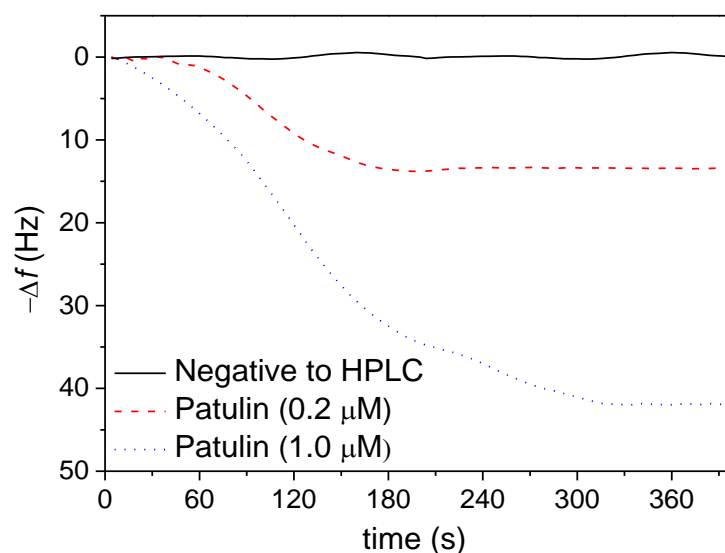
Figure 4.14. *Validation of sensor specificity. Extract from apple puree previously analyzed by HPLC have been tested using the PIT-based immunosensor. The responses due to negative to patulin sample (black solid line), 0.2 μM patulin (red dashed line) and 1 μM patulin (blue dotted line) are in fair agreement with the sensor calibration curve.*

It is worth noticing that the extracts used for these tests contain analytes which could potentially interfere with patulin detection, however, these results demonstrate that this QCM based immunosensor is suitable for real sample analysis.

4.4   Gliadin

The high risk associated to contamination of gluten-free products supports the research for user-friendly analytical tools for detecting gliadin in foods. To this end, a label-free PIT based immunosensor has been realized in collaboration with the Italian "Consiglio per la Ricerca e la Sperimentazione in Agricoltura (CRA) − Centro di ricerca per l'orticoltura". For anti-gliadin antibody, the irradiation conditions are λ = 258 nm, 10 kHz repetition rate, 250 mW of average power and 1 minute irradiation time. In view of its low solubility in water, the gliadin samples have been prepared in 20% acetonitrile aqueous solution. The calibration curve for this detection tool is shown in Figure 4.15.
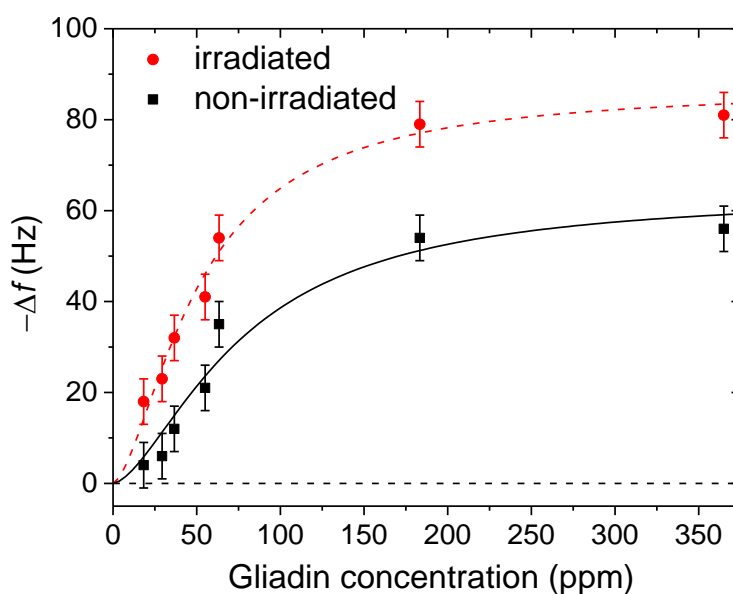
Figure 4.15. *Calibartion curves for gliadin detection using irradiated (red circles) and non-irradiated (black squares) antibodies. The experimental responses have been fitted using the model described in the text.*

The sigmoidal behaviour of the sensor responses can been attributed to interactions occurring between gliadins[114,115]. These proteins are classified into four subcategories, α-, β-, γ -, and ω-gliadins (being α, γ, and ω-types responsible for the coeliac disease), which are naturally assembled with glutenins in gluten. The bases of these connections are intermolecular disulphide bridges, hydrophobic and hydrogen bonding interactions. In view of this effect, the experimental results have been fitted using the so-called Hill equation, a mathematical model quite similar to Michaelis-Menten law, which describes cooperative binding events[110].

A biomolecule having a single binding site (*M*) interacting with a ligand (*L*) can be described by the following equilibrium:

$$M + L \rightleftarrows ML \tag{4.12}$$

$$K_{eq} = \frac{[ML]}{[M][L]} \tag{4.13}$$

K_{eq} being the equilibrium constant of the complex. The fraction of biomolecules bonded to a ligand (i.e. fractional saturation) *Y* is written as:

$$Y = \frac{[ML]}{[M] + [ML]} = \frac{[L]}{K_D + [L]} \tag{4.14}$$

where *ML* is the biomolecule-ligand complex and K_D its dissociation constant (i.e. *1/K_{eq}*). This mathematical formulation leads to the standard Michaelis-Menten equation where a certain parameter (e.g. reaction rate) is described as function of the ligand concentration (e.g. substrate concentration). Non-cooperative systems like an antigen-antibody model, where the antigen binding sites are considered completely independent, are analysed using the same approach thus resulting again in a Michaelis-Menten type equation (as shown by Equation 4.1).

On the other side, in cooperative systems, the binding of a ligand changes the other binding sites on the biomolecule. Assuming that the biomolecule has *n* binding cavities and the affinity for the remaining sites is hugely increased so that all the remaining ligands bind simultaneously, this system can be described as:

$$M + nL \rightleftarrows ML \tag{4.15}$$

$$K_{eq} = \frac{[ML]}{[M][L]^n} \tag{4.16}$$

Thus making the fractional saturation:

$$Y = \frac{[ML]}{[M] + [ML]} = \frac{[L]^n}{K_D + [L]^n} \tag{4.17}$$

This relationship leads to the so-called Hill equation which is often represented in literature as:

$$v = \frac{V_m L^n}{K_D + L^n} \tag{4.18}$$

where v is the reaction rate (i.e. for enzymatic reactions) and V_m is the saturation value. The coefficient n (number of binding sites) corresponds, in this ideal model, to the so-called Hill coefficient. In general, n is replaced with h, which usually is not an integer number thus showing the lack of this model in describing a complex phenomenon like cooperativity. The most famous example of cooperative binding concerns the haemoglobin. Even if this protein has four binding sites for molecular oxygen, the measured Hill coefficient is 2.7. When $h = 1$, the Hill equation reduces to the non-cooperative Michaelis-Menten law. If $h < 1$, an anti-cooperative binding occurs.

In addition, in this model, $\sqrt[n]{K_D}$ corresponds to the concentration of ligand giving half of fractional saturation, in analogy with K_M in the Michaelis-Menten equation. This parameter, commonly referred to as K_H, is and average dissociation constant depending on all the binding events.

The experimental results shown in Figure 4.15 have been fitted using the following Hill-type equation:

$$\Delta f(G) = \frac{(\Delta f)_{sat} G^h}{K_H^h + G^h} \tag{4.19}$$

being G the gliadin concentration. The best fit of the responses obtained when antibodies are irradiated (red dashed line in Figure 4.15) provide $(\Delta f)_{sat} = 87 \pm 5$ Hz, $K_H = 51 \pm 6$ ppm and $h = 1.6 \pm 0.3$. This value of h (i.e. $h > 1$) is consistent with a cooperative effect resulting from gliadin-gliadin interactions. This coefficient has been fixed while fitting the responses obtained when PIT is not applied using Equation 4.19 (black solid curve in Figure 4.15). In this case, $(\Delta f)_{sat} = 64 \pm 5$ Hz and $K_H = 77 \pm 13$ ppm. The increase of both saturation value and binding affinity obtained by PIT-based immunosensor is due to the lower steric hindrance of the antigen binding sites achieved when immobilized antibodies are better oriented onto the sensor surface.

By considering an overall error of about 10 Hz and inverting Equation 4.19 a LOD of about 13 ppm is estimated. This value can be significantly reduced by introducing a labelling procedure like what involved in a two-step sandwich method. These preliminary results confirm again the role of PIT in enhancing sensing efficiency. After improving the detection procedure and performing appropriate specificity tests, this PIT-based immunosensor could be used for real sample analysis.

5   Conclusions

Photonic immobilization technique has been coupled with quartz crystal microbalance technology with the aim to realize efficient and reliable detection tools for practical applications. This functionalization procedure is fast, easy and provides the effective immobilization of antibodies onto gold and thiol-reactive surfaces by exploiting the selective photoreduction of the disulphide bridge in the closely spaced cysteine-cysteine/tryptophan amino acidic triads. This structural motif is a typical characteristic of the immunoglobulin family. The UV irradiation of proteins does not affect the recognition property of the antibodies. On the other side, this activation procedure allows to achieve a better exposure of the sensitive sites of the immobilized biomolecule (i.e. the antigen binding sites) thus resulting in a valuable improvement in sensor sensitivity. The effects of this unconventional functionalization method on antibodies have been studied and characterized exploiting several investigation approaches like optical techniques, atomic force microscopy and Ellman's assay.

Using this immobilization procedure, QCM-based immunosensors have been realized for quantifying a group of analytes having significant differences in terms of size and physiochemical properties. The case study IgG-anti-IgG shows that the more correct orientation achieved when PIT is applied results in rising the maximum amount of detectable antigen as well as increasing the binding affinity of the immobilized biomolecules.

The detection of light molecules is of paramount importance in a wide range of practical applications including health diagnostic, environmental monitoring and food analysis. To this aim, PIT-based immunosensors have been realized for quantifying parathion, an organophosphorus pesticide, and patulin, a micotoxin. Since these molecules weigh only a few hundreds of Da, achieving an effective detection using a mass-based transducer like a QCM is challenging. This drawback has been overcome by adopting two strategies to increase the mass of the analyte. The first is based on the complex formation between parathion and bovine serum albumin. This big protein absorbs the small molecule through nonspecific interactions thus allowing to achieve a LOD of about 200 nM in liquid environment. The second approach mimics the sandwich configuration widely used in the ELISA assay. Basically, the antigen is recognized by its own antibody and the resulting solution is conveyed to the balance. While PIT is shown to largely increase the sensitivity of QCM, the sandwich protocol has two main advantages: it weighs down the light molecules, so that they can be revealed by the QCM, and

it inherently increases the specificity of the whole device. A well-known issue of this procedure is the decrease of the signal at high analyte concentration which can be easily solved by rising antibody concentration in the mixing volume. These immunosensors provide LODs of 50 nM and 140 nM for parathion and patulin, respectively. PIT has been involved also in developing a label-free immunosensor for detecting gliadin, the protein responsible for the coeliac disease. This QCM-based immunosensor achieves a LOD 13 ppm and can be significantly improved by introducing a sandwich type labelling. It is worth noticing that QCM-based immunosensors have non-negligible advantages in terms of rapidity in the response (only few minutes are required), flexibility and portability, thus making themselves valuable tools for in situ analysis.

In view of the results presented in this work, PIT have proven to be an effective and promising technology to couple biological sensitive elements with gold and thiol-reactive surfaces. In principle, since other transduction principles involve gold surfaces (e.g. electrochemical methods, SPR devices), PIT could be considered a valid alternative to more complex and laborious surface functionalization procedures.

References

1. Ballantine, Jr., D. S. *et al. Acoustic Wave Sensors: Theory, Design, and Physico-Chemical Applications*. (Academic Press, 1997).

2. Turner, A. P. F., Karube, I. & Wilson, G. S. *Biosensors: Fundamentals and Applications*. (Oxford University Press, 1987).

3. Grieshaber, D., MacKenzie, R., Vörös, J. & Reimhult, E. Electrochemical Biosensors - Sensor Principles and Architectures. *Sensors* **8,** 1400–1458 (2008).

4. Guth, U., Vonau, W. & Zosel, J. Recent developments in electrochemical sensor application and technology-a review. *Meas. Sci. Technol.* **20,** 042002 (2009).

5. Long, F., Zhu, A. & Shi, H. Recent Advances in Optical Biosensors for Environmental Monitoring and Early Warning. *Sensors* **13,** 13928–13948 (2013).

6. Fan, X. *et al.* Sensitive optical biosensors for unlabeled targets : A review. *Anal. Chim. Acta* **620,** 8–26 (2008).

7. Arlett, J. L., Myers, E. B. & Roukes, M. L. Comparative advantages of mechanical biosensors. *Nat. Nanotechnol.* **6,** 203–215 (2011).

8. Alvarez-lcaza, M. & Bilitewski, U. Mass Production of Biosensors. *Anal. Chem.* **65,** 525–533 (1993).

9. Clark, Jr., L. C. & Lyons, C. Electrode systems for continuous monitoring in cardiovascular surgery. *Ann. N. Y. Acad. Sci.* **102,** 29–45 (1962).

10. Cooper, M. A. & Singleton, V. T. Review A survey of the 2001 to 2005 quartz crystal microbalance biosensor literature : applications of acoustic physics to the analysis of biomolecular interactions. *J. Mol. Recognit.* **20,** 154–184 (2007).

11. Becker, B. & Cooper, M. A survey of the 2006-2009 quartz crystal microbalance biosensor literature. *J. Mol. Recognit.* **24,** 754–787 (2011).

12. Vashist, S. K. & Vashist, P. Recent Advances in Quartz Crystal Microbalance-Based Sensors. *J. Sensors* **2011,** 1–13 (2011).

13. Deakin, M. R. & Buttry, D. A. Applications of the Quartz Crystal Micro balance. *Anal. Chem.* **61,** 1147A–1154A (1989).

14. Longobardi, S. *et al.* A simple MALDI plate functionalization by Vmh2 hydrophobin for serial multi-enzymatic protein digestions. *Anal. Bioanal. Chem.* **407,** 487–496 (2015).

15. Sauerbrey, G. Verwendung von Schwingquarzen zur Wäigung diinner Schichten und zur Mikrowäigung. *Z. Phys.* **155,** 206–222 (1959).

16. Kanazawa, K. K. & Gordon, J. G. Frequency of a Quartz Microbalance in Contact with Liquid. *Anal. Chem.* **57,** 1770–1771 (1985).

17. Voinova, M. V. On mass loading and dissipation measured with acoustic wave sensors: a review. *J. Sensors* **2009,** 943125 (2009).

18. Reviakine, I., Johannsmann, D. & Richter, R. P. Hearing What You Cannot See and Visualizing What You Hear: Interpreting Quartz Crystal Microbalance Data from Solvated Interfaces. *Anal. Chem.* **83,** 8838–8848 (2011).

19. Jung, Y., Jeong, J. Y. & Chung, B. H. Recent advances in immobilization methods of antibodies on solid supports. *Analyst* **133,** 697–701 (2008).

20. Nicu, L. & Leïchlé, T. Biosensors and tools for surface functionalization from the macro- to the nanoscale: The way forward. *J. Appl. Phys.* **104,** 111101 (2008).

21. Trilling, A. K., Harmsen, M. M., Ruigrok, V. J. B., Zuilhof, H. & Beekwilder, J. The effect of uniform capture molecule orientation on biosensor sensitivity: dependence on analyte properties. *Biosens. Bioelectron.* **40,** 219–226 (2013).

22. Wilson, D. S. & Nock, S. Functional protein microarrays. *Curr. Opin. Chem. Biol.* **6,** 81–85 (2001).

23. Vijayendran, R. A. & Leckband, D. E. A quantitative assessment of heterogeneity for surface-immobilized proteins. *Anal. Chem.* **73,** 471–480 (2001).

24. Neves-Petersen, M. T., Gajula, G. P. & Petersen, S. B. in *Molecular Photochemistry - Various Aspects* 125–158 (2012). doi:10.5772/37947

25. Wink, T., van Zuilen, S. J., Bult, A. & van Bennkom, W. P. Self-assembled monolayers for biosensors. *Analyst* **122,** 43R–50R (1997).

26. Gooding, J. J. & Darwish, N. The rise of self-assembled monolayers for fabricating electrochemical biosensors-an interfacial perspective. *Chem. Rec.* **12,** 92–105 (2012).

27. Caruso, F., Rodda, E. & Furlong, D. N. Orientational Aspects of Antibody Immobilization and Immunological Activity on Quartz Crystal Microbalance Electrodes. *J. Colloid Interface Sci.* **178,** 104–115 (1996).

28. Přibyl, J., Hepel, M., Halámek, J. & Skládal, P. Development of piezoelectric immunosensors for competitive and direct determination of atrazine. *Sens. Actuators B* **91,** 333–341 (2003).

29. Hao, R. *et al.* Rapid detection of Bacillus anthracis using monoclonal antibody functionalized QCM sensor. *Biosens. Bioelectron.* **24,** 1330–1335 (2009).

30. Sharma, H. & Mutharasan, R. Half Antibody Fragments Improve Biosensor Sensitivity without Loss of Selectivity. *Anal. Chem.* **85,** 2472–2477 (2013).

31.   Byrne, B., Stack, E., Gilmartin, N. & O'Kennedy, R. Antibody-based sensors: principles, problems and potential for detection of pathogens and associated toxins. *Sensors* **9,** 4407–4445 (2009).

32.   Jiang, X. *et al.* Immunosensors for detection of pesticide residues. *Biosens. Bioelectron.* **23,** 1577–1587 (2008).

33.   Wang, Y., Knoll, W. & Dostalek, J. Bacterial pathogen surface plasmon resonance biosensor advanced by long range surface plasmons and magnetic nanoparticle assays. *Anal. Chem.* **84,** 8345–8350 (2012).

34.   Neves-Petersen, M. T., Snabe, T., Klitgaard, S., Duroux, M. E. G. & Petersen, S. B. Photonic activation of disulfide bridges achieves oriented protein immobilization on biosensor surfaces. *Protein Sci.* **15,** 343–351 (2006).

35.   Snabe, T., Røder, G. A., Neves-Petersen, M. T., Buus, S. & Petersen, S. B. Oriented coupling of major histocompatibility complex (MHC) to sensor surfaces using light assisted immobilisation technology. *Biosens. Bioelectron.* **21,** 1553–1559 (2006).

36.   Ioerger, T. R., Du, C. & Linthicum, D. S. Conservation of cys-cys trp structural triads and their geometry in the protein domains of immunoglobulin superfamily members. *Mol. Immunol.* **36,** 373–386 (1999).

37.   Parracino, A. *et al.* Arraying prostate specific antigen PSA and Fab anti-PSA using light-assisted molecular immobilization technology. *Protein Sci.* **19,** 1751–1759 (2010).

38.   Correia, M., Neves-Petersen, M. T., Parracino, A., di Gennaro, A. K. & Petersen, S. B. Photophysics, photochemistry and energetics of UV light induced disulphide bridge disruption in apo-α-lactalbumin. *J. Fluoresc.* **22,** 323–337 (2012).

39.   Janeway, Jr., C. A., Travers, P., Walport, M. & Shlomchik, M. J. *Immunobiology.* (Garland Science, 2001).

40.   Harris, L. J., Skaletsky, E. & McPherson, A. Crystallographic structure of an intact IgG1 monoclonal antibody. *J. Mol. Biol.* **275,** 861–872 (1998).

41.   Köhler, G. & Milstein, C. Continuous cultures of fused cells secreting antibody of predefined specificity. *Nature* **256,** 495–497 (1975).

42.   Roque, A. C. A., Lowe, C. R. & Taipa, M. Â. Antibodies and genetically engineered related molecules: Production and purification. *Biotechnol. Prog.* **20,** 639–654 (2004).

43.   Geschwindner, S., Carlsson, J. F. & Knecht, W. Application of optical biosensors in small-molecule screening activities. *Sensors* **12,** 4311–4323 (2012).

44.   Jones, A. M. *et al.* In vivo biochemistry: Applications for small molecule biosensors in plant biology. *Curr. Opin. Plant Biol.* **16,** 389–395 (2013).

45.   Alberts, B. *et al. Molecular Biology of the Cell*. (Garland Science, 2002).

46. Milles, H. L., Salt, H. & B. Parathion Poisoning. *Br. Med. J.* **2,** 444 (1950).

47. Jokanović, M. & Prostran, M. Pyridinium oximes as cholinesterase reactivators. Structure-activity relationship and efficacy in the treatment of poisoning with organophosphorus compounds. *Curr. Med. Chem.* **16,** 2177–2188 (2009).

48. Balali-Mood, M. & Shariat, M. Treatment of organophosphate poisoning. Experience of nerve agents and acute pesticide poisoning on the effects of oximes. *J. Physiol.* **92,** 375–378 (1998).

49. Johnson, M. K. *et al.* Evaluation of antidotes for poisoning by organophosphorus pesticides. *Emerg. Med.* **12,** 22–37 (2000).

50. Eddleston, M., Buckley, N. A., Eyer, P. & Dawson, A. H. Management of acute organophosphorus pesticide poisoning. *Lancet* **371,** 597–607 (2008).

51. Antonijevic, B. & Stojiljkovic, M. P. Unequal efficacy of pyridinium oximes in acute organophosphate poisoning. *Clin. Med. Res.* **5,** 71–82 (2007).

52. Kwakman, P. J. M., Vreuls, J. J., Brinkman, U. A. T. & Ghijsen, R. T. Determination of Organophosphorus Pesticides in Aqueous Samples by On-Line Membrane Disk Extraction and Capillary Gas Chromatography. *Chromatographia* **34,** 41–47 (1992).

53. Carabias Martinez, R., Rodriguez Gonzalo, E., Amigo Moran, M. J. & Hernandez Mendez, J. Sensitive method for the determination of organophosphorus pesticides in fruits and surface waters by high-performance liquid chromatography with ultraviolet detection. *J. Chromatogr.* **607,** 37–45 (1992).

54. Blasco, C., Fernández, M., Picó, Y. & Font, G. Comparison of solid-phase microextraction and stir bar sorptive extraction for determining six organophosphorus insecticides in honey by liquid chromatography-mass spectrometry. *J. Chromatogr. A* **1030,** 77–85 (2004).

55. Walker, J. P. & Asher, S. A. Acetylcholinesterase-Based Organophosphate Nerve Agent Sensing Photonic Crystal. *Anal. Chem.* **77,** 1596–1600 (2005).

56. Stoytcheva, M., Zlatev, R., Gochev, V., Velkova, Z. & Montero, G. Amperometric biosensor precision improvement: application to organophosphorus pesticide determination. *Anal. Methods* **6,** 8232–8238 (2014).

57. Marrazza, G. Piezoelectric Biosensors for Organophosphate and Carbamate Pesticides: A Review. *Biosensors* **4,** 301–317 (2014).

58. Bi, X. & Yang, K.-L. On-line monitoring imidacloprid and thiacloprid in celery juice using quartz crystal microbalance. *Anal. Chem.* **81,** 527–532 (2009).

59. March, C., Manclús, J. J., Jiménez, Y., Arnau, a. & Montoya, a. A piezoelectric immunosensor for the determination of pesticide residues and metabolites in fruit juices. *Talanta* **78,** 827–833 (2009).

60. Jia, K., Adam, P. M. & Ionescu, R. E. Sequential acoustic detection of atrazine herbicide and carbofuran insecticide using a single micro-structured gold quartz crystal microbalance. *Sens. Actuators B* **188,** 400–404 (2013).

61. Fox, E. M. & Howlett, B. J. Secondary metabolism: regulation and role in fungal biology. *Curr. Opin. Microbiol.* **11,** 481–487 (2008).

62. Keller, N. P., Turner, G. & Bennett, J. W. Fungal secondary metabolism - from biochemistry to genomics. *Nat. Rev. Microbiol.* **3,** 937–947 (2005).

63. Puel, O., Galtier, P. & Oswald, I. P. Biosynthesis and toxicological effects of patulin. *Toxins* **2,** 613–631 (2010).

64. Shephard, G. S. *et al.* Developments in mycotoxin analysis: an update for 2009-2010. *World Mycotoxin J.* **4,** 3–28 (2011).

65. Pereira, V. L., Fernandes, J. O. & Cunha, S. C. Mycotoxins in cereals and related foodstuffs: A review on occurrence and recent methods of analysis. *Trends Food Sci. Technol.* **36,** 96–136 (2014).

66. Vidal, J. C. *et al.* Electrochemical affinity biosensors for detection of mycotoxins: A review. *Biosens. Bioelectron.* **49,** 146–158 (2013).

67. Pohanka, M., Jun, D. & Kuca, K. Mycotoxin assays using biosensor technology: a review. *Drug Chem. Toxicol.* **30,** 253–261 (2007).

68. Prieto-Simón, B. & Campàs, M. Immunochemical tools for mycotoxin detection in food. *Monatsh. Chem.* **140,** 915–920 (2009).

69. De Champdoré, M. *et al.* A new competitive fluorescence assay for the detection of patulin toxin. *Anal. Chem.* **79,** 751–757 (2007).

70. Damián Chanique, G., Arévalo, A. H., Zon, M. A. & Fernandez, H. Eletrochemical reduction of patulin and 5-hydroxymethylfurfural in both neutral and acid non-aqueous media. Their electroanalytical determination in apple juices. *Talanta* **111,** 85–92 (2013).

71. Starodub, N. F. & Slishek, N. F. Nano-Porous Silicon Based Immune Biosensor for the Control of Level of Mycotoxins. *Adv. Biosens. Bioelectron.* **2,** 7–15 (2013).

72. Pennacchio, A. *et al.* A surface plasmon resonance based biochip for the detection of patulin toxin. *Opt. Mater.* **36,** 1670–1675 (2014).

73. Pilolli, R., Monaci, L. & Visconti, A. Advances in biosensor development based on integrating nanotechnology and applied to food-allergen management. *Trends Anal. Chem.* **47,** 12–26 (2013).

74. Leonard, P. *et al.* Advances in biosensors for detection of pathogens in food and water. *Enzyme Microb. Technol.* **32,** 3–13 (2003).

75. Mello, L. D. & Kubota, L. T. Review of the use of biosensors as analytical tools in the food and drink industries. *Food Chem.* **77,** 237–256 (2002).

76. Mowat, A. M. Coeliac disease - A meeting point for genetics, immunology, and protein chemistry. *Lancet* **361,** 1290–1292 (2003).

77. Beaudoin, K. & Willoughby, D. S. The Role of the Gluten-Derived Peptide Gliadin in Celiac Disease. *J. Nutr. Heal. Food Eng.* **1,** 1–4 (2014).

78. Tack, G. J., Verbeek, W. H. M., Schreurs, M. W. J. & Mulder, C. J. J. The spectrum of celiac disease: epidemiology, clinical aspects and treatment. *Nat. Rev. Gastroenterol. Hepatol.* **7,** 204–213 (2010).

79. Allmann, M., Candrian, U., Höfelein, C. & Lüthy, J. Polymerase chain reaction (PCR): a possible alternative to immunochemical methods assuring safety and quality of food Detection of wheat contamination in non-wheat food products. *Z. Lebensm. Unters. Forsch.* **196,** 248–251 (1993).

80. Köppel, E., Stadler, M., Luthy, J. & Hubner, P. Detection of wheat contamination in oats by polymerase chain reaction (PCR) and enzyme-linked immunosorbent assay (ELISA). *Z. Leb. Unters. Forsch.* **206,** 399–403 (1998).

81. Nicolas, Y., Martinant, J. P., Denery-Papini, S. & Popineau, Y. Analysis of wheat storage proteins by exhaustive sequential extraction followed by RP-HPLC and nitrogen determination. *J. Sci. Food Agric.* **77,** 96–102 (1998).

82. Valdés, I., García, E., Llorente, M. & Méndez, E. Innovative approach to low-level gluten determination in foods using a novel sandwich enzyme-linked immunosorbent assay protocol. *Eur. J. Gastroenterol. Hepatol.* **15,** 465–474 (2003).

83. De Stefano, L. *et al.* Glutamine-binding protein from Escherichia coli specifically binds a wheat gliadin peptide. 2. Resonance energy transfer studies suggest a new sensing approach for an easy detection of wheat gliadin. *J. Proteome Res.* **5,** 1241–1245 (2006).

84. Nassef, H. M., Civit, L., Fragoso, A. & O'Sullivan, C. K. Amperometric immunosensor for detection of celiac disease toxic gliadin based on fab fragments. *Anal. Chem.* **81,** 5299–5307 (2009).

85. Chu, P.-T., Lin, C.-S., Chen, W.-J., Chen, C.-F. & Wen, H.-W. Detection of Gliadin in Foods Using a Quartz Crystal Microbalance. *J. Agric. Food Chem.* **60,** 6483–6492 (2012).

86. Maffini, M. V., Rubin, B. S., Sonnenschein, C. & Soto, A. M. Endocrine disruptors and reproductive health: The case of bisphenol-A. *Mol. Cell. Endocrinol.* **254-255,** 179–186 (2006).

87. Soares, A., Guieysse, B., Jefferson, B., Cartmell, E. & Lester, J. N. Nonylphenol in the environment: A critical review on occurrence, fate, toxicity and treatment in wastewaters. *Environ. Int.* **34,** 1033–1049 (2008).

88. Della Ventura, B., Schiavo, L., Altucci, C., Esposito, R. & Velotta, R. Light assisted antibody immobilization for bio-sensing. *Biomed. Opt. Express* **2,** 3223–3231 (2011).

89. Neves-Petersen, M. T. *et al.* High probability of disrupting a disulphide bridge mediated by an endogenous excited tryptophan residue. *Protein Sci.* **11,** 588–600 (2002).

90. Kerwin, B. A. & Remmele, Jr., R. L. Protect from light: photo- degradation and protein biologics. *J. Pharm. Sci.* **96,** 1468–1479 (2007).

91. Bent, D. V & Hayon, E. Excited state chemistry of aromatic amino acids and related peptides. III. Tryptophan. *J. Am. Chem. Soc.* **97,** 2612–2619 (1975).

92. Neves-Petersen, M. T. *et al.* Flash photolysis of cutinase: Identification and decay kinetics of transient intermediates formed upon UV excitation of aromatic residues. *Biophys. J.* **97,** 211–226 (2009).

93. Sherin, P. S., Snytnikova, O. a. & Tsentalovich, Y. P. Tryptophan photoionization from prefluorescent and fluorescent states. *Chem. Phys. Lett.* **391,** 44–49 (2004).

94. Funari, R. *et al.* Detection of Parathion Pesticide by Quartz Crystal Microbalance Functionalized with UV-Activated Antibodies. *Anal. Chem.* **85,** 6392–6397 (2013).

95. Funari, R. *et al.* Detection of parathion and patulin by quartz-crystal microbalance functionalized by the photonics immobilization technique. *Biosens. Bioelectron.* **67,** 224–229 (2015).

96. Ellman, G. L. Tissue sulfhydryl groups. *Arch. Biochem. Biophys.* **82,** 70–77 (1959).

97. Riddles, P. W., Blakeley, R. L. & Zerner, B. Reassessment of Ellman's reagent. *Methods Enzymol.* **91,** 49–60 (1983).

98. Riener, C. K., Kada, G. & Gruber, H. J. Quick measurement of protein sulfhydryls with Ellman's reagent and with 4,4'-dithiodipyridine. *Anal. Bioanal. Chem.* **373,** 266–276 (2002).

99. Lettieri, S. *et al.* Nano- and femtosecond UV laser pulses to immobilize biomolecules onto surfaces with preferential orientation. *Appl. Phys. A* **117,** 185–190 (2014).

100. Garidel, P., Hegyi, M., Bassarab, S. & Weichel, M. A rapid, sensitive and economical assessment of monoclonal antibody conformational stability by intrinsic tryptophan fluorescence spectroscopy. *Biotechnol. J.* **3,** 1201–1211 (2008).

101. Höök, F. *et al.* A comparative study of protein adsorption on titanium oxide surfaces using in situ ellipsometry, optical waveguide lightmode spectroscopy, and quartz crystal microbalance/dissipation. *Colloids Surf. B* **24,** 155–170 (2002).

102. Wiseman, M. E. & Frank, C. W. Antibody adsorption and orientation on hydrophobic surfaces. *Langmuir* **28,** 1765–1774 (2012).

103. Trilling, A. K., Beekwilder, J. & Zuilhof, H. Antibody orientation on biosensor surfaces: a minireview. *Analyst* **138,** 1619–1627 (2013).

104. San Paulo, A. & García, R. High-resolution imaging of antibodies by tapping-mode atomic force microscopy: attractive and repulsive tip-sample interaction regimes. *Biophys. J.* **78,** 1599–1605 (2000).

105. Müller, D. J. & Engel, A. The height of biomolecules measured with the atomic force microscope depends on electrostatic interactions. *Biophys. J.* **73,** 1633–1644 (1997).

106. Balmer, T. E., Christenson, H. K., Spencer, N. D. & Heuberger, M. The effect of surface ions on water adsorption to mica. *Langmuir* **24,** 1566–1569 (2008).

107. Moreno-Herrero, F., Colchero, J. & Baró, A. M. DNA height in scanning force microscopy. *Ultramicroscopy* **96,** 167–174 (2003).

108. Santos, S., Barcons, V., Christenson, H. K., Font, J. & Thomson, N. H. The intrinsic resolution limit in the atomic force microscope: Implications for heights of nano-scale features. *PLoS One* **6,** e23821 (2011).

109. Crowther, J. R. *ELISA: Theory and practice*. (Humana Press, 1995).

110. Nelson, D. L. & Cox, M. M. *Lehninger, Principles of Biochemistry*. (Freeman, 2005).

111. Peluso, P. *et al.* Optimizing antibody immobilization strategies for the construction of protein microarrays. *Anal. Biochem.* **312,** 113–124 (2003).

112. Amarasiri Fernando, S. & Wilson, G. S. Studies of the 'hook' effect in the one-step sandwich immunoassay. *J. Immunol. Methods* **151,** 47–66 (1992).

113. Schramm, W. & Paek, S. H. Antibody-antigen complex formation with immobilized immunoglobulins. *Anal. Biochem.* **205,** 47–56 (1992).

114. Barak, S., Mudgil, D. & Khatkar, B. S. Biochemical and Functional Properties of Wheat Gliadins: A Review. *Crit. Rev. Food Sci. Nutr.* **55,** 357–368 (2015).

115. Paananen, A. *et al.* Nanomechanical Force Measurements of Gliadin Protein Interactions. *Biopolymers* **83,** 658–667 (2006).

List of publications

1. **R. Funari**, B. Della Ventura, L. Schiavo, R. Esposito, C. Altucci and R. Velotta - "Detection of Parathion Pesticide by Quartz Crystal Microbalance Functionalized with UV-Activated Antibodies" *Anal. Chem.*, 85, 6392–6397 (2013), DOI: 10.1021/ac400852c.

2. S. Lettieri, A. Avitabile, B. Della Ventura, **R. Funari**, A. Ambrosio, P. Maddalena, M. Valadan, R. Velotta, C. Altucci - "Nano- and femtosecond UV laser pulses to immobilize biomolecules onto surfaces with preferential orientation" *Appl. Phys. A*, 117, 185-190 (2014), DOI: 10.1007/s00339-014-8340-4.

3. **R. Funari**, B. Della Ventura, R. Carrieri, L. Morra, E. Lahoz, F. Gesuele, C. Altucci, R. Velotta -"Detection of parathion and patulin by quartz-crystal microbalance functionalized by the photonics immobilization technique" *Bios. Bioelectron.*, 67, 224-229 (2015), DOI: 10.1016/j.bios.2014.08.020.

4. S. Longobardi, A. M. Gravagnuolo, **R. Funari**, B. Della Ventura, F. Pane, E. Galano, A. Amoresano, G. Marino, P. Giardina - "A simple MALDI plate functionalization by Vmh2 hydrophobin for serial multi-enzymatic protein digestions" *Anal. Bioanal. Chem.*, 407, 487-496 (2015), DOI: 10.1007/s00216-014-8309-3.

5. B. Della Ventura, **R. Funari**, Anoop K.K, S. Amoruso, F.Gesuele, R. Velotta, and C. Altucci, "Nano-machining of bio-sensor electrodes through gold nanoparticles deposition produced by femtosecond laser ablation" *Appl. Phys. B*, (2015), *In Press,* DOI: 10.1007/s00340-015-6091-3.

Detection of Parathion Pesticide by Quartz Crystal Microbalance Functionalized with UV-Activated Antibodies

Riccardo Funari, Bartolomeo Della Ventura, Luigi Schiavo, Rosario Esposito, Carlo Altucci, and Raffaele Velotta*

Department of Physics, Università di Napoli Federico II, Via Cintia, 26, Naples 80126, Italy

ABSTRACT: Photonic immobilization technique (PIT) has been used to develop an immunosensor for the detection of parathion. An antibody solution has been activated by breaking the disulfide bridge in the triad Trp/Cys-Cys through absorption of ultrashort UV laser pulses. The free thiol groups so produced interact with gold lamina making the antibody oriented upside, that is, with its variable parts exposed to the environment, thereby greatly increasing the detection efficiency. PIT has been applied to anchor polyclonal antiparathion antibodies to the gold electrode of a Quartz Crystal Microbalance (QCM) giving rise to very high detection sensitivity once the parathion is made heavier by complexion with BSA (bovine serum albumin), this latter step only required by the mass based transducer used in this case. The comparison of the sensor response with irradiated antibodies against different analytes shows that the high degree of antibody specificity is not affected by PIT nor is it by the complexion of parathion with BSA. These results pave the way to important applications in biosensing, since the widespread occurrence of the Trp/Cys-Cys residues triads in proteins make our procedure very general and effective to detect light analytes.
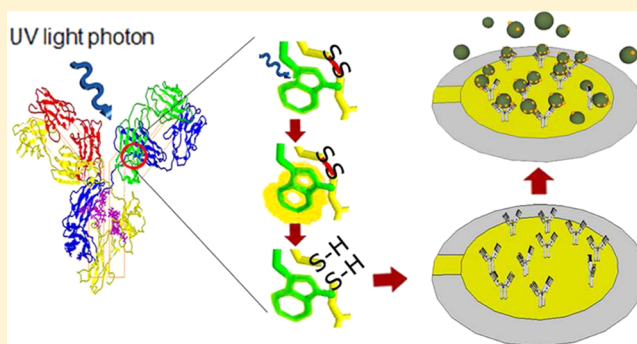
The high toxicity of pesticide residues and their bioaccumulation effects in human body underpins the research for fast response biosensors with high sensitivity and specificity for relatively light molecules.[1] Parathion (IUPAC name *O,O*-diethyl *O*-4-nitrophenil phosphorothioate) is an example of such compounds extensively used in agriculture as acaricide. As all the organophosphate insecticides, it is a selective inhibitor of acetylcholinesterase, an essential enzyme for nerve function in insects, humans, and many other animal species, thereby resulting highly toxic. The accumulation of this molecule leads to respiratory distress and muscular problems. Once absorbed, the parathion acts indirectly on the acetylcholinesterase since it is oxidized by enzymes of the host in its more reactive form, the paraoxon, which is capable of irreversible covalent binding the acetylcholinesterase.[2] The use of parathion is forbidden in the European Union.

Since the toxicity manifests its effects only several hours after exposure it is of paramount importance the availability of a tool allowing real-time analysis in environmental monitoring and particularly over agricultural waste. The lowest limit of detection (LOD) for parathion, and more in general measured for organophosphate, in aqueous solution has been achieved by Walker et al.[3] using a photonic crystal device. They developed a polymerized crystalline colloidal array (PCCA) photonic crystal sensing material that reaches a detection limit of 0.001 ppt. The crystals were coupled with acetylcholinesterase, which is irreversibly bonded by the organophosphate compound. The experiments were performed exposing the PCCAs to sample solutions as large as 100 mL thereby requiring up to 30 min for the analysis. Disadvantages of these devices include complex nanofabrication processes and the high cost of commercially modified substrates.

Amperometric devices allow rapid and low cost detection of organophosphates. A sensitive method for the detection of parathion has been developed by Zen et al.,[4] who reached a LOD of 50 nM (0.9 ppb) using a Nafion-coated glassycarbon electrode. Other detectors involve electrodes functionalized using organophosphorus hydrolase. Mulchandani et al.[5] reached a LOD of 20 nM (0.4 ppb) for both methyl-parathion and paraoxon, whereas Sacks et al.[6] efficiently detected parathion at nanomolar concentration. It is worth to mention that electrochemical devices are effective tools for analysis of aqueous solutions providing that the molecules to be detected are electroactive. In addition, this kind of sensors can be easily influenced by other oxidizable species that may well be present in a real sample.

Because of their cost-effectiveness, flexibility, and reliability, quartz crystal microbalance (QCM) based sensors have received an increasing interest in recent years[7,8] with wide applications to liquid samples. For instance, Bi and Yang[9] detected pesticides in aqueous environment using a QCM based method. They used molecular imprinted monolayers (MIMs), obtained from hexadecanethiol self-assembling on the

QCM gold electrode, to detect imidacloprid and thiacloprid in celery juice reaching a LOD of 1 μM by using an extremely sensitive QCM apparatus with a resolution of 0.1 Hz. Marx et al.[10] developed a sol−gel functionalization method based on MIP (molecularly imprinted polymer) films for the detection of parathion. They applied this technique for the development of both cyclic voltammetry devices and QCM based sensors, but despite their high sensitivity, sol−gel-based functionalizations can be easily affected by cross-sensitivity phenomena.

The sensor specificity is inherently warranted when antibodies are used as linkers, but in this case, the surface functionalization becomes a crucial phase in the realization of the sensor, the antibody orientation being one of the main issues.[11] Usually a biological molecule moves into aqueous environment and its functions are characterized by parameters, which can change significantly when the same molecule is, instead, immobilized. So, there is a strong interest in the research of new immobilization and functionalization techniques which allows better sensitivity and lower LOD as witnessed by the vast literature on this topics.[12,13]

The most suitable functionalization procedure depends both on the nature of the biological sensitive element and on the transduction principle. Besides that, functionalization of gold laminas entices many efforts in view of their use not only in QCM-based immunosensors[14−17] but also in surface plasmon resonance (SPR).[18−20] Moreover, gold is an inert metal having a low tendency to oxidize and is biocompatible and easily cleaned by chemical treatments such as piranha solution (a mixture of sulfuric acid and hydrogen peroxide). The stability of gold−sulfur interaction is one of the mechanisms exploited to immobilize molecules on a support, since the only requirement is the availability of a thiol group. To this end, it is possible both to use a chemical marker of the molecule, usually easy to realize by chemical synthesis, or to exploit existing thiol groups within proteins and peptides.[21]

UV induced immobilization is a novel technology that results in spatially oriented and spatially localized anchoring of biomolecules onto thiol-reactive surfaces as demonstrated by Neves-Petersen et al.[22] The reaction mechanism behind this immobilization technique involves the photonic activation of disulfide bridges, that is, the light-induced breakage of disulfide bridges in proteins through UV illumination of nearby aromatic amino acids.

In a previous paper, we have demonstrated that no pretreatment to the surface is necessary, the presence of this structural characteristic being the only condition required to apply this approach that we will refer as photonic immobilization technique (PIT).[23] The mechanism of photonic activation of the Trp/Cys-Cys triads and the crystallographic structure of a type G immunoglobulin (IgG)[24] are shown in figure 1. Basically, the UV photon energy is absorbed by Tryptophan and then transferred to the close Cys-Cys thereby forming free reactive thiol groups which interact with thiol-reactive surfaces (like gold plates or surfaces treated with alkanethiols). Thus, the "driving force" for a possible side-up orientation of the antibody onto the gold surface is provided by the open disulfide bridges; these are produced in a selective way because the occurrence of a solvent accessible triad Try/Cys-Cys, which is required by PIT, is limited to interdomain region.[22]

The UV radiation may reduce or vanish the biological activity of proteins and enzymes, causing also structural changes in the biomolecules,[25] but PIT preserves the native structure and the
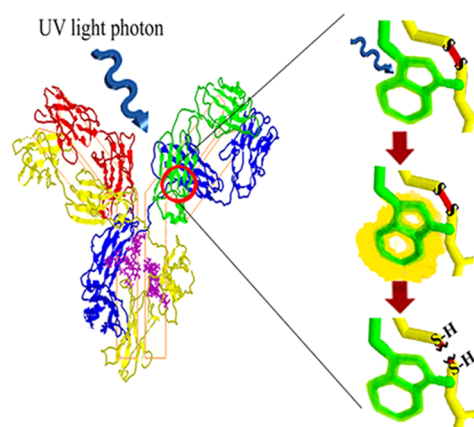
Figure 1. UV photonic activation of a generic IgG (1IGY). (a) The protein solution is irradiated. (b) One UV photon is absorbed by a tryptophan side-chain which transfers the energy to the near cysteines. (c) The disulfide bridge opens and the thiol groups so produced can effectively interact with the gold surface.

functional properties of the immobilized proteins while favoring the proper orientation of the biomolecule on the support,[23] and this is achieved by avoiding any chemical and thermal treatment.

One of the advantages of PIT relies in the wide field of application since the closely spaced triad of residues Trp/Cys−Cys is present in all members of the immunoglobulin superfamily. Every IgG has twelve intradomain disulfide bridges near a tryptophan residue, one of them being present in every domain of the protein. It is likely to induce the opening of these disulfide bonds through UV irradiation of the near aromatic residue. With the breaking of these disulfide bridges there is an increase of free thiol groups, which can react with a gold or thiol-rich surface. The same geometry of the Trp/Cys−Cys triad is observable in structures of several IgSF (immunoglobulin superfamily) molecules as well as in TCRs (T cell receptors), MHCs (major histocompatibility complex),[26] cell surface antigens (CD4 and CD8), and various cell-adhesion molecules. It is suggested that the conservation of the geometrical relationship between this three aminoacids is due to the role played by tryptophan in stabilizing or protecting the disulfide bridge.[27]

The proof of principle of PIT reported in our previous paper concerned the detection of murine immunoglobulin by QCM based immunosensor for which the sensitivity improved only by a factor of 2.[23] This result is in agreement with the findings reported in a recent paper by Trilling et al.[28] who show that the effect of the antibody orientation on the capture of the analyte is strongly dependent on the mass of the analyte. In particular, lighter analytes are more sensitive to the side-up orientation of the antibodies, so that PIT can render effective several techniques (e.g., QCM) otherwise impractical.

In this paper, we demonstrate how PIT improves the sensitivity of a QCM by about 1 order of magnitude compared to that achieved when the antibodies are tethered randomly oriented. The main drawback of a mass-based transducer like QCM in detecting light molecules (parathion weighs only about 300 Da), is the small frequency shift associated with their tethering to the antibody. We overcame this problem through a procedure that makes the molecules heavier so that a LOD of 4 ppb was achieved with an analysis requiring less than 10 min. We also demonstrate that PIT does not affect the specificity

features of the antibody as the test with similar compounds have shown.

■ EXPERIMENTAL SECTION

Chemicals. Antiparathion polyclonal antibodies were purchased from antibodies-online.com as rabbit serum (ABIN113883). Protein A agarose (Pierce) from Thermo Scientific has been used for the antibodies purification, whereas bovine serum albumin (A2153), parathion (45607), bisphenol A (239658), p-nonylphenol (46018), dichlorvos (45441), and paraoxon (36186) were purchased from Sigma-Aldrich. Since these compounds are highly toxic, all the samples were prepared in the fume hood. Other materials we have used are PBS 1× buffer solution pH 7.4, Helix water, sulfuric acid 98%, and hydrogen peroxide 30%.

Experimental Apparatus. The QCM is a μLibra from Technobiochip, Italy. The frequency variation of the balance in the cell is displayed on a connected computer by a producer-released software. The quartz crystals are from ICM Manufacturer, Oklahoma city (U.S.A.). They are AT-CUT quartz with a fundamental frequency of 10 MHz. The crystal diameter is 1.37 cm while the diameter of the gold lamina is 0.68 cm. The electrodes are cleaned using the Piranha solution (3:1 ratio between concentrated sulfuric acid and 30% hydrogen peroxide solution).

The fluidic apparatus consists of a GILSON peristaltic pump, Tygon silicone tubes with different diameters (0.51 mm for input into the cell and 0.64 mm for output) and the cell which contains the crystal placed on the electronic console for the measurement of frequency oscillation. The volume just above the electrode is approximately 40 μL and the fluidic apparatus is designed so that the whole replacement of the solution takes about 80 s when the flow rate is 3.3 μL/s. This was tested by measuring the time required by PBS to remove completely a colored solution (Flavin adenine dinucleotide) from the cell. The permanence of BSA above the electrode entails that this protein is still present when the parathion reaches the cell, so that a complex between the protein and the analyte is formed as a consequence of unspecific interactions. This is sketched in figure 2 where the BSA and the analyte are represented as big green and small orange balls, respectively. To check the complex formation between parathion and BSA we measured the BSA fluorescence spectrum (λ_{ex} = 278 nm) observing a
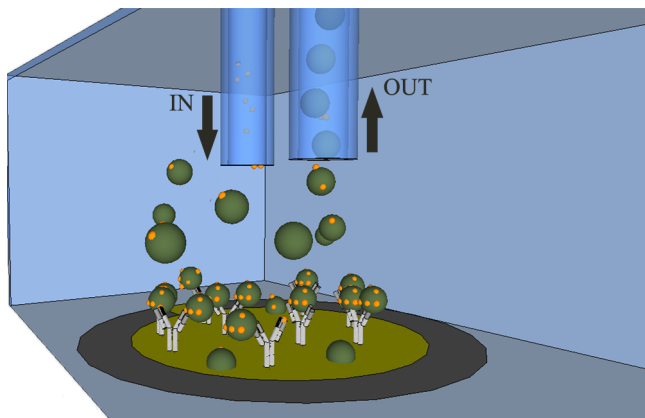
strong reduction of the yield as a function of the parathion concentration. This quenching effect of parathion on BSA fluorescence shows the interaction between these two partners.

The UV light source used is a custom femtosecond PHAROS laser system having a high tunable pulse repetition rate (Light Conversion, Ltd., www.lightcon.com). UV laser pulses having a length of approximately 120 fs are obtained coupling the laser with a harmonic generator stage (HIRO), which provides the conversion to 515, 343, or 258 nm wavelengths of the IR fundamental radiation.

UV Activation of the Antibody Solution. Aliquots of 1 mL, containing 5 μg of antiparathion polyclonal antibody, have been irradiated by means of the femtosecond laser system previously described. The laser source operates, in this case, at a pulse repetition rate of 10 kHz and delivers 250 mW of average power at λ = 258 nm (resulting in energy per pulse of 25 μJ). These irradiation conditions guarantee the maximum efficiency in disulfide bond breaking as demonstrated by Della Ventura et al.[23] through the Ellman's assay.[29]

QCM Protocol. The experimental protocol consists of the following steps: (1) Reaching of the basal frequency stabilization by washing the electrode surface with 1× phosphate buffer (PBS) pH 7.4. (2) UV-assisted adsorption or passive adsorption of antiparathion polyclonal antibodies. (3) Blocking the remaining gold free surface with bovin serum albumin (BSA) solution (50 μg/mL) to avoid nonspecific-interactions. (4) Flowing of parathion solution in the fluidic circuit that interacts with BSA solution still inside the volume above the electrode. The complex so formed is subsequently recognized by the antibody (see Figure 2). (5) Final washing step with PBS 1× to eliminate weakly bonded antigen.

Figure 3 shows typical QCM outputs obtained when the antibodies are irradiated (black continuous line) and not-irradiated (red dashed line). To be noted that the first drop in the frequency shift (~−300 Hz, step 2 of the protocol) is the same in both cases (irradiated and not irradiated) so that we can assume that PIT does not change the amount of antibody

Figure 2. Antigen binding on the functionalized gold electrode. The big green spheres are the BSA macromolecules which are complexed with the smaller antigens (orange spheres). The model is not in scale.
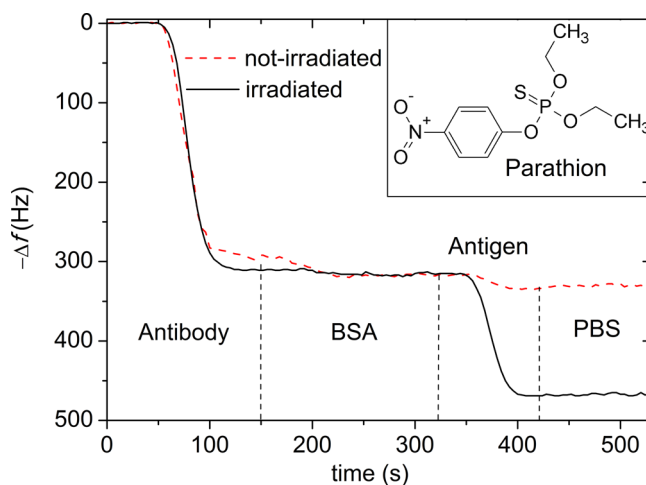
Figure 3. QCM responses of irradiated (black solid line) and not-irradiated (red dashed line) antibody samples with a protein concentration of 5 μg/mL. The first drop at ~50 s corresponds to the antibodies tethered to the electrode and is not affected by PIT, whereas the second drop at ~350 s is given by an antigen solution (parathion 51.5 μM) conveyed to the cell and is much larger when PIT is used. The vertical dashed lines show the steps described in the text.

tethered to the electrode. This is in fair agreement with the surface density measurements reported by Peluso et al. who studied the effects produced by orientation on both full-sized antibodies and Fab' fragments, finding comparable surface densities between aligned and not-aligned antibodies in three different cases (Mab602, Mab208, and Mab9647).[30]

When BSA reaches the electrode (step 3) no frequency shift is observed demonstrating that the surface is fully covered by antibodies. Subsequently, the analyte is conveyed to the electrode (step 4) and a completely different response is observed whether PIT is used or not. Such a difference is kept even when the electrode is washed by means of PBS (step 5).

■ RESULTS AND DISCUSSION

Sensitivity and LOD. The response of the QCM is proportional to the mass tethered to the electrode[31] so that the frequency shift $\Delta f(P)$, P being the concentration of parathion, is a measure of the amount of analyte bound to the antibodies. As reported in the Experimental Section, when the parathion reaches the volume above the electrode, the BSA solution is still there in high concentration thereby allowing the complex formation. The BSA molecules (approximately 66 kDa) bind the organophosphate compound by means of unspecific interactions and plays a "ballast" role, making the analyte "heavier" and detectable by a balance. In fact, even if all the antibodies on the electrode bound one parathion molecule (∼300 Da), the QCM frequency shift would be only few hertz and, thus, not detectable by our device. This has been verified by washing the fluidic circuit, thus removing the BSA, and checking that the parathion is not detectable any more, even if PIT is used. It is worth to stress that this unconventional labeling of the analyte does not affect the features of the sensor which is fully insensitive to BSA once the antibodies are tethered to the electrode. Figure 3 shows that when BSA is conveyed to the QCM the crystal oscillation frequency keeps constant (see the signal in the interval 150−330 s). Thus, with a relatively high concentration of BSA in the fluidic circuit we have compared the response of QCM to irradiated (PIT) and nonirradiated antibodies obtaining the results shown in figure 4.

It is readily seen that no significant signal is measurable when the parathion concentration is lower than 50 μM (15 μg/mL) if the antibodies are not irradiated, the signal being already in the saturation region in the opposite case. By considering the law of mass action and given the free diffusion conditions of our experiment, the analysis of the interaction kinetic between the analyte and the antibody leads to a Michaelis−Menten type equation:

$$\Delta f(P) = \frac{(\Delta f)_{sat}P}{P + K_M} \tag{1}$$

where $(\Delta f)_{sat}$ contains the instrument response and K_M is the so-called Michaelis−Menten constant. The former parameter includes the number of antibodies tethered on the balance as well as their effectiveness in capturing the analyte, that is, their orientation, whereas the latter provides estimation for the range of linearity of the realized sensor. The fitting of the experimental results obtained with irradiated antibodies by eq 1 (solid line in figure 4) provides $(\Delta f)_{sat} = 151 \pm 5$ Hz and $K_M = 2.2 \pm 0.7$ μM. The uncertainty in our measurements is due to instrumental limitations in the performances of our QCM, as well as to the fluctuations in some steps of the procedure. Although we expect a remarkable improvement of the
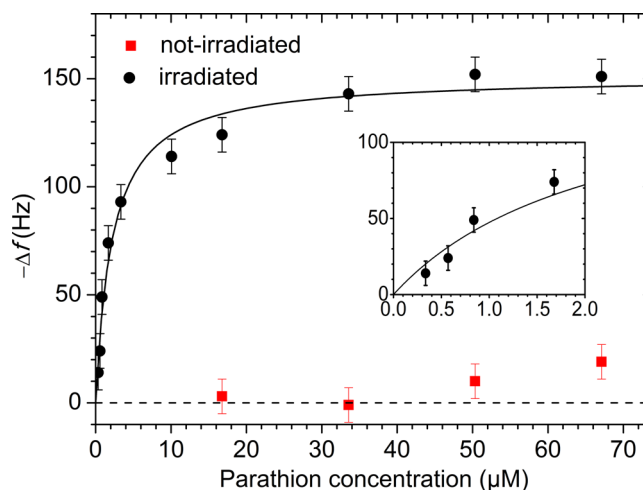
Figure 4. Response of the QCM versus the parathion concentration with irradiated (circles) and not-irradiated (squares) antibodies. The experimental points obtained with the irradiated antibody are fitted by a Michaelis−Menten type equation (black solid line). The low frequency change achieved when the antibody is not irradiated does not allow any significant fit of the experimental data. The inset is the enlargement of the low concentration region.

reproducibility by an up-to-date QCM as well as an improved fluidic circuit setup, currently we consider a conservative frequency error of 15 Hz (see also the inset in figure 4). Thus, a minimum frequency change $(\Delta f)_{min} = 15$ Hz is required for a measurement to be significantly different from zero. An evaluation of the lower LOD can, then, be obtained by inverting eq 1

$$LOD \approx \frac{(\Delta f)_{min}K_M}{(\Delta f)_{sat}} \approx 2 \times 10^{-7}M \approx 60 \; \frac{ng}{mL} \tag{2}$$

Since the concentration of water is about 55 M a LOD better than 4 ppb for parathion in water results from our functionalization technique applied to a QCM.

By considering the response at the concentration of 51.5 μM (see figure 4) we can estimate an increase in the sensitivity by at least 1 order of magnitude when PIT is used. Such a result can only be attributed to the side-up orientation of the antibodies and is much more significant than that achieved with heavier analytes,[23] in agreement with the mass dependence effects of antibody orientation recently reported by Trilling et al.[28]

Specificity. To test the sensor specificity, the same experimental procedure has been used for four compounds, progressively similar to parathion, from the chemical and structural point of view. They are bisphenol A (4,4′-(propane-2,2-diyl)diphenol), p-nonylphenol, dichlorvos (2,2-dichlorovin-yl dimethyl phosphate), and paraoxon (diethyl 4-nitrophenyl phosphate). At concentrations of approximately 1.7 μM, where parathion exhibits a significant response (see inset of Figure 4), all the four compounds showed no detectable frequency shift when they were tested separately. Thus, we tested the sensor response with a mixture of the four compounds at an even higher concentration (3.5 μM). thereby mimicking a real complex matrix. The results are reported in Figure 5a, where the last steps of the protocol are highlighted. The frequency shift measured when only the four compounds are in the solution is just few hertz (mix), but the frequency goes back to the previous value when PBS is made to flow (blue dotted line).
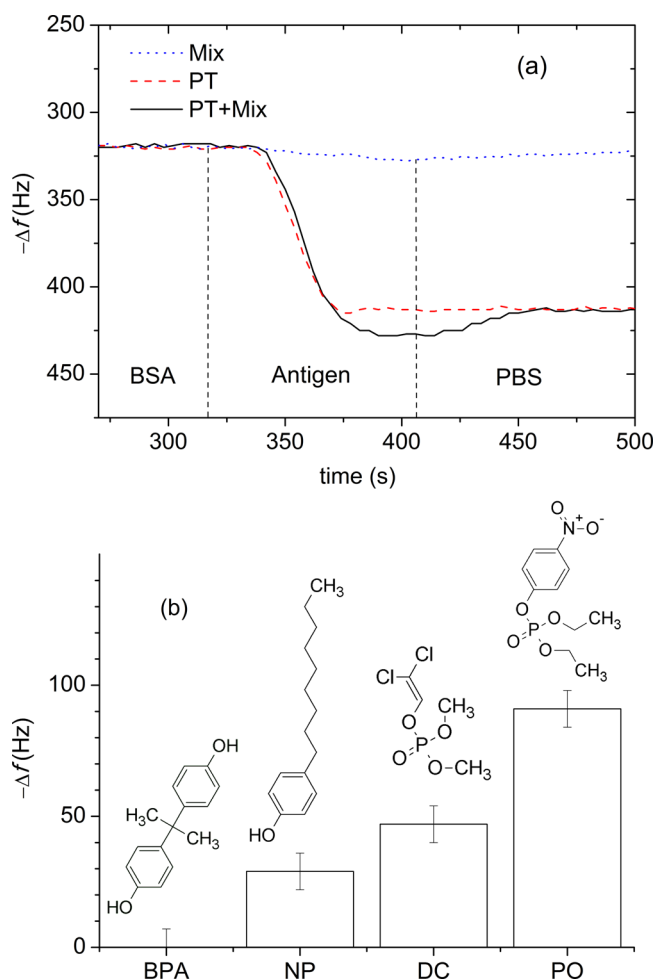
Figure 5. Sensor specificity i.e. sensor responses against different pollutants similar to parathion (their structures are reported in the panel b). (a) QCM response to parathion (PT) (red dashed line), to a mixture (mix) of bisphenol A (BPA), p-nonylpheno (NP), dichlorvos (DC), paraoxon (PO) (blue dotted line), and to PT + mix (solid black line). The concentration of all the compounds is 3.5 μM. (b) Frequency shift of the single compounds at the concentration of 172 μM, that is, one hundred times higher than that for which the parathion yields approximately 70 Hz.

The parathion alone at 3.5 μM gives rise to a frequency shift of approximately 90 Hz (red dashed line). The addition of the four compounds (Pt + mix) produces a slightly larger shift (solid black line) that disappear after purging with PBS. Thus, the concentrations were increased by 2 orders of magnitude (170 μM) compared to the initial one (1.7 μM), but despite such high concentration, the QCM responses were always lower than those provided by parathion in the saturation regime of the dose−response curve. It is also noticeable to look at the sensor response as a function of "similarity" with the parathion, reported in Figure 5b. Such data are internally consistent showing once again that the recognition capability of antibodies is unaffected by PIT.

■ CONCLUSIONS

The side-up orientation of antibodies is the most effective way to improve the sensitivity of immunosensors designed for light molecules and becomes a necessary condition when QCMs are going to be used. By applying the novel photonic immobilization technique to antibodies to be tethered to the gold electrodes of a QCM, we have been able to achieve a sensitivity that allows the detection of a light molecule like parathion (291.26 Da) in water with a LOD lower than 4 ppb (60 ng/mL). This value has been reached with a QCM capable to detect frequency shift of approximately 10 Hz and, although the resulting LOD is already competitive with those obtained with similar devices, we anticipate a significant improvement if an up-to-date QCM capable to detect frequency shift as low as 0.1 Hz is used.[9] Thus, in principle, by adopting PIT, as well as the complexion with a heavy molecule like BSA, we expect to be able to reach LOD much better than 1 ppb. This kind of immunosensor is inherently highly specific and provides fast response (only few minutes are required for the whole analysis). Moreover, in view of its flexibility and portability, such a device is suitable for in situ analysis. On the basis of our microscopic interpretation of the experimental findings and given the widespread presence of the triad Trp/Cys-Cys in all the antibodies, PIT can be considered as a general technique to anchor oriented antibodies on thiol reactive surfaces thereby paving the way to use this cost-effective technology for the detection of a variety of analytes.

■ AUTHOR INFORMATION

Corresponding Author

*E-mail: rvelotta@unina.it.

Notes

The authors declare no competing financial interest.

■ REFERENCES

(1) Liu, S.; Zheng, Z.; Li, X. *Anal Bioanal. Chem.* **2013**, *405*, 63−90.
(2) Milles, H. L.; Salt, H. *Br. Med. J.* **1950**, *2*, 444.
(3) Walker, J. P.; Asher, S. A. *Anal. Chem.* **2005**, *77*, 1596−1600.
(4) Zen, J.-M.; Jou, J.-J.; Senthil Kumar, A. *Anal. Chim. Acta* **1999**, *396*, 39−44.
(5) Mulchandani, P.; Chen, W.; Mulchandani, A. *Environ. Sci. Technol.* **2001**, *35*, 2562−2565.
(6) Sacks, V.; Eshkenazi, I.; Neufeld, T.; Dosoretz, C.; Rishpon, J. *Anal. Chem.* **2000**, *72*, 2055−2058.
(7) Cooper, M. A.; Singleton, V. T. *J. Mol. Recognit.* **2007**, *20*, 154−184.
(8) Becker, B.; Cooper, M. *J. Mol. Recognit.* **2011**, *24*, 754−787.
(9) Bi, X.; Yang, K.-L. *Anal. Chem.* **2009**, *81*, 527−532.
(10) Marx, S.; Zaltsman, A.; Turyan, I.; Mandler, D. *Anal. Chem.* **2004**, *76*, 120−126.
(11) Trilling, A. K.; Beekwilder, J.; Zuilhof, H. *Analyst* **2013**, *138*, 1619−1627.
(12) Nicu, L.; Leïchlé, T. *J. Appl. Phys.* **2008**, *104*, 111101.
(13) Jung, Y.; Jeong, J. Y.; Chung, B. H. *Analyst* **2008**, *133*, 697−701.
(14) Caruso, F.; Rodda, E.; Furlong, D. N. *J. Colloid Interface Sci.* **1996**, *178*, 104−115.
(15) Přibyl, J.; Hepel, M.; Halámek, J.; Skládal, P. *Sens. Actuators, B* **2003**, *91*, 333−341.
(16) Hao, R.; Wang, D.; Zhang, X.; Zuo, G.; Wei, H.; Yang, R.; Zhang, Z.; Cheng, Z.; Guo, Y.; Cui, Z.; Zhou, Y. *Biosens. Bioelectron.* **2009**, *24*, 1330−1335.
(17) Sharma, H.; Mutharasan, R. *Anal. Chem.* **2013**, *85*, 2472−2477.
(18) Byrne, B.; Stack, E.; Gilmartin, N.; O'Kennedy, R. *Sensors* **2009**, *9*, 4407−4445.
(19) Jiang, X.; Li, D.; Xu, X.; Ying, Y.; Li, Y.; Ye, Z.; Wang, J. *Biosens. Bioelectron.* **2008**, *23*, 1577−1587.
(20) Wang, Y.; Knoll, W.; Dostalek, J. *Anal. Chem.* **2012**, *84*, 8345−8350.
(21) Karyakin, A. A.; Presnova, G. V; Rubtsova, M. Y.; Egorov, A. M. *Anal. Chem.* **2000**, *72*, 3805−3811.
(22) Neves-Petersen, M. T.; Snabe, T.; Klitgaard, S.; Duroux, M. E. G.; Petersen, S. B. *Protein Sci.* **2006**, *15*, 343−351.

6396

dx.doi.org/10.1021/ac400852c | *Anal. Chem.* 2013, 85, 6392−6397

(23) Della Ventura, B.; Schiavo, L.; Altucci, C.; Esposito, R.; Velotta, R. *Biomed. Opt. Express* **2011**, *2*, 3223−3231.

(24) Harris, L. J.; Skaletsky, E.; McPherson, A. *J. Mol. Biol.* **1998**, *275*, 861−72.

(25) Neves-Petersen, M. T.; Gryczynski, Z.; Fojan, P.; Pedersen, S.; Petersen, E.; Petersen, S. B. *Protein Sci.* **2002**, *11*, 588−600.

(26) Snabe, T.; Røder, G. A.; Neves-Petersen, M. T.; Buus, S.; Petersen, S. B. *Biosens. Bioelectron.* **2006**, *21*, 1553−1559.

(27) Ioerger, T. R.; Du, C.; Linthicum, D. S. *Mol. Immunol.* **1999**, *36*, 373−386.

(28) Trilling, A. K.; Harmsen, M. M.; Ruigrok, V. J. B.; Zuilhof, H.; Beekwilder, J. *Biosens.Bioelectron.* **2013**, *40*, 219−226.

(29) Ellman, G. L. *Arch. Biochem. Biophys.* **1959**, *82*, 70−77.

(30) Peluso, P.; Wilson, D. S.; Do, D.; Tran, H.; Venkatasubbaiah, M.; Quincy, D.; Heidecker, B.; Poindexter, K.; Tolani, N.; Phelan, M.; Witte, K.; Jung, L. S.; Wagner, P.; Nock, S. *Anal. Biochem.* **2003**, *312*, 113−124.

(31) Sauerbrey, G. *Z. Phys.* **1959**, *155*, 206−222.

Nano- and femtosecond UV laser pulses to immobilize biomolecules onto surfaces with preferential orientation

**S. Lettieri · A. Avitabile · B. Della Ventura ·
R. Funari · A. Ambrosio · P. Maddalena ·
M. Valadan · R. Velotta · C. Altucci**

Abstract By relying on the photonic immobilization technique of antibodies onto surfaces, we realized portable biosensors for light molecules based on the use of quartz crystal microbalances, given the linear dependence of the method on the laser pulse intensity. Here, we compare the quality of the anchoring method when using nanosecond (260 nm, 25 mJ/pulse, 5 ns, 10 Hz rep. rate) and femtosecond (258 nm, 25 μJ/pulse, 150 fs, 10 kHz rep. rate) laser source, delivering the same energy to the sample with the same average power. As a reference, we also tethered untreated antibodies by means of the passive adsorption. The results are striking: When the antibodies are irradiated with the femtosecond pulses, the deposition on the gold plate is much more ordered than in the other two cases. The effects of UV pulses irradiation onto the antibodies are also analyzed by measuring absorption and fluorescence and suggest the occurrence of remarkable degradation when nanosecond pulses are used likely induced by a larger thermal coupling. In view of the high average power required to activate the antibodies for the achievement of the photonic immobilization technique, we conclude that femtosecond rather than nanosecond laser pulses have to be used.

1 Introduction

The quest for developing more and more sophisticated and efficient techniques for surface functionalization is of extreme importance in the current scenario of applied sciences, ranging from sensing [1, 2] to bioelectronics [3]. Here, we report on the role played by a pulsed UV radiation source in the surface functionalization of a quartz crystal microbalance (QCM) by means of the Photonic Immobilization Technique (PIT) for the detection of a light pesticide such as parathion (IUPAC name *O,O*-diethyl *O*-4-nitrophenil phosphorothioate) [2, 4]. In QCMs, the detection of the analyte occurs thanks to its specific recognition by bioreceptors (antibodies) immobilized on the sensor surface. The strategy to anchor bio-receptors on a metallic surface element is a key issue to improve the sensor performances and for any requirement of surface functionalization. We demonstrated an increase in the QCM sensitivity and its linear range extension when antibodies were irradiated with 258-nm laser pulses [2, 5]. It is important stressing that the increase in the antibodies efficiency due to laser pulse irradiation is linear with the peak intensity, namely the pulse power per unit surface, of the UV laser pulses in the investigated intensity range, as demonstrated in [2]. This has the consequence to rule out any nonlinear phenomenon essentially based on two-photon absorption in the antibody response, thus indicating the delivered energy dose as the laser source key parameter for antibody treatment. Such linear response, moreover, would somehow entail that any source delivering the same energy dose to the target, even

S. Lettieri · A. Avitabile · R. Funari · A. Ambrosio ·
P. Maddalena · M. Valadan · R. Velotta · C. Altucci (✉)
Dipartimento di Fisica, Università degli Studi di Napoli Federico
II, Complesso Universitario Monte S. Angelo, Via Cintia,
Naples 80126, Italy
e-mail: carlo.altucci@unina.it

S. Lettieri · A. Ambrosio
CNR-SPIN, UOS Napoli, Complesso Universitario Monte S.
Angelo, Via Cintia, Naples 80126, Italy

B. Della Ventura
Dipartimento di Fisica, Università di Roma, La Sapienza, Rome,
Italy

R. Velotta · C. Altucci
Consorzio Nazionale Interuniversitario per le Scienze Fisiche
della Materia, Naples, Italy

conventional lamps of photo-reactors, should be equally efficient in triggering the PIT mechanism. Nonetheless, we have found here that different UV sources imply very much different efficiencies in triggering PIT, due to the different nature of the stimulated molecular dynamics, once a single UV photon has been absorbed by an antibody. Here, we compare the quality of the PIT-based anchoring method when using nanosecond (260 nm, 25 mJ/pulse, 5 ns, 10 Hz rep. rate) and femtosecond (258 nm, 25 μJ/pulse, 150 fs, 10 kHz rep. rate) laser source, delivering the same energy dose to the sample. The results show that QCM is effective in the antigen detection only when PIT is realized with fs UV pulses.

The mechanism underlying the PIT relies on the photonic activation of disulfide bridges into the antibody, i.e., the light-induced breakage of the disulfide bridges in proteins through UV illumination of nearby aromatic amino acids [4]. Such a mechanism favors the proper orientation of the biomolecule on the surface so as the antibody can easily catch its antigen.

Nevertheless, irradiating biomolecules with 260-nm light leads to the denaturation of the molecules. Proteins and enzymes, for instance, can substantially reduce their biological activity as a consequence of induced structural changes [6]. Thus, we seek for the best trade-off between efficient tethering of the antibodies onto the surface, due to UV irradiation, and the lowest possible damage produced to the biomolecules. This latter feature was characterized by analyzing molecular absorption and fluorescence UV spectra: Differently from the femtosecond treatment case and likely due to thermal coupling, nanosecond UV pulses induce severe damages to the antibodies, as witnessed by significant changes in absorption and fluorescence spectra. Thus, femtosecond UV pulses confirm their capability to trigger important processes, otherwise inaccessible, even in antibodies beside their effectiveness already demonstrated in nucleic acids both in vitro [7] and in living cells [8].

2 PIT and its application to bio-sensing

We have recently demonstrated PIT to be an efficient method to anchor antibodies onto gold surfaces in order to realize sensors for the detection of heavy [2] and light [5] molecules. Briefly, the underlying idea is that, thanks to PIT based on fs UV pulse irradiation of antibodies, these proteins are tethered to the gold surface of a QCM-based biosensor with their variable part (i.e., the region that recognize the antigen,) pointing up[9–12]. The driving force for such a mechanism is provided by disulfide bridges disrupted by absorption of 260-nm photons; these are selectively produced since the occurrence of a solvent accessible triad Tryptophan/Cysteine–Cysteine, which is

required by PIT, is limited to the specific interdomain region of the antibody [4].

Details of device realization to detect heavy and light analytes, based on PIT, can be found elsewhere [2, 5]. Here, it is useful to summarize that the frequency variation of the quartz crystal microbalance is displayed and acquired in real time on a computer by producer-released software. The quartz crystal fundamental frequency is in our case 10 MHz. Antibodies and, successively, antigens are circulated in liquid phase by means of a fluidic apparatus consisting of a peristaltic pump and a cell containing the quartz crystal. The suitable antibody aqueous solution needed to detect the analyte is pre-treated by means of a preliminary irradiation in cuvette, to obtain the desired UV activation. In the case reported in Fig. 1, we detected a light pesticide, parathion, and used its polyclonal antibody having a concentration of 50 μg/1 mL. When using fs UV laser pulses, we utilized the fourth harmonic (258 nm, ≈180 fs, 25 μJ/pulse) of a PHAROS system operated at a repetition rate of 10 kHz, thus reaching the UV average power of 250 mW. The maximum efficiency in disulfide bond breaking was reached in this case after 60 s irradiation and monitored by the Ellman's assay on the irradiated antibodies that quantify the amount of thiol groups produced by UV absorption [13]. We tried also PIT with ns UV sources, by using the fourth harmonic (260 nm, ≈3 ns, 25 mJ/pulse) of a Nd:YAG system operated at 10-Hz repetition rate. The maximum efficiency in disulfide bond breaking was reached again after
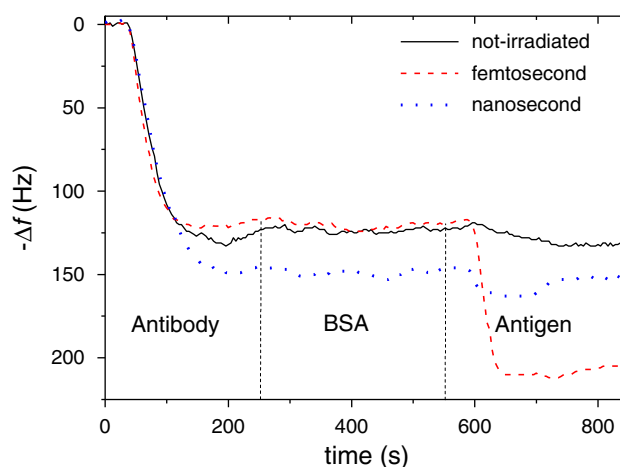
Fig. 1 QCM-based biosensor response for parathion detection in real time. *Black solid line* no PIT is used. *Red dashed line* femtosecond-based PIT is carried out. *Blue dotted line* nanosecond-based PIT is used. The first drop between ∼0 and 150 s corresponds to the antibodies tethered to the electrode and is poorly affected by PIT only with nanosecond irradiation, whereas the second drop at ∼550 s is given by an antigen solution (parathion 1.5 μM) conveyed to the cell and is effective only when femtosecond-based PIT is carried on. *The vertical dashed lines* show the steps of the protocol described in the text. The reported experiment was performed at a parathion concentration of 1.5 μM

60 s irradiation, although the corresponding Ellman's assay indicated that the number of opened disulfide bonds by fs treatment was about double than that for ns. Moreover, no measurable response of the sensor was detected for ns irradiation of the antibody in the above as well as in other tested conditions, indicating that PIT is highly efficient only when coupled to fs antibody irradiation.

A typical biosensor response for parathion detection is reported in Fig. 1, where the ordinary QCM response with no PIT is compared to PIT with fs and ns pulses, in the conditions of antibody concentration and laser irradiation reported above. The experimental protocol, which mimics the so-called SANDWICH [14] method widely spread in several biochemical assays, consists of the following steps. (1) Reaching of the basal frequency stabilization by washing the electrode surface with 1× phosphate buffer (PBS). (2) UV-assisted adsorption or passive adsorption of antiparathion polyclonal antibodies. (3) Wash with PBS to eliminate the excess of IgG. (4) Blocking the remaining gold-free surface with bovin serum albumin (BSA) solution (50 μg/mL) to avoid nonspecific interactions. (5) Flowing of PBS to clean the fluidic circuit. (6) Flowing of a para-thion-antibody sample where the labeled antigen is cap-tured by the immobilized antibodies. The mixture of pesticide and protein solution has been prepared 24 h before the experiment. By using a SANDWICH-type pro-tocol, we can make heavier and detectable the light para-thion analyte (∼300 Da), the antibody molecules playing the twofold role of "specific ballasts", rendering the device inherently specific. (7) Final washing step with PBS 1× eliminates weakly bonded antigen. We notice also that the first drop in the frequency shift (∼ −150 Hz, step 2 of the protocol) is nearly the same in all the cases, being the ns irradiation shift slightly higher than the other two cases, likely due molecular fragmentation induced by ns pulse irradiation, with the consequence of a partial deposit of small antibody peptides with no active recognition func-tion. Thus, in fair agreement with previous results [15], we can assume that PIT does not change the amount of anti-body immobilized onto the electrode. As a final result, we have that no measurable response is provided by the device both when the antibodies are tethered by spontaneous adsorption, and the PIT is realized with ns UV pulses, in contrast to the nice and very well detectable response of the QCM when fs-based PIT is used (≈100 Hz frequency shift is detected with a solution of 1 μM).

3 Optical characterization of activated antibodies

It is well known for long that technologies based on UV irradiation of biomolecules in general, and in particular proteins, imply a nonnegligible disadvantage as both molecular structure and biological activity can be severely affected. Thus, we characterized the effect of irradiating antibodies with UV fs laser pulses, which is an essential step of PIT [2, 5], in order to verify two important issues of our application: (1) Finding the irradiation conditions allowing the best trade-off between UV activation in PIT and protein denaturation and (2) Assuring that the funda-mental biological properties of the irradiated antibodies are preserved, in particular looking at the antigen-binding capability. This has been done by investigating the absorption and fluorescence UV spectra of irradiated pro-teins (nanosecond and femtosecond) in comparison with those of the nonirradiated species.

A typical UV absorption spectrum (recorded with the Jenway 6715 UV–visible spectrophotometer) displays two peaks at 220 nm (ammidic bond) and ≈280 nm (aromatic amino acids, particularly tryptophan). Generally, a nice and well-behaved peak at 280 nm indicates a protein well fol-ded with its natural conformation. This is, indeed, the case of the curves obtained for no irradiation (initial species) in Fig. 2 (a) and (b), where the UV absorption spectra of the anti-parathion are reported at several irradiation times for fs (a) and ns (b) laser irradiation. In both cases, the irra-diation leads to a significant change in the protein spectrum with the consequent almost complete disappearance of the peak at 280 nm. This phenomenon requires much shorter irradiation times if the protein sample is irradiated using the ns rather than the fs laser source. It is worth noticing that after short irradiation times (18, 30 and 60 s), there is still a shoulder at 280 nm. Spectral changes, in this case, can be due to a structural modification of the protein which does not affect the ability of the immunoglobulin to bind the antigen. This means that most likely such changes occurred in a region of the immunoglobulin far from the structural characteristic involved in the photonic activation (cys–cys trp triads), since PIT-enhanced immuno-recogni-tion of the antibody is properly working, as demonstrated by a very effective response of the QCM-based sensor.

Stationary fluorescence is a rapid, low-cost, and effec-tive method to monitor structural changes and is based on the emissions of intrinsic protein probes (the aromatic amino acids: tryptophan, phenylalanine, and tyrosine) which are strongly affected by both chemical environment and protein structure [16]. The photonic activation of antibodies results in the breakage of the sulfur–sulfur bonds placed nearby the tryptophan side chain so that the protein structure becomes less compact. The new conformations allow the penetration of water molecules inside the protein resulting in a change of the fluorescence spectrum. The data are acquired using a Perkin Elmer LS55 spectrofluo-rometer, the excitation wavelength being 278 nm. The fluorescence emission is mainly due to the tryptophan residues which strongly absorb at that wavelength. In
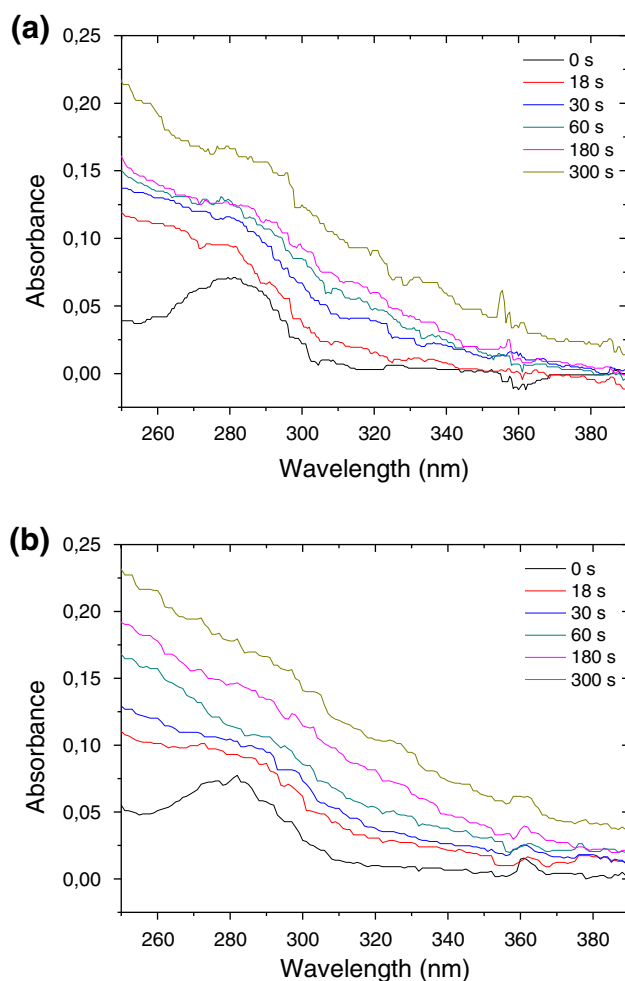
Fig. 2 UV Absorption spectra of antiparathion solutions for **a** fs and **b** ns UV pulse pre-treatment at various irradiation times. The antibody concentration is 50 µg/1 mL, whereas the laser source irradiation conditions are 25 µJ/pulse—10 kHz repetition rate for the 150-fs system and 25 mJ/pulse—10 Hz for the 3-ns source. In this way, the same UV dose is delivered to the target in the two cases in correspondence with the same irradiation time

Fig. 3 (a) and (b), we report the stationary fluorescence of antibody samples as function of the irradiation time using either fs (a) or ns (b) laser source. UV irradiation leads to two different phenomena: protein activation and denaturation. Given the optimal irradiation time for maximizing the sensor efficiency (60 s), we have found that the reduced emission has to be related to a prompt structural change that does not entail a complete denaturation, the latter occurring only after several minutes of irradiation. These two phenomena can be easily observed in Fig. 4 where the fluorescence signal integrated in the 320–370 nm range is reported. If the protein sample is irradiated using fs laser pulses, there is a prompt rapid variation in fluorescence emission related to protein activation and a subsequent decrease due to the denaturation. This difference is not so
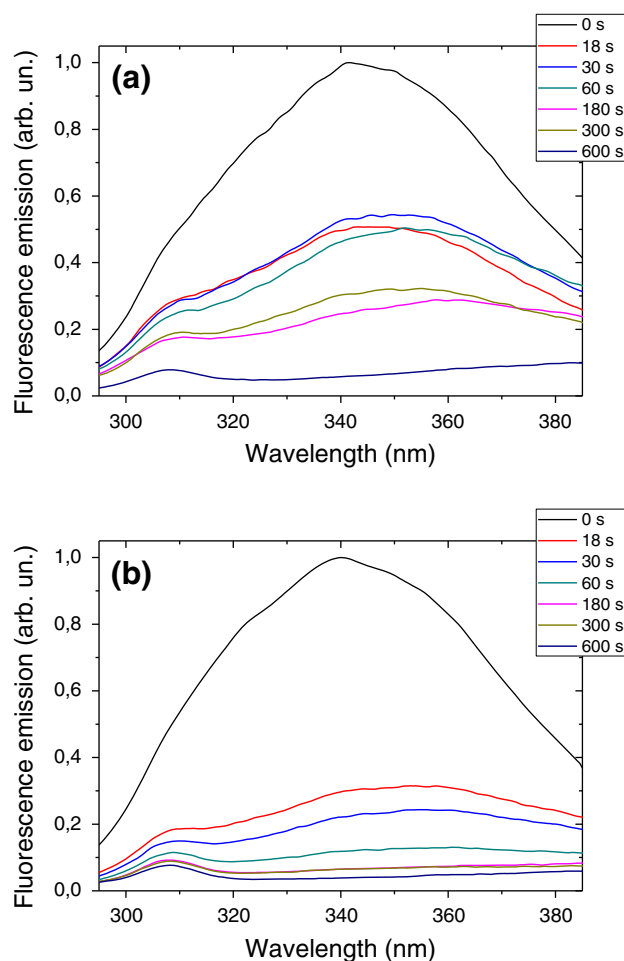
Fig. 3 UV Fluorescence spectra of antiparathion solutions for **a** fs and **b** ns UV pulse pre-treatment at various irradiation times. The excitation wavelength is 278 nm. Experimental parameters concerning antibody concentration and laser irradiation are the same as in Fig. 2

evident if the antibodies are irradiated using much more energetic UV pulses. Nanosecond irradiated antibodies show a more rapid drop in fluorescence emission due to denaturation phenomena.

The conformational change induced by the femtosecond laser source does not prevent the antibody from recognizing the analyte, while making more effective its orientation once immobilized on the gold surface of a QCM. On the other side, it is plausible that the irradiated antibody may lose its ability to recruit the elements required for the immune response. This "immune function" is related to a different part of the biomolecule and does not affect the antigen recognition [16, 17].

The solid lines in Fig. 4 are the result of best fits to the experimental points. For the nanosecond measurement, a single exponential model has been used, whereas a double exponential best fits the femtosecond behavior for which, indeed, we observed a much longer tail. The amplitudes of the
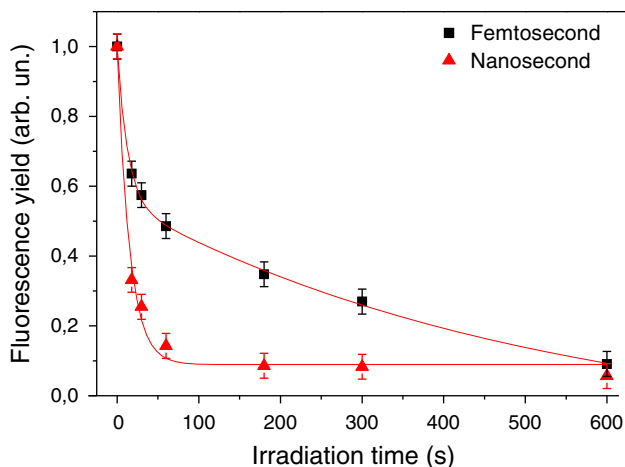
Fig. 4 Integrated fluorescence emission in the 320–370 nm spectral window for antiparathion activated with fs (*black squares*) and ns (*red triangles*) pulses versus the UV laser irradiation time. Red bold lines: best fits using a double exponential model for (**a**) and a single exponential model for (**b**)

two exponential decays turn out to be $A_{short} = 0.44 \pm 0.03$ and $A_{long} = 0.7 \pm 0.1$ for the short- and for long-lived decay, respectively. Most likely, such a substantial difference between nanosecond and femtosecond irradiation indicates a conformational change in the antibody occurring when femtosecond rather than nanosecond pulses are used for PIT. It is well known the fluorescence of proteins in the UV is mostly due to aromatic amino acids, and in particular to tryptophan, which has a fluorescence quantum yield about one order of magnitude higher than that of the tyrosine and phenylalanine [18]. It is also known that in a large number of cases, tryptophan fluorescence yield and dynamics in proteins are closely related to the molecular conformation as demonstrated for the electron transfer in myoglobins [19], for protein photo-activation in bacteria [20], and for the influence of tryptophan in ligand recognition of nicotinic receptors [21]. Such a change might be induced in the antibody only by shining femtosecond and not nanosecond pulses, as tryptophan exhibits two fluorescence lifetimes in the UV equal to ≈ 0.4 and ≈ 2.8 ns [22], in correspondence with the $S_0 \rightarrow {}^1L_a$ and $S_0 \rightarrow {}^1L_b$ transitions. These lifetimes are much longer than our femtosecond pulses, whereas they are shorter than the used nanosecond pulses. As a consequence, conformational changes induced in the antibody by the dynamics triggered by the $S_0 \rightarrow {}^1L_a$ and $S_0 \rightarrow {}^1L_b$ transitions in tryptophan can be observed only when using femtosecond pulse irradiation, since our relatively long nanosecond pulses will likely also deplete the excited ${}^1L_a$ and ${}^1L_b$ states due to stimulated emission. This has the natural counterpart, typical of the nanosecond regime, of inducing stronger damages than in the femtosecond case, due to thermal coupling.

4 Conclusions

We have shown here a successful application of fs pulse-based PIT to the realization of a portable immune-sensor for the detection of a light pesticide such as parathion. In particular, the application of fs pulse-based PIT to functionalize the electrode of a QCM sensor makes the difference between the possibility of a good sensing against no response at all from the device. Such a negative result occurs indeed both when passive adsorption and nanosecond PIT are used to functionalize the gold electrode.

We then characterized the effects of a robust 260-nm pulse irradiation onto the antiparathion molecules by measuring absorption and fluorescence spectra for initial and irradiated species in several different experimental conditions. We found that using fs pulse irradiation of the antibodies represents the best trade-off between efficient tethering of the antibodies onto the surface and the lowest possible damage induced to the biomolecules by UV radiation. This finding strongly suggests to carry on a dynamic study of the tryptophan UV photo-excitation into the antibody with the consequent relaxation and related conformational dynamics.

References

1. J.L. Arlett, E.B. Myers, M.L. Roukes, Nat. Nanotechnol. **6**(4), 203–215 (2011)
2. B. Della Ventura, L. Schiavo, C. Altucci, R. Esposito, R. Velotta, Biomed. Opt. Expr. **2**(11), 3223–3231 (2011)
3. J. Cheng, G. Zhu, L. Wu, X. Du, H. Zhang, B. Wolfrum, Q. Jin, J. Zhao, A. Offenhäuser, Y. Xu, J. Neurosci. Methods **213**(2), 196–203 (2013)
4. M.T. Neves-Petersen, T. Snabe, S. Klitgaard, M. Duroux, S.B. Petersen, Protein Sci. **15**(2), 343–351 (2006)
5. R. Funari, B. Della Ventura, L. Schiavo, R. Esposito, C. Altucci, R. Velotta, Anal. Chem. **85**, 6392–6397 (2013)
6. M.T. Neves-Petersen, Z. Gryczynski, Z. Fojan, S. Pedersen, E. Petersen, S.B. Petersen, Protein Sci. **11**, 588–600 (2002)
7. C. Russmann, M. Beato, J. Stollhof, C. Weiss, R. Beigang, Nucl. Acid Res. **26**, 3697 (1998)
8. C. Altucci, A. Nebbioso, R. Benedetti, R. Esposito, V. Carafa, M. Conte, M. Micciarelli, L. Altucci, R. Velotta, Laser Phys. Lett. **9**, 234–239 (2012)
9. F. Caruso, E. Rodda, D.N. Furlong, J. Colloid Interface Sci. **178**, 104–115 (1996)
10. J. Pribyl, M. Hepel, J. Halámek, P. Skládal, Sens. Actuators, B **91**, 333–341 (2003)
11. R. Hao, D. Wang, X. Zhang, G. Zuo, H. Wei, R. Yang, Z. Zhang, Z. Cheng, Y. Guo, Y. Zhou, Biosens. Bioelectron. **24**, 1330–1335 (2009)
12. H. Sharma, R. Mutharasan, Anal. Chem. **85**, 2472–2477 (2013)
13. G.L. Ellman, Arch. Biochem. Biophys. **82**, 70–77 (1959)

14. C. Davies, *The immunoassay handbook* (Stockton Press, New York, 1994)
15. P. Peluso, D.S. Wilson, D. Do, H. Tran, M. Venkatasubbaiah, D. Quincy, B. Heidecker, K. Poindexter, N. Tolani, M. Phelan, K. Witte, L.S. Jung, P. Wagner, S. Nock, Anal. Biochem. **312**, 113–124 (2003)
16. P. Garidel, M. Hegyi, S. Bassarab, M. Weichel, Biotechnol. J. **3**, 1201–1211 (2008)
17. C.A. Janeway Jr., P. Travers, M. Walport, and M.J. Schlomchiket, Immunobiology, Garland Science Ed. (2001)
18. J.R. Lakowicz, *Principles of fluorescence spectroscopy*, 3rd edn. (Springer, New York, 2006)
19. C. Consani, G. Auböck, F. van Mourik, M. Chergui, Science **339**, 1586–1589 (2013)
20. J. Léonard, E. Portuondo-Campa, A. Cannizzo, F. Van Mourik, G. Van der Zwan, J. Tittor, S. Haacke, M. Chergui, Proc. Nat. Ac. Sci. **106**, 7718–7723 (2009)
21. S.B. Hansen, Z. Radi¢, T.T. Talley, B.E. Molles, T. Deerinck, I. Tsigelny, P. Taylor, J. Biol. Chem. **277**, 41299–41302 (2002)
22. J.R. Albani, J. Fluoresc. **19**, 1061–1071 (2009)

Detection of parathion and patulin by quartz-crystal microbalance functionalized by the photonics immobilization technique

Riccardo Funari [a], Bartolomeo Della Ventura [a], Raffaele Carrieri [b], Luigi Morra [b], Ernesto Lahoz [b], Felice Gesuele [a], Carlo Altucci [a], Raffaele Velotta [a,*]

[a] CNISM and Dipartimento di Fisica, Università di Napoli "Federico II", Via Cintia, 26, Naples 80126, Italy
[b] Consiglio per la Ricerca e la Sperimentazione in Agricoltura – Unità di Ricerca per le Colture Alternative al Tabacco, Via P. Vitiello, 108, Scafati 84018, Italy

ABSTRACT

Oriented antibodies are tethered on the gold surface of a quartz crystal microbalance through the photonics immobilization technique so that limit of detection as low as 50 nM and 140 nM are achieved for parathion and patulin, respectively. To make these small analytes detectable by the microbalance, they have been weighed down through a "sandwich protocol" with a second antibody. The specificity against the parathion has been tested by checking the immunosensor response to a mixture of compounds similar to parathion, whereas the specificity against the patulin has been tested with a real sample from apple puree. In both cases, the results are more than satisfactory suggesting interesting outlook for the proposed device.

© 2014 Elsevier B.V. All rights reserved.

1. Introduction

The effective detection of small molecular weights analytes is of paramount importance in a wide range of scientific topics like investigating the molecular recognition phenomena and sensing of toxic molecules (Cooper and Singleton, 2007; Geschwindner et al., 2012; Jones et al., 2013; Vashist and Vashist, 2011). In particular, in the field of environmental monitoring it would be of great importance the availability of cost-effective and sensitive tools allowing the detection of low soluble and harmful compounds like steroids, herbicides, pesticides, toxins and combustion products like polycyclic aromatic hydrocarbon (PAH). As case studies to test our approach, we focused on parathion (IUPAC name O,O-diethyl O-4-nitrophenil phosphorothioate, MW=297 Da) and patulin (IUPAC name 4-hydroxy-4,6-dihydrofuro[3,2-c]pyran-2-one, MW= 154 Da), which share a relatively low molecular weight and high interest for environment and health safety. Parathion is an organophosphate pesticide widely used to enhance agricultural production, but for its toxicity (Milles and Salt, 1950) it is now forbidden within the European Union which sets the limits of pesticide residues in food between 50 and 100 µg/kg (Commission Regulation (EC) no. 839/2008). Patulin is an example of mycotoxin which is most likely to be found in crops as a result of fungal

infection. Both molecules are highly resistant to degradation and the patulin high toxicity for human and animal health has been recently pointed out in a review by Puel et al. (2010). Patulin level in food is strictly regulated in European countries (Commission Regulation (EC) no. 1881/2006) which set a maximum level of 50 µg/kg for fruit juices and derived products, 25 µg/kg for solid apple products and 10 µg/kg for baby foods. Both parathion and patulin are usually quantified by exploiting expensive, time consuming and relatively complex techniques like high-performance-liquid-chromatography (HPLC) and/or mass spectrometry [see (Blasco et al., 2004; Carabias Martinez et al., 1992; Kwakman et al., 1992) for parathion and (Berthiller et al., 2014; Pereira et al., 2014) for patulin]. Thus, the lack of any commercial and standard immunochemical methods underpins the research for biosensor based detection allowing *in situ* and real-time analysis for environmental monitoring and food quality control.

Amperometric devices are used for parathion in view of their feature to provide cheap, rapid and effective analysis of aqueous samples if the molecules to be detected are electroactive. Zen et al. (1999) developed a sensitive technique for the detection of parathion using a Nafion-coated glassycarbon electrode thus reaching a limit of detection (LOD) of 50 nM. Other sensing strategies are based on electrodes functionalized using enzymes like organophosphorus hydrolase. Exploiting this principle Mulchandani et al. (2001) were able to detect methyl-parathion and paraoxon with a LOD of 20 nM. Even if this kind of devices

* Corresponding author. Tel.: +39 081 6 76148.
  E-mail address: rvelotta@unina.it (R. Velotta).

offers several advantages for water analysis, electrochemical detection can be easily influenced by other oxidizable molecules eventually present in a real sample.

Electrochemical (Vidal et al., 2013), optical (Pereira et al., 2014) and piezoelectric (Pohanka et al., 2007; Prieto-Simón and Campàs, 2009), sensors and biosensors for the detection of mycotoxins are reported in literature, but quite few results are reported for patulin detection. A fluorescence assay was proposed by De Champdoré et al. (2007) with a LOD of 10 µg/L (less than 0.1 µM), but no test on a real sample was carried out. Damián Chanique et al. (2013) have developed a detection method based on the electrochemical reduction of patulin using glassy carbon electrodes. With this strategy they reached a LOD of 300 nM quantifying patulin in commercial apple juices. Starodub and Slishek (2012) proposed a nano-porosus silicon based immunosensor for measuring the level of patulin and T2 mycotoxin in real samples reaching a sensitivity of about 10 ng/mL for both pollutants. More recently, Pennacchio et al. (2014) proposed a competitive surface plasmon resonance (SPR) based bioassay with an estimated LOD of 0.1 nM, but it is worth noticing that the accuracy of SPR measurements can be influenced by interfering effects like temperature and sample composition fluctuation which produce a change in the refractive index not related to the analyte binding.

In view of their robustness, flexibility and cost-effectiveness, quartz crystal microbalance (QCM) technology has achieved an important role in fields like sensing, material science, environmental monitoring and protein studying (Vashist and Vashist, 2011). It is possible use QCM devices for small molecule detection exploiting several principles and configurations (Cooper and Singleton, 2007). All these advantages led to a wide range of publications involving QCM based detection of both pesticides and mycotoxins. For instance, Bi and Yang (2009) used molecular imprinted monolayers (MIMs) self-assembled onto the QCM gold electrode to effectively detect imidacloprid and thiacloprid pesticides in celery juice. They used an extremely sensitive QCM device getting a LOD of 1 µM. Concerning mycotoxin detection an indirect competitive immunological strategy has been adopted by Jin et al. (2009) for the quantification of aflatoxin B1. They significantly improved the sensitivity of the QCM based biosensor coupling the indirect competitive immunoassay with biocatalyzed deposition amplification using enzyme labeled secondary antibodies. Horseradish peroxidase was used to catalyze the oxidation of 4-chloro-1-naphthol to form an insoluble product which deposits onto the QCM electrode thus resulting in a huge increase in the sensor response. This procedure requires several time consuming incubation steps and allows to reach a LOD of about 32 pM.

Surface functionalization is one the main issue in biosensor development, in fact, recent publications show the strong interest in the research of innovative immobilization and functionalization strategies which provide better sensitivity and lower LOD (Jung et al., 2008; Nicu and Leïchlé, 2008). In particular, protein orientation is of paramount importance for immobilized antibodies which have to well expose their sensitive parts, the so called antigen binding sites, to effectively capture the antigens. Trilling et al. (2013) have recently investigated the relationship between analyte characteristics and capture molecule anchoring showing that the uniform orientation of the recognition elements provides a huge systematic improvement in sensitivity for weak interactions. They observed that the smaller the molecule, the lower the epitope number per analyte and, hence, the more important is the orientation of the sensitive biomolecule. By an appropriate antibody surface functionalization, Funari et al. (2013) were able to use a simple transducer like quartz-crystal microbalance (QCM) to detect a concentration of about 200 nM of parathion. This result was achieved by adopting the photonic immobilization technique (PIT) (Della Ventura et al., 2011), so that a gold surface fully

covered by oriented antibodies was realized, but also by "weighing down" the molecule through the complexion of parathion with bovine serum albumin (BSA). Since not all the molecules are able to complex with BSA, in this paper we propose a more general approach leading to higher sensitivity and specificity. Essentially, parathion and patulin are "weighed down" by the same antibodies used for the detection onto QCM, mimicking the so called sandwich configuration widely used in the ELISA assays. To this end, the pollutant sample is mixed with an antibody solution before the latter is conveyed to the QCM and LODs of approximately 50 nM and 140 nM are achieved for parathion and patulin, respectively.

2. Materials and methods

2.1. Chemicals

Parathion (45607) and patulin (P1639) were purchased from Sigma-Aldrich. Anti-parathion (ABIN113883) and anti-patulin (AS11-1699) polyclonal antibodies were purchased as rabbit sera from antibodies-online.com and Agrisera respectively. The type G immunoglobulins were purified using the Protein A Antibody Purification Kit (PURE1A) from Sigma-Aldrich. 5,5′-dithiobis-(2-nitrobenzoic acid) also known as Ellman's reagent (D8130), bovine serum albumin (A2153) and the compounds used for the specificity tests, bisphenol A (239658), p-nonylphenol (46018), dichlorvos (45441), diazinon (45428) and paraoxon (36186), were from Sigma-Aldrich. The pollutant samples were prepared using PBS $1 \times$ buffer solution in the fume hood. Helix water, sulfuric acid 98% and hydrogen peroxide 40% were used for the cleaning procedure of the QCM gold surfaces.

2.2. Patulin extraction from real sample

For the specificity test, we used real samples of patulin extracted from apple puree obtained from apple processing plant. To this end a commercial kit (Polyintell Affinimip® SPE cartridges) was used. The extraction was performed as follows: 10 g of apple puree were treated with 150 µL of a pectinase enzyme solution followed by 10 mL water and mixed. Solution was left at room temperature overnight, or for 2 h at 40 °C, centrifuged at 4500g for 5 min and then filtered with a 0.2 µM filter. This solution is used as the loading solution. SPE Cartridge was conditioned with 2 mL of acetonitrile (ACN), then with 1 mL of deionised water. 5 mL of the loading solution was put in the cartridge, which was subsequently washed with 4 mL of deionized water containing 1% of acetic acid. Water was forced down into the cartridge. The cartridge was treated with 1 mL of CHCl$_3$ and patulin was eluted with 2 mL of ACN containing 1% acetic acid. The SPE procedure lasted approximately 30 min. The elution fraction was then evaporated and dissolved in water containing 0.1% acetic acid. This fraction was submitted to a Perkin Elmer HPLC with UV detector to determine the patulin concentration. The same sample was used in QCM validation analysis.

2.3. UV laser source

The immunoglobulin samples were irradiated using the UV laser pulses provided by a custom femtosecond PHAROS laser system with high tunable pulse repetition rate coupled with a harmonic generator stage (HIRO) which allows the conversion to 515 nm, 343 nm and 258 nm wavelengths of the IR fundamental radiation. Both PHAROS and HIRO were from Light Conversion Ltd.

2.4. Quartz crystals

The quartz oscillators (151218) are from ICM, Oklahoma city (USA). They are AT-CUT quartz with a fundamental frequency of 10 MHz. The crystal and the gold electrode diameters are 1.37 cm and 0.68 cm respectively. The gold surfaces are cleaned by immersing the oscillators for 1 min in a glass beaker containing Piranha solution (5:1 ratio between concentrated sulfuric acid and 40% hydrogen peroxide solution), then the quartzes are washed with helix water. The whole cleaning procedure is performed in the hood and can be repeated 3–4 times before the quartz needs to be changed. The QCM device is a μLibra from Technobiochip, Italy. The gold-quartz wafer is placed on the electronic console and the resonance frequency of the oscillator is monitored by producer released software. The QCM is integrated in a microfluidic circuit consisting of the cell which contains the oscillator, platinum threaded silicon tubes and a GILSON peristaltic pump. The volume of the circuit is about 300 μL and the flow rate is 3 μL/s. A gentle cleaning with glycine HCl 0.2 M at pH 2.8 allows the removal of only the antigen without significant loss of the tethered antibodies thus leading to the regeneration of the functionalized gold surface. This procedure can be safely applied approximately three times.

2.5. UV activation of antibody solution

Photonic immobilization technique (PIT) (Della Ventura et al., 2011) is a method to immobilize antibodies onto gold based on the photonic reduction of disulfide bridges in proteins by UV illumination of near aromatic amino acid (Neves-Petersen et al., 2002). PIT leads to antibodies oriented side-up i.e. they expose the Fab onto thiol-reactive surfaces like gold plates. The only requirement for applying this technique is the presence into the protein of a closely spaced tryptophan/cysteine–cysteine (Trp/Cys–Cys) triad which is a typical structural characteristic of the immunoglobulin family (Ioerger et al., 1999). The details of this photonic activation have been recently reported by Neves-Petersen et al. (2012). Basically the UV-excitation of tryptophan can result in its photoionization thus generating solvated electrons which are captured by the near electrophillic species like cystines. In this case the result is the breakage of the disulfide bridge thereby generating new thiol functions (red part in the constant region of the antibody) which can easily react with other free thiol groups or with thiol reactive surfaces like gold plates. The rise of the number of the SH groups onto the protein allows new structural conformation for the immobilized immunoglobulin which are characterized by a well exposure of the antigen binding sites thus greatly improving sensor sensitivity. It is well known that UV radiation strongly affects both structure and activity of biomolecules, but we have recently demonstrated that the photonic activation of immunoglobulins by femtosecond UV pulses does not affect their ability to capture the antigen (Funari et al., 2013; Lettieri et al., 2014).

To realize the PIT, antibody samples of 500 μL with a protein concentration of 50 μg/mL were activated using the UV laser source previously described (Fig. 1). In order to find the irradiation conditions which maximize the number of thiol groups per molecule we exploited the so called Ellman's assay (Ellman, 1959) (data not shown). For both anti-parathion and anti-patulin antibodies, the irradiation conditions are $\lambda = 258$ nm, 10 kHz repetition rate, 250 mW of average power, and 1 min irradiation time.

2.6. QCM measurements

Before the experiment each pollutant sample has been incubated for 30 min with the same volume of immunoglobulin solution at a fixed concentration (25 μg/mL), corresponding to an
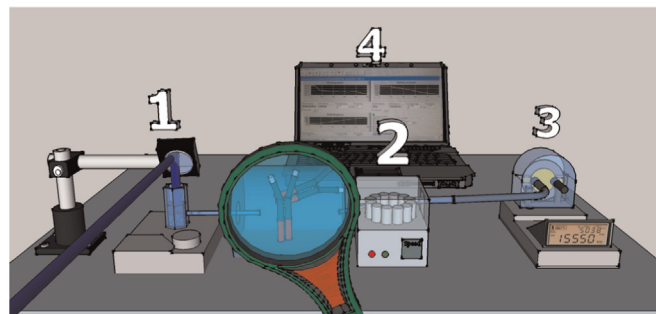
Fig. 1. Experimental layout for PIT. The antibodies are "activated" in the cuvette (1) and conveyed through a peristaltic pump (2) to the QCM (3). The electronics of the QCM is interfaced with a PC (4) so that the frequency shift due to the antibody tethering is controlled in real time. The white end of the antibodies in the pipe is the antigen binding site, whereas the red part highlights the region where the free thiols are produced. (For interpretation of the references to color in this figure legend, the reader is referred to the web version of this article.)

initial concentration of Ab$_{free}$ (*free* antibody in solution) of $[Ab_{free}]_0 \approx 0.17$ μM. This mixture is then tested by the QCM based immunosensor. The experimental procedure consists in the flowing of different solutions onto the gold sensitive surface of the crystal using the fluidic apparatus previously described. Typical QCM outputs involving either irradiated or non-irradiated antibodies in the detection of parathion are shown in Fig. 2.

The first step is the reaching of the basal frequency stabilization by flowing PBS solution. Then the surface is functionalized using either irradiated or non-irradiated antibody sample. This step gives rise to a first frequency drop of about 140 Hz, which is the same in both conditions showing that PIT does not affect significantly the total amount of tethered antibodies. This result is in fair agreement with the surface density measurements reported by Peluso et al. (2003) and can be explained by considering that even oriented side up the antibodies can tether with an arbitrary azimuthal, which prevents the possibility to line them up. Subsequently, a washing step with PBS is used to purge the circuit from the excess of immunoglobulins. Then a BSA solution (50 μg/mL) flows into the cell filling the remaining free space on the gold surface. This blocking step is crucial in order to avoid non-specific
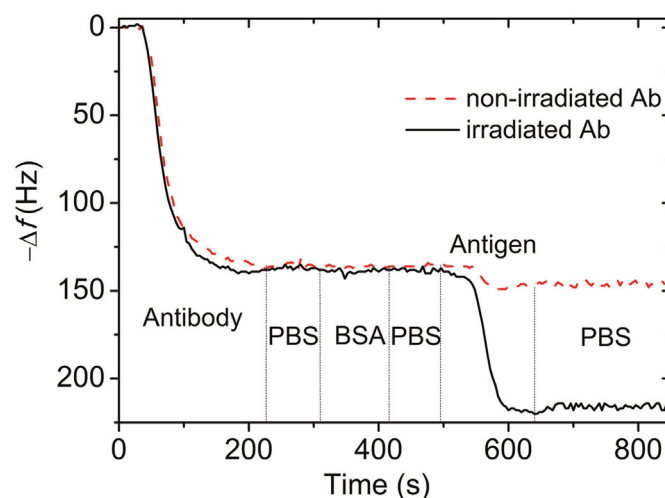
Fig. 2. QCM-based immunosensor outputs for parathion detection using either irradiated (black solid line) or non-irradiated (red dashed line) antibodies. The first frequency shift at about 150 s corresponds to the antibody immobilization onto the sensor surface, while the second drop at about 550 s is due to the detection of analyte–antibody complex (parathion 0.85 μM). The vertical dashed lines highlight the phases of the protocol described in the text. (For interpretation of the references to colour in this figure legend, the reader is referred to the web version of this article.)
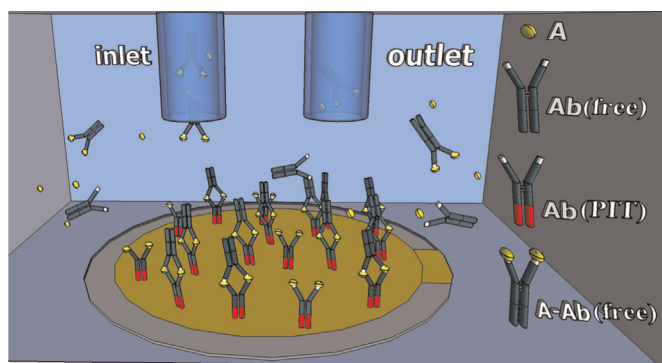
Fig. 3. Sketch of the cell containing the surface detector. The antibodies activated by the PIT are shown with their lower part in red and are tethered side-up on the gold electrode. The solution flowing through the cell contains analyte (small yellow particles) bound to the Ab (green Y-shape), but also "free" Ab and "free" analytes. When a free analyte is recognized by the Ab tethered to the gold, there is no effect on the QCM frequency since the deposited mass is too small. Only when the "sandwich" configuration is realized there is a detectable response. (For interpretation of the references to colour in this figure legend, the reader is referred to the web version of this article.)

interactions between the further flowing molecules and the gold plate. It is worth notice that this phase results in a negligible change in the resonance frequency, therefore proving that the gold surface is quite completely covered by the antibodies. After another cleaning step with PBS, the analyte–antibody sample flows into the circuit and the labeled antigens are captured by the immobilized antibodies, thus resulting in the second frequency shift. This signal is much bigger when the sensor surface is functionalized using UV activated antibodies. A final washing step is then used to remove weakly bonded analytes.

It is important to highlight that in this scheme three species can interact with the sensor (Fig. 3): A (antigen), A–Ab$_{free}$ (antigen–antibody complex) and Ab$_{free}$ (antibody).

The advantage of the simultaneous injection of the three species (A, Ab$_{free}$ and A–Ab$_{free}$) rather than the sequential injection of A and Ab$_{free}$, as it occurs in the "standard sandwich ELISA" protocol (Crowther, 1995), relies in the higher *effective* concentration of the analyte in the interaction volume. In fact, due to the stationary equilibrium conditions occurring in the interaction volume of the QCM, when the antibodies are mixed with the solution to be analyzed, the *effective* antigen concentration in the interaction volume coincides with the antigen concentration in the original solution. On the opposite, when the original solution is injected first into QCM and the antibody is injected in a second

step after a necessary washing (as in the "standard sandwich ELISA" protocol), the *effective* antigen concentration is lower since there are no free antigens that could replace those detached from the QCM plate by the free antibodies. This, in turn, leads to a reduction of the QCM frequency shift which we measured to be approximately two. Since the aim of this work was the search for the highest sensitivity, the injection of the solution mixed with antibodies was preferred. The drawback of such an approach relies in the need of high antibody concentration in the original solution so that virtually all the antigens are bound and the probability of finding free antigen is negligible. At antigen concentration much higher than the antibody concentration there will be free antigens that would bind the antibodies tethered to the gold plate. In this case the QCM will not provide a detectable signal because of the low antigen mass giving rise to the so-called "hook effect" which can be shifted to high analyte concentration by simply increasing the antibody concentration (Amarasiri Fernando and Wilson, 1992).

3. Results and discussion

The response of the QCM is proportional to the mass tethered to the electrode (Sauerbrey, 1959) so that through the measurement of the frequency shift $\Delta f([A]_0)$, we measure the concentration of the analyte in the solution. While a detailed description of the process in terms of chemical kinetic would require a complex analysis which should also include the diffusion of the several species, we can easily model the observed dynamics by considering the law of mass action and the free diffusion conditions of our experiment. In fact, in this case a Michaelis–Menten type equation is expected to well describe the process when $[A]_0 \ll [Ab_{free}]_0$:

$$\Delta f([A]_0) = \frac{(\Delta f)_{sat}[A]_0}{K_M + [A]_0} \tag{1}$$

In Eq. (1) $(\Delta f)_{sat}$ contains the instrument response and K_M is the so-called Michaelis–Menten constant. The former parameter includes the number of antibodies tethered on the balance as well as their effectiveness in capturing the analyte, i.e. their orientation, whereas the latter provides an estimation of the linear range of the sensor. As explained in Section 2.6, an excess of analyte concentration in the original solution ($[A]_0 \gg [Ab_{free}]_0$) makes high the probability that tethered antibodies bind the analytes (A) rather than the complexed analytes (A–Ab$_{free}$), but due to the small mass of the analyte such a recognition does not lead to a measurable frequency shift. Thus, when [A] increases and the
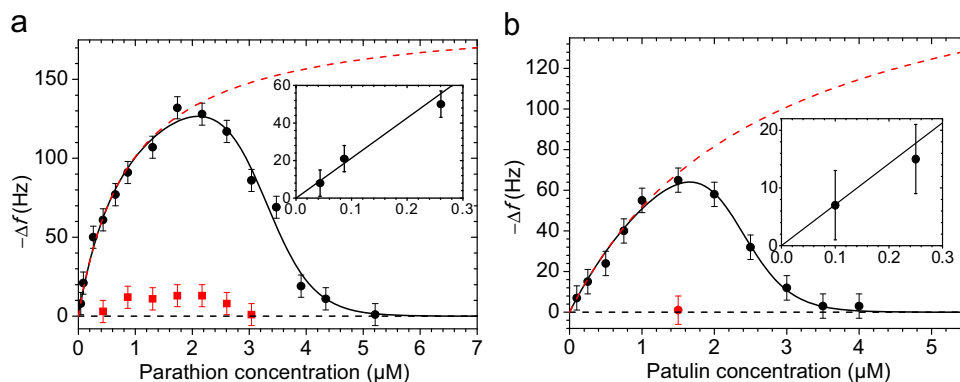
Fig. 4. Response of the QCM to (a) parathion and (b) patulin concentrations when the antibody is irradiated (circle points) and not irradiated (square points). The points achieved with the irradiated antibody are fitted by Eq. (2) (bold line). The low frequency change achieved when the antibody is not irradiated does not allow any significant fit of the experimental data. The inset is the enlargement of the low concentration region, whereas the dashed red lines are the plots of Eq. (1), i.e. the inhibition effect of the free antigens is hampered by high Ab$_{free}$ concentration. (For interpretation of the references to color in this figure legend, the reader is referred to the web version of this article.)

Table 1
Values of the three free parameters as deduced from the best fit of the experimental data.

	K_M [μM]	b [μM]$^{-1}$	$[A]_M$ [μM]
Parathion	0.90 ± 0.05	2.4 ± 0.1	3.3 ± 0.1
Patulin	2.70 ± 0.05	3.0 ± 0.1	2.3 ± 0.1

condition $[A]_0 \approx [Ab_{free}]_0$ is reached an "inhibition effect" starts and further increase of [A] results in a reduction of Δf rather than in its increase. This is observable in Fig. 4 where at low [A] the frequency shift follows Eq. (1), whereas a reduction of the frequency shift occurs at high analyte concentration. A simple way to model the inhibition role played by the free analyte is through a two parameters logistic function, in which one parameter accounts for the analyte concentration at which the inhibition becomes important and the other takes into account the decay rate of the available recognition site. Thus, we can fit our experimental results with the following function:

$$\Delta f([A]_0) = \frac{(\Delta f)_{sat}[A]_0}{K_M + [A]_0} \times \frac{1}{1 + e^{b([A]_0 - [A]_M)}} \quad (2)$$

In the Eq. (2) b and $[A]_M$ are two free parameters accounting for the different kinetics the analytes and antibodies may have, whereas $(\Delta f)_{sat} = 192 \pm 2$ Hz has been determined by measuring the saturation value one measures when a layer of antibodies covers the surface. Although such a value refers to irradiated antibodies, it is essentially the same even when the antibodies are not irradiated (Della Ventura et al., 2011).

The fitting of the experimental results obtained with irradiated antibodies by Eq. (2) (solid black lines in both panels of Fig. 4) provides the results reported in Table 1, while the square red points in Fig. 4 are the results obtained if PIT is not adopted and the antibodies are only tethered spontaneously on the gold. In this latter case it is readily seen that no significant signal is measurable. The dashed red lines in Fig. 4 are the plots of Eq. (1), i.e. the response one obtains when $[Ab_{free}]_0 \gg K_M$, showing that an initial Ab concentration of 1 mg/mL is more than enough in many practical conditions to achieve a monotonic response from our sensor.

The uncertainty in our measurements is due to instrumental limitations in the performances of our QCM as well as to the unavoidable fluctuations in the several steps of the procedure. Assuming an overall error of 10 Hz, (see also the insets in Fig. 4) so that a minimum frequency change $(\Delta f)_{min} = 10$ Hz is required for a measurement to be significantly different from zero, an evaluation

of the lower LOD can be obtained by inverting Eq. (1)

$$LOD \approx \frac{(\Delta f)_{min}K_M}{(\Delta f)_{sat}}. \quad (3)$$

Eq. (3) leads to a LOD in water of approximately 50 nM and 140 nM, for parathion and patulin, respectively.

To ascertain the sensor specificity, the same experimental procedure has been used to test the response of the QCM when compounds similar to the analytes to be detected are in the solution. For parathion, we prepared a mixture of bisphenol A (4,4′-(propane-2,2-diyl)diphenol), p-nonylphenol, dichlorvos (2,2-dichlorovinyl dimethyl phosphate), diazinon (O,O-diethyl O-[4-methyl-6-(propan-2-yl)pyrimidin-2-yl] phosphorothioate), and paraoxon (diethyl 4-nitrophenyl phosphate) each of them at a concentration of 2 μM. When only this mixture is made to flow into the QCM no response is provided by the sensor (black solid line in Fig. 5(a)). On the opposite, when parathion at 0.2 μM is added to this mixture, the sensor exhibits a frequency shift of approximately 35 Hz (dashed red line in Fig. 5(a)) in very good agreement with the curve shown in Fig. 4(a) (see the inset), thereby evidencing that pollutants other than parathion have no effect in the QCM response.

As it concerns patulin, Fig. 5(b) reports the QCM response to real samples previously analyzed by HPLC. When there is no patulin in the extract from apple puree, no frequency shift is observed (black solid line); on the opposite, when we analyze extracts from apple puree containing 0.2 μM and 1.0 μM of patulin measured by HPLC, the response of QCM (− 12 Hz and − 43 Hz, for the two concentrations, respectively) is in very satisfactory agreement with the calibration curve reported in Fig. 4(b). It is worth mentioning, that the real samples we analyzed contained all the possible analytes which could potentially interfere with the patulin measurement; nevertheless, our results show that the technique and the protocol adopted is robust and highly specific.

4. Conclusion

We report here a method to detect light molecules which combines the recently proposed Photonic Immobilization Technique for the antibody functionalization of the gold surfaces, and the antibody-sandwich protocol, to realize an immunosensor based on a QCM. Essentially, in our device the antigen is recognized by its own antibody and the resulting solution is conveyed to the balance. While PIT is shown to largely increase the sensitivity of QCM, the sandwich protocol has a twofold effect: on the one hand it weighs down light molecules, so that they can be "weighed" by QCM, on the other hand it inherently increases even more the
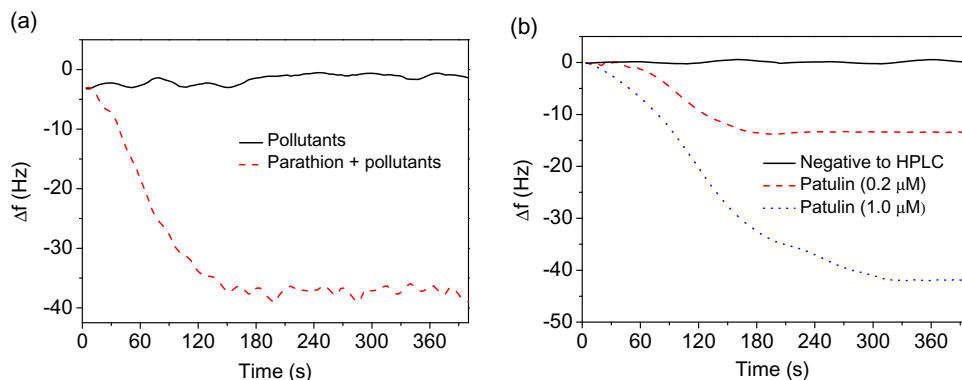
Fig. 5. Sensor specificity i.e.. QCM responses against different pollutants. (a) Parathion at 0.2 μM tested against bisphenol A, p-nonylphenol, dichlorvos, diazinon and paraoxon each of them at 2 μM. (b) Extract from apple puree previously analyzed by HPLC. (——) Negative to patulin; (‑‑‑) 0.2 μM patulin; (·····) 1 μM patulin. (For interpretation of the references to color in this figure, the reader is referred to the web version of this article.)

specificity of the whole device. The sandwich protocol proposed here considers the inclusion of free antibody in the solution to be analyzed, so that the formation of the analyte-antibody complex takes place in the cuvette, and a subsequent injection of the whole solution into QCM. Compared to the typical sandwich ELISA protocol, in which the solution is conveyed as it is to the tethered antibodies and the second antibody is added after a washing, our approach leads to higher sensitivity, the drawback of the decrease of the signal in presence of high analyte concentration being easily overcome by using higher antibody concentration in the mixing volume. On the opposite, one of the advantages of our immuno-sensors relies in its generality, since in practice antibodies can be produced for any analyte. We have applied our device to parathion and patulin for which LODs of 50 nM and 140 nM were achieved, respectively. In a scenario with lack of simple and reliable immunochemical analysis for two important analytes such as parathion and patulin, our QCM based immunosensor has notice-able advantages in terms of rapidity in the response (only few minutes are required), flexibility and portability, lending itself appropriate for *in situ* analysis.

Acknowledgments

References

Amarasiri Fernando, S., Wilson, G.S., 1992. J. Immunol. Methods 151, 47–56.
Berthiller, F., Burdaspal, P.A., Crews, C., Iha, M.H., Krska, R., Lattanzio, V.M.T., MacDonald, S., Malone, R.J., Maragos, C., Solfrizzo, M., Stroka, J., Whitaker, T. B., 2014. World Mycotoxin J. 7, 3–33.
Bi, X., Yang, K.-L., 2009. Anal. Chem. 81, 527–532.
Blasco, C., Fernández, M., Picó, Y., Font, G., 2004. J. Chromatogr. A 1030, 77–85.
Carabias Martinez, R., Rodriguez Gonzalo, E., Amigo Moran, M.J., Hernandez Mendez, J., 1992. J. Chromatogr. A 607, 37–45.
Cooper, M.A., Singleton, V.T., 2007. J. Mol. Recognit. 20, 154–184.

Crowther, J.R., 1995. ELISA: Theory and Practice. Humana Press, Totowa, NJ.
Damián Chanique, G., Heraldo Arévalo, A., Alicia Zon, M., Fernández, H., 2013. Talanta 111, 85–92.
De Champdoré, M., Bazzicalupo, P., De Napoli, L., Montesarchio, D., Di Fabio, G., Cocozza, I., Parracino, A., Rossi, M., D'Auria, S., 2007. Anal. Chem. 79, 751–757.
Della Ventura, B., Schiavo, L., Altucci, C., Esposito, R., Velotta, R., 2011. Biomed. Opt. Express 2, 3223–3231.
Ellman, G.L., 1959. Biophysics 82, 70–77.
Funari, R., Della Ventura, B., Schiavo, L., Esposito, R., Altucci, C., Velotta, R., 2013. Anal. Chem. 85, 6392–6397.
Geschwindner, S., Carlsson, J.F., Knecht, W., 2012. Sensors 12, 4311–4323.
Ioerger, T.R., Du, C., Linthicum, D.S., 1999. Mol. Immunol. 36, 373–386.
Jin, X., Jin, X., Liu, X., Chen, L., Jiang, J., Shen, G., Yu, R., 2009. Anal. Chim. Acta 645, 92–97.
Jones, A.M., Grossmann, G., Danielson, J.Å., Sosso, D., Chen, L.-Q., Ho, C.-H., Frommer, W.B., 2013. Curr. Opin. Plant Biol. 16, 389–395.
Jung, Y., Jeong, J.Y., Chung, B.H., 2008. Analyst 133, 697–701.
Kwakman, P.J.M., Vreuls, J.J., Brinkman, U.A.T., Ghijsen, R.T., 1992. Chromatographia 34, 41–47.
Lettieri, S., Avitabile, A., Della Ventura, B., Funari, R., Ambrosio, A., Maddalena, P., Valadan, M., Velotta, R., Altucci, C., 2014. Appl. Phys. A, http://dx.doi.org/10.1007/s00339-014-8340-4, in press.
Milles, H.L., Salt, H.B., 1950. Brit Med. J. 2, 444.
Mulchandani, P., Chen, W., Mulchandani, A., 2001. Sci. Technol. 35, 2562–2565.
Neves-Petersen, M.T., Petersen, S., Gajula, G.P., 2012. In: Satyen Saha (Ed.). UV Light Effects on Proteins: From Photochemistry to Nanomedicine in Molecular Photo-chemistry: Various Aspects. Tech-Open Access Company. http://dx.doi.org/10.5772/37947. Available from: http://www.intechopen.com/books/molecular-photochemistry-various-aspects/uv-light-effects-on-proteins-from-photochemistry-to-nanomedicine.
Neves-Petersen, M.T., Gryczynski, Z., Lakowicz, J., Fojan, P., Pedersen, S., Petersen, E., Bjørn Petersen, S., 2002. Protein Sci. 11, 588–600.
Nicu, L., Leïchle, T., 2008. J. Appl. Phys. 104, 111101.
Peluso, P., Wilson, D.S., Do, D., Tran, H., Venkatasubbaiah, M., Quincy, D., Heidecker, B., Poindexter, K., Tolani, N., Phelan, M., Witte, K., Jung, L.S., Wagner, P., Nock, S., 2003. Anal. Biochem. 312, 113–124.
Pennacchio, A., Ruggiero, G., Staiano, M., Piccialli, G., Oliviero, G., Lewkowicz, A., Synak, A., Bojarski, P., D'Auria, S., 2014. Opt. Mater. (Amst) 36, 1670–1675.
Pereira, V.L., Fernandes, J.O., Cunha, S.C., 2014. Trends Food Sci. Technol. 36, 96–136.
Pohanka, M., Jun, D., Kuca, K., 2007. Drug Chem. Toxicol. 30, 253–261.
Prieto-Simón, B., Campàs, M., 2009. Monatshefte für Chem. – Chem. Mon. 140, 915–920.
Puel, O., Galtier, P., Oswald, I.P., 2010. Toxins 2, 613–631.
Sauerbrey, G., 1959. Z. Phys. 155, 206–222.
Starodub, N.F., Slishek, N.F., 2012. Adv. Biosens. Bioelectron. 2, 7–15.
Trilling, A.K., Harmsen, M.M., Ruigrok, V.J.B., Zuilhof, H., Beekwilder, J., 2013. Biosens. Bioelectron. 40, 219–226.
Vashist, S.K., Vashist, P., 2011. J. Sensors 2011, 1–13.
Vidal, J.C., Bonel, L., Ezquerra, A., Hernández, S., Bertolín, J.R., Cubel, C., Castillo, J.R., 2013. Biosens. Bioelectron. 49, 146–158.
Zen, J.-M., Jou, J.-J., Senthil Kumar, A., 1999. Anal. Chim. Acta 396, 39–44.

A simple MALDI plate functionalization by Vmh2 hydrophobin for serial multi-enzymatic protein digestions

**Sara Longobardi · Alfredo Maria Gravagnuolo · Riccardo Funari ·
Bartolomeo Della Ventura · Francesca Pane · Eugenio Galano ·
Angela Amoresano · Gennaro Marino · Paola Giardina**

Abstract The development of efficient and rapid methods for the identification with high sequence coverage of proteins is one of the most important goals of proteomic strategies today. The on-plate digestion of proteins is a very attractive approach, due to the possibility of coupling immobilized-enzymatic digestion with direct matrix-assisted laser desorption/ionization (MALDI)-time of flight (TOF)-mass spectrometry (MS) analysis. The crucial step in the development of on-plate immobilization is however the functionalization of the solid surface. Fungal self-assembling proteins, the hydrophobins, are able to efficiently functionalize surfaces. We have recently shown that such modified plates are able to absorb either peptides or proteins and are amenable to MALDI-TOF-MS analysis. In this paper, the hydrophobin-coated MALDI sample plates were exploited as a lab-on-plate for noncovalent immobilization of enzymes commonly used in protein identification/characterization, such as trypsin, V8 protease, PNGaseF, and alkaline phosphatase. Rapid and efficient on-plate reactions were performed to achieve high sequence coverage of model proteins, particularly when performing multiple enzyme digestions. The possibility of exploiting this direct on-plate MALDI-TOF/TOF analysis has been investigated on model proteins and, as proof of concept, on entire whey milk proteome.

This article is dedicated to the memory of Prof. Alessandro Ballio, a Master of Life and Science.

S. Longobardi (✉) · A. M. Gravagnuolo · F. Pane · E. Galano · A. Amoresano · G. Marino · P. Giardina
Department of Chemical Sciences, University of Naples "Federico II", Via Cintia 4, 80126 Naples, Italy
e-mail: sara.longobardi@unina.it

R. Funari · B. Della Ventura
Department of Physics, University of Naples "Federico II", Via Cintia 4, 80126 Naples, Italy

Introduction

Mass spectrometry-based proteomics is currently the most valuable analytical tool for identification of proteins present in complex biological samples such as cell lysates, body fluids, or tissues [1]. In a typical bottom-up analytical strategy, proteins are enzymatically digested into peptide fragments, before a mass spectrometric (MS) analysis. Peptide mass mapping and MS/MS sequence analysis are key methods currently used in protein identification [2, 3]. It is generally considered that the in-solution digestion is the most time-consuming step in this workflow. The enzyme/substrate ratio has to be kept low (generally 1:50) to prevent protease autodigested products. For this reason, the incubation with free proteases is usually performed for 12–24 h at 37 °C to achieve an efficient proteolysis.

To try to address the demands of reducing digestion times, while maintaining high sequence coverage, immobilization of proteases onto a solid support has emerged as a promising alternative to the in-solution digestion. Immobilization leads to increased enzyme stability, reduced autolysis, and improved digestion efficiency due to the increased enzyme-to-protein ratio [4–6]. Trypsin is the most widely used enzyme in proteomics [7–10], particularly due to its restricted specificity (Arg-X, Lys-X) [11]. Several methods for trypsin immobilization have been explored, such as adsorption [12–15], encapsulation [16, 17], and covalent binding [18, 19]. Different materials (such as silica, PTFE, magnetic nanoparticles, and so on) have also been tested for both offline digestion and microfluidic devices [20–23].

Despite the many advantages of trypsin, the use of other proteases or other enzymes is often necessary. Tryptic digestion can often result in limited sequence coverage [24] because of the following: (i) lack or excess of Lys and Arg residues, (ii) length of the digested fragments due to missed cleavages, and (iii) the presence of posttranslational modification (i.e., phosphorylation and glycosylation) which can affect the extent of digestion and/or lower the ionization efficiency. To overcome these potential issues, the use of other enzymes, including pepsin [25, 26] chymotrypsin [27, 28], and alkaline phosphatase [28], has been suggested.

The application of matrix-assisted laser desorption/ionization (MALDI)-time of flight (TOF) on-plate digestion is a very attractive strategy due to the possibility of coupling immobilized-enzymatic reactions with direct mass spectrometry analysis [29–31]. However, to the best of our knowledge, no multi-enzymatic digestion directly on MALDI plate has so far been reported. The crucial step in development of on-plate enzyme immobilization is in reality the functionalization of the solid surface.

Design and realization of stable bio/non-biointerfaces able to immobilize biomolecules are key features in several processes. In particular, protein immobilization on surfaces is currently a hot topic in biotechnology, since commercial solutions are of limited availability. It is worth considering that it is extremely difficult to find a common surface suitable for the adsorption of different proteins having a broad range of molecular weights and physicochemical properties, such as charge and hydrophobicity [32].

Recent studies from our research group have demonstrated an efficient surface functionalization by means of a nanostructured layer of amphiphilic proteins, named hydrophobins [33].

Hydrophobins are a family of small amphipathic proteins produced by filamentous fungi, able to self-assemble on hydrophobic or hydrophilic solid surfaces [34]. Due to their interesting properties, several biotechnological applications have been reported [35–37]. In particular, hydrophobin coating has been used as an intermediate layer to attach cells, proteins, or other biomolecules to surfaces for development of several biotools such as biosensors [38–41]. However, the mechanism of binding of proteins to hydrophobin-coated surfaces is still a matter of discussion [40].

A class I hydrophobin secreted by the basidiomycete fungus *Pleurotus ostreatus* (Vmh2) has been extensively studied in our lab [42]. We have demonstrated that Vmh2 spontaneously forms a stable and homogeneous layer on hydrophilic or hydrophobic surfaces, which are able to strongly bind proteins, including enzymes in their active form [33]. Recently, we reported a novel surface biofunctionalization of steel MALDI sample plates by self-assembling of Vmh2, for on-plate high-throughput desalting of proteins and peptides in real samples and offline coupled with MS analysis [43]. No background interference due to Vmh2 molecular ion signals

was detected in any mass range, possibly because of the low amount of protein in the nanometric layer. This low-cost, fast, and environmentally friendly strategy allows a remarkable increase of the signal-to-noise ratio of the MALDI mass spectra. Following on from these results, we have investigated a strategy aimed at including the proteolytic steps on the hydrophobin-coated MALDI sample plate. It is worth considering that only few examples of phosphatase or deglycosidase immobilization are reported [28, 44, 45] in comparison with the ample literature concerning trypsin immobilization. As proof of concept, we have used trypsin, V8 protease, PNGaseF, and alkaline phosphatase to achieve high sequence coverage of model proteins, particularly when performing multiple enzyme digestions. Moreover, the possibility of exploiting this technique coupled to MALDI-TOF/TOF sequencing has been applied on both model proteins and on the entire whey milk proteome.

Experimental section

Materials Nα-p-tosyl-L-arginine methyl ester hydrochloride (TAME), lysozyme from chicken egg white, ovalbumin from chicken egg white, α-casein and β-casein from bovine milk were purchased from Sigma (St. Louis, MO, USA). Recombinant human erythropoietin (rhEPO) was purchased in pharmacy (α-darbepoetin from Amgem). Laccase phenol oxidase C (POXC) was purified from cultural broth of *P. ostreatus* (type: Florida no. MYA-2306) [46]. PD-10 desalting columns were purchased from GE Healthcare (Milan, Italy). Calibration mixtures were obtained from AB SCIEX (Framingham, MA, USA).

Stock enzyme solutions Trypsin from bovine pancreas, bovine alkaline phosphatase, and V8 protease were purchased from Sigma (St. Louis, MO, USA). PNGaseF was purchased from Roche. Trypsin stock solution was prepared at 6 mg mL^{-1} in 0.1 % formic acid. The specific activity using TAME as substrate was about 500 U mg^{-1}. Alkaline phosphatase was diluted at 1 U μL^{-1} in 5 mM Tris, 5 mM MgCl$_2$, and 0.1 mM ZnCl$_2$, pH 7.0. PNGaseF was used undiluted (1 U μL^{-1}). V8 protease was dissolved in 0.1 M ammonium bicarbonate, pH 8.0, at 0.5 U μL^{-1}. One unit is defined as the amount of enzymatic activity converting 1 μmol of substrate per minute.

Vmh2 purification Vmh2 was prepared from *P. ostreatus* mycelia as previously described [42]. Preparation basically consists in growing mycelia at 28 °C in static cultures in 2-L flasks containing 500 mL of potato dextrose (24 g/L) broth with 0.5 % yeast extract. After 10 days of fungal growth, hydrophobins released into the medium were aggregated by air bubbling using a Waring blender and collected by centrifugation at 4,000×*g*. The precipitate was freeze dried, left to dissolve under mechanical agitation with trifluoroacetic acid

(TFA) for 2 h, and treated in bath sonicator (operating at 35 kHz and at 240 W) for 30 min. The TFA solution was dried in a stream of air and Vmh2 dissolved in 60 % ethanol, resulting in a stock solution (100 μg mL^{-1}) which was used for further experiments.

Functionalization of steel surface Vmh2-coated steel was prepared and characterized as previously reported [43]. Briefly, 1 μL of Vmh2 solution was spotted on each MALDI plate well. After 1 h, samples were dried for 10 min at 80 °C and washed with 60 % ethanol. Deposition was repeated twice and finally the plate was washed with 2 % SDS at 100 °C for 10 min. The coated MALDI wells were used to noncovalently immobilize a set of four enzymes, usually employed in proteomics. In our current experience, the same coated plate has been used still after 3 weeks storage at room temperature. For trypsin adsorption, the enzyme was diluted in 0.1 % formic acid at different concentrations (from 0.3 to 6 mg mL^{-1} corresponding to 0.15–3 U mL^{-1}). One microliter of these solutions was spotted on Vmh2-coated wells. After 5-min incubation at room temperature, wells were washed three times to remove the excess of enzyme. The adsorbed trypsin was characterized and employed for further experiments. For alkaline phosphatase, PNGaseF, and V8 protease, 1 μL of enzyme stock solutions was spotted on Vmh2-coated wells and immobilized following an identical procedure. Since the immobilization is a very rapid step, we have routinely used freshly immobilized enzymes, to perform the required hydrolytic reaction.

Mass spectral determination of immobilized trypsin activity The enzymatic activity of trypsin in solution was spectrophotometrically determined at 247 nm with 10 mM TAME as a substrate in 50 mM Tris–HCl pH 8.0, by using Beckman DU 7500 spectrophotometer (Beckman Instruments). For quantitative analysis of TAME converted by on-plate trypsin, liquid chromatography–tandem quadrupole mass spectrometry (LC–MS/MS) in the multiple reaction monitoring (MRM) was performed by using a 6420 triple Q system with a HPLC 1100 series binary pump (Agilent, Waldbronn, Germany). The analytical column was a Phenomenex Kinetex 5u 100 A C18. The mobile phase was generated by mixing eluent A (2 % acetonitrile (ACN) and 0.1 % formic acid) and eluent B (95 % ACN and 0.1 % formic acid) and the flow rate was 0.200 mL min^{-1}. The HPLC gradient was from 5 to 95 % B in 8 min then to 100 % for 2 min. Standard solutions were prepared by dissolving the equivalent of 1 mg of TAME in 1 mL of methanol. A standard solution of 500 pg μL^{-1} of each metabolite was used for optimization of the MRM transition. The ideal mass spectrometric parameters for detection were determined via MassHunter Optimizer software, resulting in 343.43 *m/z* as precursor ion, 91.1 and 65.1 *m/z* product ions, and 48 and 92 V optimized voltages.

Quartz crystal microbalance (QCM) determination of immobilized trypsin amount The QCM device is a μLibra from Technobiochip, Italy, and the resonance frequency of the oscillating crystal is monitored by a producer-released software. The oscillators (151218) are AT-CUT quartz with a fundamental frequency of 10 MHz purchased from ICM Oklahoma City (USA). The diameters of the crystal and of the gold sensitive surface are 1.37 and 0.68 cm, respectively. Before the functionalization with Vmh2, the electrodes were cleaned using piranha solution (5:1 sulfuric acid/40 % hydrogen peroxide solution) thus removing any impurity and organic compound from the gold plates. Then, in order to test the Vmh2–trypsin interaction, the protein-coated oscillator is placed in a microfluidic apparatus consisting of the cell which contains the crystal, a GILSON peristaltic pump, and Tygon silicone tubes. The volume of the circuit is 300 μL, while the flow rate is about 50 μL min^{-1}. The volume of the sample to test is 1 mL. Using this experimental setup, it was possible to estimate the amount of trypsin adsorbed onto the Vmh2-coated gold surface at several enzyme concentrations.

Substrate preparation Lysozyme, ovalbumin, POXC, α-darbepoetin, and whey milk proteins were dissolved at 5 μM in 0.5 M Tris–HCl pH 8.0 containing 6 M guanidinium chloride, then reduced in 10 mM dithiothreitol for 2 h at 37 °C, and carboxamidomethylated in 50 mM iodoacetamide for 30 min, in the dark, at room temperature. Samples were desalted on a PD10 column using 10 mM NH$_4$HCO$_3$ (AMBIC) as eluting buffer. Fractions containing proteins were pooled and lyophilized before the analyses.

In-solution hydrolysis Trypsin (substrate/enzyme ratio, 50:1 *w/w*) was added to the aliquots of denatured proteins and incubated for 18 h at 37 °C. Then, the reactions were stopped by adding 0.1 % formic acid. Three microliters of stock enzyme solutions was added to the aliquots of boiled tryptic hydrolyzed samples.

Setting up on-plate hydrolysis One microliter of denatured proteins in 10 mM AMBIC was spotted on Vmh2-adsorbed enzyme wells. In the case of trypsin, reaction was carried out for 5 min, 10 min, 3 h, 6 h, or 18 h at room temperature, in a wet atmosphere. The reaction was stopped by addition of matrix solution, α-cyano-4-hydroxycinnamic acid (CHCA) (10 mg mL^{-1} in acetonitrile/0.1 % TFA 7/3 (*v/v*)). Once having set up the best reaction time (see "Results and discussion" section), the serial reactions (trypsin-alkaline phosphatase, trypsin-PNGaseF, and trypsin-V8 protease) were carried out as above described for trypsin (1 μL, 5 min).

MALDI-MS analysis MALDI-TOF/MS spectra were acquired by a Voyager-DE STR MALDI-TOF mass spectrometer (Applied Biosystems, Framingham, MA, USA) equipped

with a nitrogen laser (337 nm). Peptides were detected in reflector mode using CHCA as matrix. Spectra were acquired using a mass range of 500–5,000 amu. Acceleration and voltages were set up as follows: target voltage at 20 kV, grid at 66 % of target voltage, and delayed extraction at 150 ns to obtain the best signal-to-noise (S/N) ratios and the best possible isotopic resolution. Spectra were accumulated in multiples of 50 laser shots, with 50–2,000 shots in total. The molecular weight standards for the calibration of the Voyager-DE STR system were AB SCIEX calibration mixtures 1 and 2.

MS/MS experiments were carried out on a 4800 Plus MALDI-TOF/TOF™ Analyzer AB SCIEX. All acquisitions were generated automatically in the instrument software and based on averaging 500 shots per spectrum, with 1,000–2,000 shots in total.

Results and discussion

Trypsin immobilization on hydrophobin-coated MALDI sample wells

The ability of the Vmh2-coated MALDI sample plates to bind peptides and proteins has been previously demonstrated [43]. In this work, the most commonly used enzymes in proteomic research, including posttranslational demodifying enzymes, have been adsorbed on this layer and their performances have been exploited.

Preliminary experiments were aimed at evaluating the catalytic activity of the enzyme which was actually adsorbed. Because of the low sensitivity of the spectrophotometric assay, a mass spectrometry method was set up, by using LC–MS/MS MRM ion mode [47]. Two micrograms of trypsin was deposited on the Vmh2 layer and left standing for 5 min. After thoroughly washing the wells with repeated aliquots of 0.1 % formic acid followed by equilibration with AMBIC, the TAME assay was performed. TAME was completely converted in less than 30 s, thus qualitatively indicating that the adsorbed trypsin was fully active. Since we reached the TAME solubility limit (40 mg mL^{-1}), quantitative activity data were obtained by depositing 1 μg of enzyme. Results demonstrated that about 0.1 μmol of substrate was hydrolyzed in 1 min, indicating that 0.1 U of trypsin per well was immobilized. Since Vmh2-coated well surface was equivalent to 7 mm^2, the activity/surface ratio was 14 mU mm^{-2}.

To evaluate the actual amount of trypsin adsorbed on a Vmh2 layer, QCM was used [48]. The QCM gold sensor was coated with hydrophobin, taking into consideration that the physical characteristics of the Vmh2 layer on the gold surface are quite similar to those observed on the steel plate (data not shown). After coating, three different amounts of trypsin (1, 3, and 5 μg in 1 mL of 0.1 % formic acid) were tested by

monitoring the resonance frequency of the crystal after the injection of the sample in the fluidic circuit. Since the frequency shifts (Δf) are related to the amount of material adsorbed on sensor [49], we were able to extrapolate the weight of enzyme immobilized. Results (see Electronic Supplementary Material (ESM) Fig. S1) indicated that 100, 220, and 250 ng of enzyme were, respectively, adsorbed, corresponding to 3, 6, and 7 ng mm^{-2}, thus suggesting that the latter value approximately corresponds to that of saturation of the functionalized surface.

In order to evaluate the enzyme-specific activity, we took into account that the QCM gold sensor surface (36 mm^2) is about fivefold wider than that of the MALDI sample plate well (7 mm^2). The specific activity was calculated by dividing the enzyme activity measured by MRM analysis (14 mU mm^{-2}) with the weight measured by QCM (7 ng mm^{-2}), values obtained incubating the same amount of enzyme per square millimeter. Hence, the specific activity of immobilized trypsin was considered to be about 2,000 U mg^{-1}, some fourfold higher than that of the free form. This increase may be ascribed to a greater accessibility of substrate molecules to active sites of immobilized enzyme as reported elsewhere [50, 51].

Protein digestion by on-plate immobilized trypsin

To test the performance of trypsin immobilized on Vmh2-coated MALDI wells, lysozyme and ovalbumin were used as reference proteins. After reduction, carbamidomethylation, and desalting, protein samples were spotted on the trypsin-immobilized wells and incubated for 5 min, 10 min, 3 h, 6 h, or 18 h at room temperature.

Spectra obtained (Fig. 1) showed that the on-plate immobilized trypsin was able to extensively hydrolyze the denatured proteins after 5 min of incubation. As expected, no digestion was observed in the absence of the Vmh2 coating. Eleven unique peptides for lysozyme and 15 unique for ovalbumin (ESM Table S1) were identified, allowing 90 and 60 % of sequence coverage, respectively (ESM Table S2). No improvement of sequence coverage was observed with increases in incubation time, even after incubating for 18 h. It is noteworthy that the spectra used for peptide mapping were recorded without any further sample manipulation. Indeed, the reaction was stopped by addition of the appropriate matrix solution, and spectra were recorded immediately after drying in ambient atmosphere. Therefore, the performance of on-plate trypsin was comparable to that of conventional in-solution digestion (18 h at 37 °C) (ESM Fig. S2) but with a very significant reduction in reaction and sample workup time (about 2 h for plate preparation, which can be used even for 100 hydrolysis, and 5 min for the reaction). These results could be ascribed to the in situ high enzyme/substrate ratios (about 1:1) with respect to those commonly used. In the conventional (in solution) method, this ratio is kept low
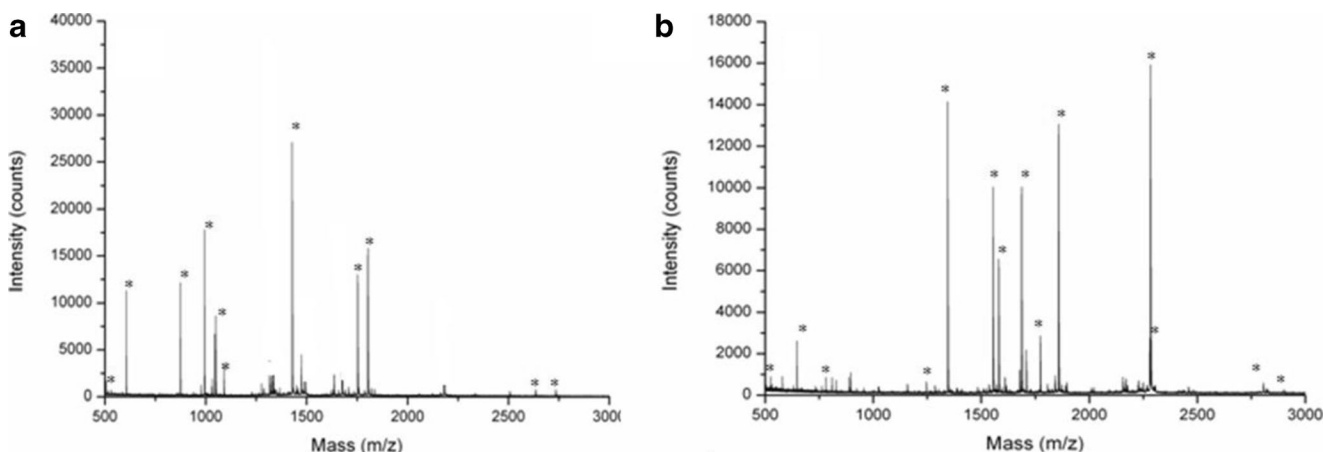
Fig. 1 MALDI spectra of lysozyme (**A**) and ovalbumin (**B**) after 5 min of on-plate hydrolysis. The assigned signals are marked with *asterisks*. List of peptides with their *m/z* values is reported in ESM Table S1

(generally 1:50 *w/w*) to prevent excessive formation of autodigested products. In the reported on-plate method, rapid and efficient proteolysis was achieved with undetectable autodigestion products. As matter of fact, no detectable autoproteolysis product or Vmh2 tryptic peptides were observed in any of the tested conditions (ESM Fig. S3). The absence of autoproteolysis products can be due to the restricted accessibility of an immobilized trypsin molecule to the active site of another one. As expected, Vmh2 was not digested by trypsin because the lone basic amino acid residue is probably hidden in the very compact structure of the layer.

In order to evaluate the reproducibility of the methodology, 10 replicates of each sample were prepared and the MALDI mass spectrometer was set in automatic mode. Spectra accumulated in multiples of 200 laser shots in 10 random positions of the well (2,000 shots in total) were compared. Peaks/spectrum (12.1±0.6) related to lysozyme were detected (1.8 standard deviation). Moreover, all the replicate allowed to obtain the same sequence coverage, thus indicating the reproducibility of these analyses.

Immobilization of other enzymes and on-plate serial reactions

The ionization efficiency of a digested fragment depends on its size, sequence, and, possibly, posttranslational modifications, all factors affecting sequence coverage of the target protein by MS analysis. Therefore, digestion with other proteases, the removal of posttranslational modifications by suitable enzymes, such as phosphatases or deglycosidase often have to be performed to increase the sequence coverage and/or the general sensitivity of the analysis.

Our previous results suggest that the Vmh2 layers are able to bind proteins irrespective of their molecular weights or physicochemical properties [43]. Therefore, once the use of immobilized trypsin was assessed, the on-plate immobilization of other enzymes commonly used in proteomic research was tested in order to further improve sequence coverage,

eventually exploiting multiple hydrolysis experiment on the same plate.

V8 protease, N-glycosidase F, and alkaline phosphatase (1 µL of stock solutions) were loaded on Vmh2-coated MALDI wells, using the same procedure described for trypsin. We did not attempt any further investigation on the on-plate enzyme activity as we did in the case of trypsin and directly tested the performance of these enzymes on protein substrates: ovalbumin for V8, ovalbumin and POXC laccase for PNGaseF, and α-casein and β-casein from bovine milk for alkaline phosphatase. Substrate proteins were hydrolyzed first by on-plate immobilized trypsin and then the tryptic digests were transferred by pipetting about 0.8÷0.9 µL on the appropriate immobilized enzyme wells and incubated for 5 min.

Results of V8 activity on the ovalbumin tryptic hydrolyzed are shown in Fig. 2. The detection of 11 new peaks (marked with asterisks) due to the expected hydrolysis after Asp and Glu demonstrated that the enzyme was active and able to hydrolyze the substrate in some 5 min.

† Typtic peptides		* V8 peptides	
Mass (m/z)	peptide	Mass (m/z)	peptide
580.75	124-127	605.20	201-205
647.86	281-285	850.43	285.264
888.56	279-285	887.25	111-117
1248.45	361-370	947.23	19-26
1345.61	371-382	965.45	193-200
1555.74	188-200	1133.17	324-334
1581.74	265-277	1238.10	268-277
1687.92	128-143	1461.19	321-334
1773.80	324-340	1515.39	72-85
1858.86	144-159	2741.92	204-227
2283.02	1-20	3031.64	230-257
2284.02	201-219		

Fig. 2 MALDI-TOF spectra of ovalbumin after trypsin-V8 on-plate hydrolysis. Eleven new peptides that appeared after V8 digestion are marked with *asterisks* and reported in the *inset table*

The performance of immobilized PNGaseF was tested using ovalbumin and POXC laccase (Fig. 3). In the case of ovalbumin, a new signal appeared at 3,294.44 m/z which can be attributed to the peptide 292-323 lacking the glycosidic moiety, where Asn293 has been converted into Asp by the PNGaseF reaction. Similarly, in the case of laccase POXC, a new signal appeared at 1,646.77 m/z which can be attributed to the peptide 433-448 without glycosidic moiety and with Asn 444 converted into Asp[46]. The identity of these peptides was confirmed by MALDI-TOF/TOF analysis (an example of MS/MS spectra is reported in ESM Fig. S4).

Caseins from bovine milk are phosphoproteins with well-characterized phosphorylated sites [52]. Phosphopeptides are not easily detectable by using MALDI mass spectrometer in positive ion mode, due to the presence of negative charges. Spectra recorded after 5 min of phosphatase reaction on the tryptic peptides showed the presence of the α-casein peptides containing the Ser130-dephosphorylated, 119-134 and 121-134 (1,871.92 and 1,580.76 m/z, respectively), and β-casein-dephosphorylated peptide 1-25 (2,802.34 m/z) (Fig. 4), confirmed by MALDI-TOF/TOF analysis. Even in this case,

tryptic digestion and dephosphorylation were performed in a total time of 10 min.

Since the setup method gives us the opportunity to perform a number of on-plate reactions in very short times, it can be exploited to achieve an even higher sequence coverage of proteins by multiple hydrolytic steps. In addition to the N-glycosylation site at Asn293, ovalbumin has a phosphorylation site at Ser69. As reported above, a 60 % of sequence coverage was achieved after trypsin hydrolysis. When trypsin-digested samples were incubated for 5 min on V8, PNGaseF, and phosphatase-immobilized wells, respectively, new peptides were generated: four new unique peptides (605.43, 850.50, 2,741.48, 3,031.64 m/z; peptides 201-205, 258-264, 204-227, 230-257, respectively) by V8 reaction (see Fig. 2), one peptide (3,294.45 m/z; peptide 292-323) by PNGaseF reaction, and one peptide (2,282.45 m/z; peptide 60-85) by phosphatase reaction, allowed to increase the sequence coverage to some 85 %.

The effectiveness of the setup method has also been tested on a real sample of pharmaceutical interest. α-Darbepoetin is a second-generation rhEPO with five modified amino acids
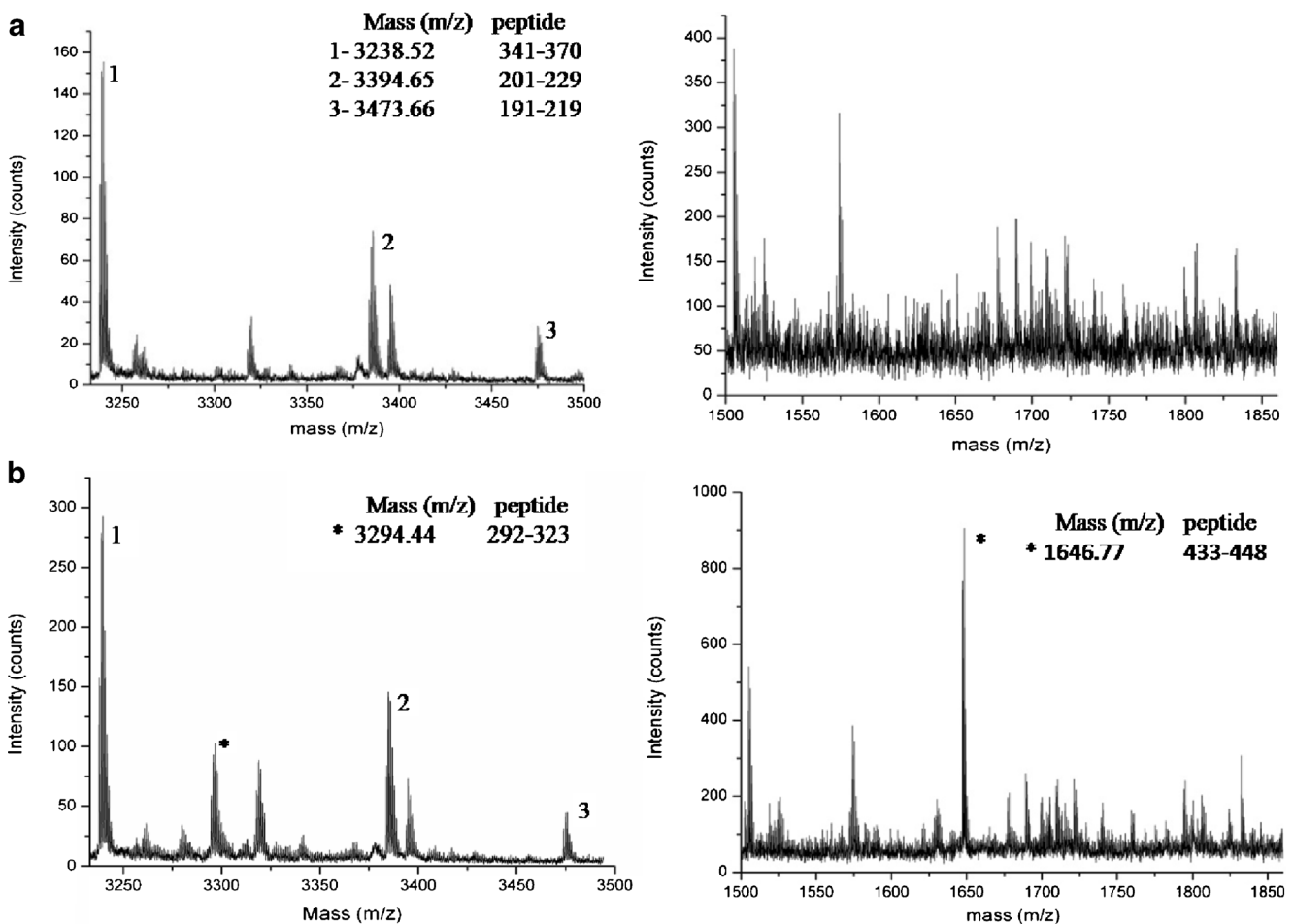
Fig. 3 Section of MALDI-TOF spectra of ovalbumin (*on the left*) and POXC (*on the right*) tryptic peptides, before (**A**) and after (**B**) on-plate deglycosylation. Deglycosylated peptides are marked with *asterisks*

a (left spectrum)

Mass (m/z)	peptide
1- 2061.16	33–48
2- 2186.16	184–202
3- 2480.15	29–48
4- 2909.54	184–209

(right spectrum)

Mass (m/z)	peptide
1- 1195.70	130–140
2- 1267.69	106–115
3- 1337.68	95–105
4- 1384..47	38–49
5- 1760.86	3–18
6- 1928.13	91–105

b (left spectrum)

Mass (m/z)	peptide
* 2802.34 m/z	1–25

(right spectrum)

Mass (m/z)	peptide
* 1580.76 m/z	119–134
** 1871.92 m/z	121–134
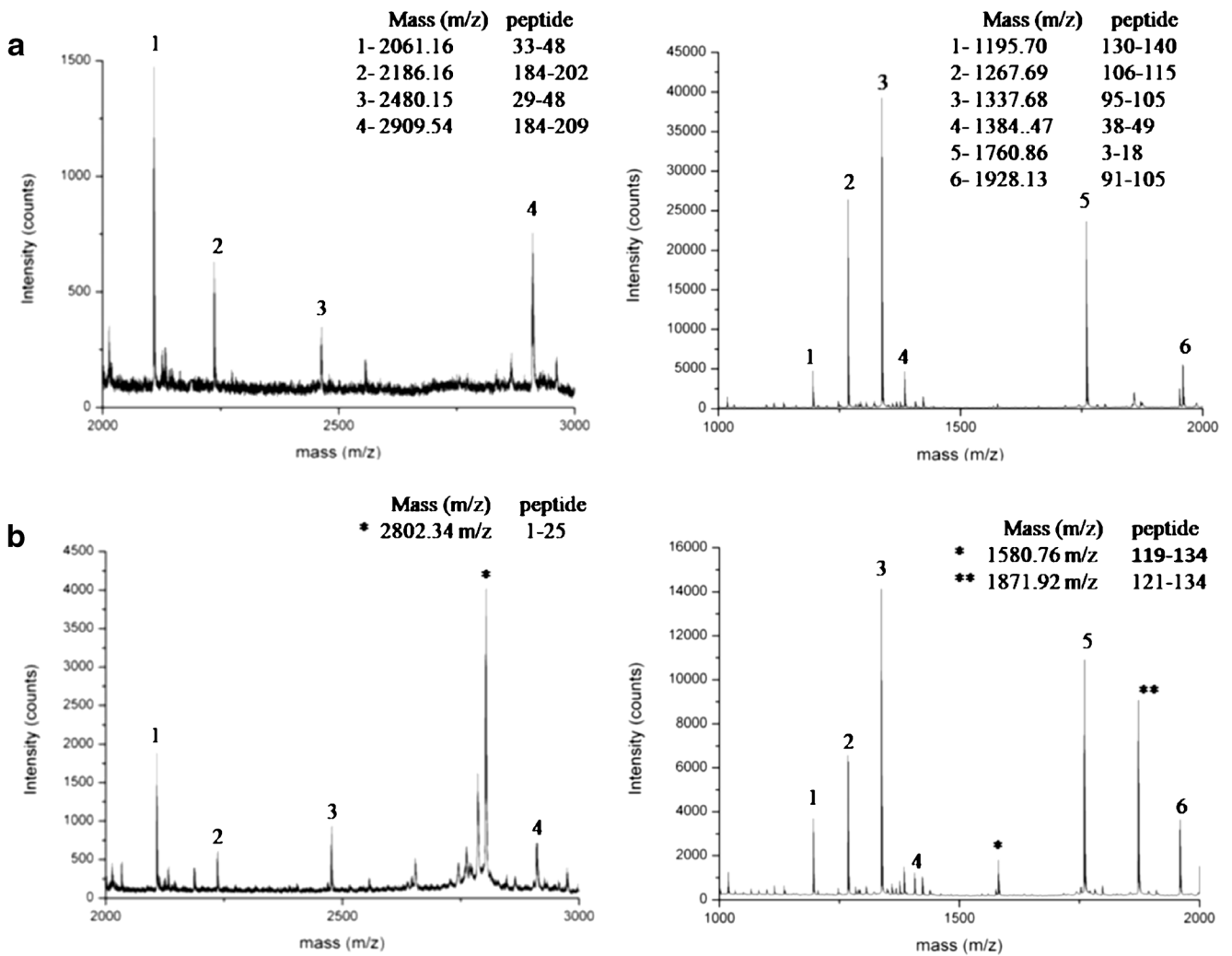
Fig. 4 Section of MALDI-TOF spectra of β-casein (*on the left*) and α-casein (*on the right*) tryptic peptides, before (**A**) and after (**B**) on-plate dephosphorylation. Dephosphorylated peptides are marked with *asterisks*

Table 1 List of unique peptides of rhEPO obtained by on-plate coupled hydrolysis

Signals (*m/z*)	Start	End	Sequences	Trypsin	Trypsin + PNGase	PNGase + trypsin
1,184.68	1	10	(−)APPRLIC*DSR(V)	+	+	+
516.42	11	14	(R)VLER (Y)	+	+	+
736.48	15	20	(R)YLLEAK (E)	+	+	+
2,815.66	21	45	(K)EAE**NIT**TGC***NET**C*SLNE**NIT**VPDTK(V)			+
1,083.90	46	53	(K)VNFYAWKR(M)			+
2,526.70	54	76	(R)MEVGQQAVEVWQGLALLSEAVLR (G)	+	+	+
2,295.27	77	97	(R)GQALLV**NSS**QV**NET**LQLHVDK (A)		+	+
602.45	98	103	(K)AVSGLR(S)			+
803.60	104	110	(R)SLTTLLR(A)			+
1,465.93	117	131	(K)EAISPPDAASAAPLR(T)			+
1,052.68	132	140	(R)TITADTFRK(L)	+	+	+
2,481.24	117	140	(K)EAISPPDAASAAPLRTITADTFRK(L)	+	+	+
563.44	140	143	(R)KLFR(V)	+	+	+
2,274.32	144	162	(R)VYSNFLRGKLKLYTGEAC*R(T)	+	+	+

Glycosylation sites are presented in bold

Fig. 5 MALDI-TOF/TOF spectrum of milk proteins after on-plate digestion (**A**). Panel **B** shows the MS/MS spectrum of precursor peptide 830.57 m/z (192–198) of β-casein peptide
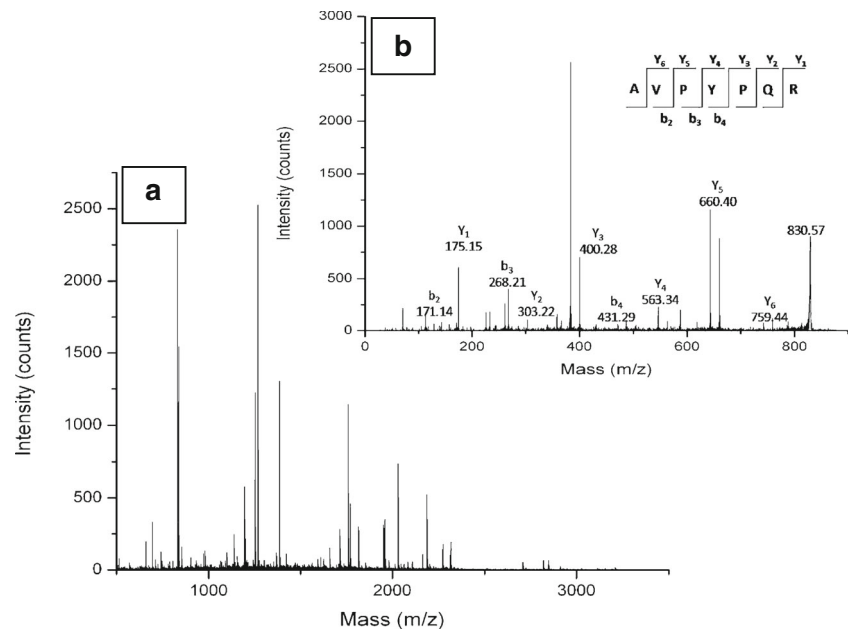
(Ala30Asn, His32Thr, Pro87Val, Trp88Asn, and Pro90Thr). These amino acidic substitutions insert other two N-glycosylation sites (in addition to the three N-glycosylation sites of human EPO) at positions Asn30 and Asn88. Hyperglycosylation enhances serum half-life, reducing frequency of injections [53]. The presence of high content of carbohydrates, typically tetra-antennary N-glycans containing up to four sialic acids [54], may interfere with proteolysis and MALDI/MS analysis. For this reason, an on-plate digestion protocol for mapping of rhEPO was ad hoc set up. Coupled reactions were performed as already described, and MALDI spectra were acquired after deglycosylation–tryptic digestion or tryptic digestion–deglycosylation steps and compared. Results (Table 1) showed that, when deglycosylation was performed after trypsin hydrolysis, only one deglycosylated peptide was observed (peptide 77-97, two glycosylation sites), while the peptide 21-45 (three glycosylation sites) as well as regions downstream of the glycosylated peptides were not detected. On the other hand, higher sequence coverage (up

to 94 %) was obtained when the deglycosylation step was performed prior to trypsin digestion.

Milk proteins

In order to verify the feasibility of our strategy of on-plate coupled reactions on a complex biological sample, whey milk proteins were analyzed. After acetone precipitation, proteins were suspended in denaturing buffer, then were reduced and carbamidomethylated. Finally, samples were incubated for 5 min at room temperature on immobilized trypsin wells. MALDI spectra showed the presence of 48 signals related to 9 milk proteins (ESM Table S3). Because of the complexity of these spectra, the same experiment was performed on MALDI-TOF/TOF plate. Amino acidic sequences of peptides were determined by MS/MS analysis, allowing us to unequivocally identify these proteins. In Fig. 5, the MALDI spectrum of tryptic digested milk proteins is reported, together with an

Fig. 6 A graphical overview of the workflow
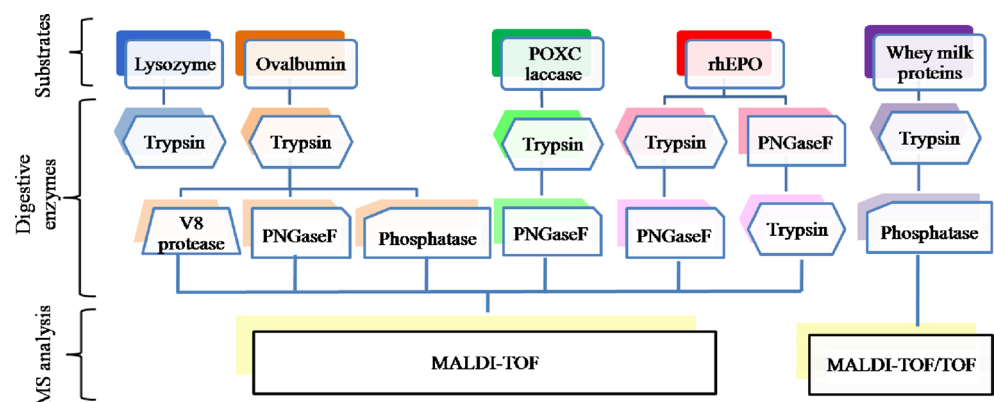
example of MS/MS spectrum. It is worth noting that some of them are among the less abundant milk proteins.

Whey milk is rich in phosphoproteins (caseins); thus, denatured samples were incubated on trypsin-immobilized well and then on alkaline phosphatase-immobilized well. Spectra acquired after double-reaction steps showed the presence of the expected dephosphorylated peptides for α-casein (1,871.92 *m/z*), and β-casein (2,802.34 *m/z*), confirmed by MS/MS analysis. Results showed that both immobilized enzymes were able to carry out their function in 10 min even in complex samples.

Conclusions

Efficient, fast, and reproducible protein digestion is of utmost importance in bottom-up proteomics. Albeit several trypsin-immobilized systems have been developed for proteolysis, only few studies have described multi-enzymatic immobilized systems [28] and analysis of posttranslational modification in proteins [44, 45]. Our approach is based on the formation of a protein layer on the MALDI sample plate formed by the self-assembling fungal protein hydrophobin. We have demonstrated that this layer is able to immobilize different enzymes involved in proteomic studies, providing a simple and rapid procedure for the analysis of protein sequences, including posttranslational modifications. Several advantages of this in situ procedure can easily be envisaged: (i) rapid analysis, with a reduction of digestion time to few min; (ii) use of very low sample volumes, in the order of magnitude of some microliters; (iii) multi-proteolysis steps directly on the same MALDI sample plate, and (iv) posttranslational modification analysis, thanks to the opportunity of immobilization of different enzymes on the same system. As a consequence, very high sequence coverage has been obtained. Using MALDI-TOF/TOF, the strategy can be extended to protein identification/characterization in complex proteomes, through peptide mass fingerprinting or (selected) peptide sequencing. The potential of this method can be greatly exploited by immobilizing other enzymes and/or setting ad hoc protocols for specific proteins using a combination of proteases and other posttranslational demodifying enzymes (Fig. 6). The demonstration of achieving an almost complete sequence coverage of rhEPO merely by using two immobilized enzymes is highly significant. The strategy demonstrated in this paper can be further developed to be fully automated thus leading to a high-throughput proteome lab-on-plate platform.

References

1. Angel TE, Aryal UK, Hengel SM et al (2012) Mass spectrometry-based proteomics: existing capabilities and future directions. Chem Soc Rev 41:3912–3928. doi:10.1039/c2cs15331a
2. Yamaguchi H, Miyazaki M (2013) Enzyme-immobilized reactors for rapid and efficient sample preparation in MS-based proteomic studies. Proteomics 13:457–466. doi:10.1002/pmic.201200272
3. Aebersold R, Mann M (2003) Mass spectrometry-based proteomics. Nature 422:198–207. doi:10.1038/nature01511
4. Switzar L, Giera M, Niessen WMA (2013) Protein digestion: an overview of the available techniques and recent developments. J Proteome Res 12:1067–1077. doi:10.1021/pr301201x
5. Massolini G, Calleri E (2005) Immobilized trypsin systems coupled on-line to separation methods: recent developments and analytical applications. J Sep Sci 28:7–21. doi:10.1002/jssc.200401941
6. Girelli AM, Mattei E (2005) Application of immobilized enzyme reactor in on-line high performance liquid chromatography: a review. J Chromatogr B Analyt Technol Biomed Life Sci 819:3–16. doi:10.1016/j.jchromb.2005.01.031
7. Vestling MM, Fenselau C (1994) Poly(vinylidene difluoride) membranes as the interface between laser desorption mass spectrometry, gel electrophoresis, and in situ proteolysis. Anal Chem 66:471–477. doi:10.1021/ac00076a009
8. Sun J, Hu K, Liu Y et al (2013) Novel superparamagnetic sanoparticles for trypsin immobilization and the application for efficient proteolysis. J Chromatogr B Analyt Technol Biomed Life Sci 942–943:9–14. doi:10.1016/j.jchromb.2013.10.015
9. Bao H, Zhang L, Chen G (2013) Immobilization of trypsin via graphene oxide-silica composite for efficient microchip proteolysis. J Chromatogr A 1310:74–81. doi:10.1016/j.chroma.2013.08.040
10. Fan C, Shi Z, Pan Y et al (2014) Dual matrix-based immobilized trypsin for complementary proteolytic digestion and fast proteomics analysis with higher protein sequence coverage. Anal Chem 86:1452–1458. doi:10.1021/ac402696b
11. Brownridge P, Beynon RJ (2011) The importance of the digest: proteolysis and absolute quantification in proteomics. Methods 54:351–360. doi:10.1016/j.ymeth.2011.05.005
12. Liu Y, Lu H, Zhong W et al (2006) Multilayer-assembled microchip for enzyme immobilization as reactor toward low-level protein identification. Anal Chem 78:801–808. doi:10.1021/ac051463w
13. Liu Y, Zhong W, Meng S et al (2006) Assembly-controlled biocompatible interface on a microchip: strategy to highly efficient proteolysis. Chemistry 12:6585–6591. doi:10.1002/chem.200501622
14. Gao J, Xu J, Locascio LE, Lee CS (2001) Integrated microfluidic system enabling protein digestion, peptide separation, and protein identification. Anal Chem 73:2648–2655
15. Qiao L, Liu Y, Hudson SP et al (2008) A nanoporous reactor for efficient proteolysis. Chemistry 14:151–157. doi:10.1002/chem.200701102
16. Min Q, Zhang X, Wu R et al (2011) A novel magnetic mesoporous silica packed S-shaped microfluidic reactor for online proteolysis of low-MW proteome. Chem Commun (Camb) 47:10725–10727. doi:10.1039/c1cc13969j
17. Qu H, Wang H, Huang Y et al (2004) Stable microstructured network for protein patterning on a plastic microfluidic channel: strategy and characterization of on-chip enzyme microreactors. Anal Chem 76:6426–6433. doi:10.1021/ac049466g
18. Lee J, Musyimi HK, Soper SA, Murray KK (2008) Development of an automated digestion and droplet deposition microfluidic chip for

MALDI-TOF MS. J Am Soc Mass Spectrom 19:964–972. doi:10.1016/j.jasms.2008.03.015

19. Kim BC, Lopez-Ferrer D, Lee S-M et al (2009) Highly stable trypsin-aggregate coatings on polymer nanofibers for repeated protein digestion. Proteomics 9:1893–1900. doi:10.1002/pmic.200800591

20. Dodds ED, Seipert RR, Clowers BH et al (2009) Analytical performance of immobilized pronase for glycopeptide footprinting and implications for surpassing reductionist glycoproteomics. J Proteome Res 8:502–512. doi:10.1021/pr800708h

21. López-Ferrer D, Hixson KK, Smallwood H et al (2009) Evaluation of a high-intensity focused ultrasound-immobilized trypsin digestion and 18O-labeling method for quantitative proteomics. Anal Chem 81:6272–6277. doi:10.1021/ac802540s

22. Casadonte F, Pasqua L, Savino R, Terracciano R (2010) Smart trypsin adsorption into N-(2-aminoethyl)-3-aminopropyl-modified mesoporous silica for ultra fast protein digestion. Chemistry 16:8998–9001. doi:10.1002/chem.201000120

23. Lim LW, Tomatsu M, Takeuchi T (2006) Development of an on-line immobilized-enzyme reversed-phase HPLC method for protein digestion and peptide separation. Anal Bioanal Chem 386:614–620. doi:10.1007/s00216-006-0458-6

24. Guo X, Trudgian DC, Lemoff A et al (2014) Confetti: a multiprotease map of the HeLa proteome for comprehensive proteomics. Mol Cell Proteomics 13:1573–1584. doi:10.1074/mcp.M113.035170

25. Cingöz A, Hugon-Chapuis F, Pichon V (2010) Total on-line analysis of a target protein from plasma by immunoextraction, digestion and liquid chromatography-mass spectrometry. J Chromatogr B Analyt Technol Biomed Life Sci 878:213–221. doi:10.1016/j.jchromb.2009.07.032

26. Geiser L, Eeltink S, Svec F, Fréchet JMJ (2008) In-line system containing porous polymer monoliths for protein digestion with immobilized pepsin, peptide preconcentration and nano-liquid chromatography separation coupled to electrospray ionization mass spectroscopy. J Chromatogr A 1188:88–96. doi:10.1016/j.chroma.2008.02.075

27. Temporini C, Calleri E, Campèse D et al (2007) Chymotrypsin immobilization on epoxy monolithic silica columns: development and characterization of a bioreactor for protein digestion. J Sep Sci 30:3069–3076. doi:10.1002/jssc.200700337

28. Yamaguchi H, Miyazaki M, Kawazumi H, Maeda H (2010) Multidigestion in continuous flow tandem protease-immobilized microreactors for proteomic analysis. Anal Biochem 407:12–18. doi:10.1016/j.ab.2010.07.026

29. Urban PL, Amantonico A, Zenobi R (2011) Lab-on-a-plate: extending the functionality of MALDI-MS and LDI-MS targets. Mass Spectrom Rev 30:435–478. doi:10.1002/mas.20288

30. Jiang B, Yang K, Zhang L et al (2014) Dendrimer-grafted graphene oxide nanosheets as novel support for trypsin immobilization to achieve fast on-plate digestion of proteins. Talanta 122:278–284. doi:10.1016/j.talanta.2014.01.056

31. Li Y, Yan B, Deng C et al (2007) On-plate digestion of proteins using novel trypsin-immobilized magnetic nanospheres for MALDI-TOF-MS analysis. Proteomics 7:3661–3671. doi:10.1002/pmic.200700464

32. De Stefano L, Rea I, Rendina I et al (2011) Organic–inorganic interfaces for a new generation of hybrid biosensors. Biosens Health Environ Biosecurity

33. De Stefano L, Rea I, De Tommasi E et al (2009) Bioactive modification of silicon surface using self-assembled hydrophobins from Pleurotus ostreatus. Eur Phys J E Soft Matter 30:181–185. doi:10.1140/epje/i2009-10481-y

34. Linder MB (2009) Hydrophobins: proteins that self assemble at interfaces. Curr Opin Colloid Interface Sci 14:356–363. doi:10.1016/j.cocis.2009.04.001

35. Hektor HJ, Scholtmeijer K (2005) Hydrophobins: proteins with potential. Curr Opin Biotechnol 16:434–439. doi:10.1016/j.copbio.2005.05.004

36. Zampieri F, Wösten HAB, Scholtmeijer K (2010) Creating surface properties using a palette of hydrophobins. Materials (Basel) 3:4607–4625. doi:10.3390/ma3094607

37. Wohlleben W, Subkowski T, Bollschweiler C et al (2010) Recombinantly produced hydrophobins from fungal analogues as highly surface-active performance proteins. Eur Biophys J 39:457–468. doi:10.1007/s00249-009-0430-4

38. Sun T, Qing G, Su B, Jiang L (2011) Functional biointerface materials inspired from nature. Chem Soc Rev 40:2909–2921. doi:10.1039/c0cs00124d

39. Qin M, Wang L-K, Feng X-Z et al (2007) Bioactive surface modification of mica and poly(dimethylsiloxane) with hydrophobins for protein immobilization. Langmuir 23:4465–4471. doi:10.1021/la062744h

40. Wang Z, Lienemann M, Qiau M, Linder MB (2010) Mechanisms of protein adhesion on surface. Films Hydrophobin 57:8491–8496. doi:10.1021/la101240e

41. Zhao Z-X, Wang H-C, Qin X et al (2009) Self-assembled film of hydrophobins on gold surfaces and its application to electrochemical biosensing. Colloids Surf B Biointerfaces 71:102–106. doi:10.1016/j.colsurfb.2009.01.011

42. Armenante A, Longobardi S, Rea I et al (2010) The Pleurotus ostreatus hydrophobin Vmh2 and its interaction with glucans. Glycobiology 20:594–602

43. Longobardi S, Gravagnuolo AM, Rea I et al (2014) Hydrophobin-coated plates as matrix-assisted laser desorption/ionization sample support for peptide/protein analysis. Anal Biochem 449:9–16

44. Weng Y, Qu Y, Jiang H et al (2014) An integrated sample pretreatment platform for quantitative N-glycoproteome analysis with combination of on-line glycopeptide enrichment, deglycosylation and dimethyl labeling. Anal Chim Acta 833:1–8. doi:10.1016/j.aca.2014.04.037

45. Krenkova J, Szekrenyes A, Keresztessy Z et al (2013) Oriented immobilization of peptide-N-glycosidase F on a monolithic support for glycosylation analysis. J Chromatogr A 1322:54–61. doi:10.1016/j.chroma.2013.10.087

46. Giardina P, Aurilia V, Cannio R et al (1996) The gene, protein and glycan structures of laccase from Pleurotus ostreatus. Eur J Biochem 235:508–515

47. Luo B, Groenke K, Takors R et al (2007) Simultaneous determination of multiple intracellular metabolites in glycolysis, pentose phosphate pathway and tricarboxylic acid cycle by liquid chromatography-mass spectrometry. J Chromatogr A 1147:153–164. doi:10.1016/j.chroma.2007.02.034

48. Cooper MA, Singleton VT (2001) A survey of the 2001 to 2005 quartz crystal microbalance biosensor literature: applications of acoustic physics to the analysis of biomolecular interactions. J Mol Recognit 20:154–184. doi:10.1002/jmr.826

49. Sauerbrey SG (1959) Verwendung von Schwingquarzen zur Wägung dünner Schichten und zur Mikrowägung. Z Phys 155:206–222

50. Kannan K, Jasra RV (2009) Immobilization of alkaline serine endopeptidase from Bacillus licheniformis on SBA-15 and MCF by surface covalent binding. J Mol Catal B: Enzym 56:34–40. doi:10.1016/j.molcatb.2008.04.007

51. Li S, Wu Z, Lu M et al (2013) Improvement of the enzyme performance of trypsin via adsorption in mesoporous silica SBA-15: hydrolysis of BAPNA. Molecules 18:1138–1149. doi:10.3390/molecules18011138

52. Han G, Ye M, Jiang X et al (2009) Comprehensive and reliable phosphorylation site mapping of individual phosphoproteins by combination of multiple stage mass spectrometric analysis with a target-decoy database search. Anal Chem 81:5794–5805. doi:10.1021/ac900702g

53. Egrie JC, Browne JK (2001) Development and characterization of novel erythropoiesis stimulating protein (NESP). Br J Cancer 84(Suppl 1):3–10. doi:10.1054/bjoc.2001.1746

54. Llop E, Gallego RG, Belalcazar V et al (2007) Evaluation of protein N-glycosylation in 2-DE: erythropoietin as a study case. Proteomics 7:4278–4291. doi:10.1002/pmic.200700572

Nano-machining of biosensor electrodes through gold nanoparticles deposition produced by femtosecond laser ablation

B. Della Ventura[1] · R. Funari[1] · K. K. Anoop[1,2] · S. Amoruso[1,2] · G. Ausanio[1,2] ·
F. Gesuele[1] · R. Velotta[1] · C. Altucci[1]

Abstract We report an application of femtosecond laser ablation to improve the sensitivity of biosensors based on a quartz crystal microbalance device. The nanoparticles produced by irradiating a gold target with 527-nm, 300-fs laser pulses, in high vacuum, are directly deposited on the quartz crystal microbalance electrode. Different gold electrodes are fabricated by varying the deposition time, thus addressing how the nanoparticles surface coverage influences the sensor response. The modified biosensor is tested by weighting immobilized IgG antibody from goat and its analyte (IgG from mouse), and the results are compared with a standard electrode. A substantial increase of biosensor sensitivity is achieved, thus demonstrating that femtosecond laser ablation and deposition is a viable physical method to improve the biosensor sensitivity by means of nanostructured electrodes.

1 Introduction

A biosensor is an analytical device used for the detection of an analyte combining biological components with a physical and/or chemical detector and a signal transducer. A biosensor based on a quartz crystal microbalance (QCM) registers the variation of the quartz crystal resonance frequency upon deposition of an analyte on the sensor surface, thus allowing to measure its mass. The sensor surface can be functionalized with appropriate bio-receptors capable of recognizing a specific analyte, thus gaining a high specificity thanks to immune recognition. Usually, analyte detection with QCM biosensors occurs in liquid phase.

It has been recently demonstrated that QCM sensor sensitivity can be increased through deposition of nanoparticles (NPs) on its electrode surface. This was explained by considering that NPs can enhance the effective surface of the QCM electrode where the bio-receptor is anchored and the analyte is caught. The QCM modification was achieved by means of a chemical approach based on precipitation of 50-nm gold NPs onto the QCM gold lamina [1].

Here, we report on the application of femtosecond laser ablation (fs-LA) as a possible alternative to improve the sensitivity of a QCM biosensor. In particular, in the present work we choose as analyte the IgG from mouse and as bio-element the IgG antibody (anti-IgG from goat), because it is characterized by a high specificity for the analyte. Moreover, this complex represents a good case study, since we have used it in previous experiments exploiting standard QCM electrodes [2].

Fs-LA is a viable and versatile physical method to generate NPs and NPs-assembled film of a number of materials [3, 4]. In particular, it has been shown that NPs form as a result of the relaxation dynamics of the irradiated target driven into a high non-equilibrium state [4, 5]. One advantage of fs-LA is the generation and subsequent expansion of the produced NPs in high vacuum conditions, which allows avoiding all the complications introduced by the presence of a background gas or a liquid environment typical of other methods of NPs production. This, in turn, precludes any possible effect related to possible environmental impurities that could influence the biosensor response.

✉ S. Amoruso
  amoruso@na.infn.it

1 Dipartimento di Fisica, Università degli Studi di Napoli Federico II, Complesso Universitario di Monte S. Angelo, Via Cintia, 80126 Naples, Italy

2 CNR-SPIN, UOS Napoli Complesso Universitario di Monte S. Angelo, Via Cintia, 80126 Naples, Italy

Fs-LA is used to generate and deposit gold NPs on the QCM lamina, thus addressing the possible improvement of the device sensitivity due to the modified surface of gold electrodes. A larger available surface induced by the presence of gold NPs might increase the number of bio-receptors onto the gold transducers, which should allow catching a larger quantity of analytes, hence enhancing the sensitivity of the biosensor. Our experimental findings address an interesting fourfold increase in detection efficiency of NPs-modified QCM (Nm-QCM) compared to standard QCM electrodes.

2 Experimental methods

Figure 1a reports a schematic layout of the system used for QCM measurements. The QCM is integrated in a microfluidic circuit consisting of a cuvette, containing the sample under study, a Gilson peristaltic pump, and a cell, which contains the gold-quartz oscillator of the QCM. The QCM oscillator is placed on an electronic console that monitors its resonance frequency. The volume of the circuit is about 300 µL, and the flow rate is 3 µL/s. The quartz oscillators (151218) are from ICM, Oklahoma City (USA). They are AT-cut quartz with a fundamental frequency of 10 MHz. The crystal and the gold electrode diameters are 1.37 and 0.68 cm, respectively. The gold surfaces are cleaned by immersing the oscillators for 1 min in a glass beaker containing piranha solution (3:1 ratio between concentrated sulfuric acid and 40 % hydrogen peroxide solution). Then, the quartz crystals are washed with Elix water, i.e., a purified water with a certified standard of purity [6]. The whole cleaning procedure is performed in the hood and can be repeated 3–4 times before the quartz needs to be changed. The QCM device is a µLibra from Technobiochip, Italy.

Figure 1b shows a typical output of the QCM device separated in the three regions I–III, while the cartoon on the right side of panel (b) schematically illustrates the diverse steps of the measurement procedure. A frequency downshift of about 140 Hz is observed in region I, due to the linkage of anti-IgG from goat to the sensitive gold surface. The passage to region II corresponds to washing with PBS 1X followed by circulation of BSA solution (50 µg/mL). PBS 1X purges the fluidic circuit and fluidic cell from the excess of immunoglobulins anti-IgG from goat, while BSA fills possible free sites still available on gold surface to avoid specific interactions between the antigen and the gold surface. In the case shown in Fig. 1d, a negligible variation of the frequency shift is observed in region II, suggesting that the surface is fully covered with antibodies. Finally, an antigen solution of IgG from
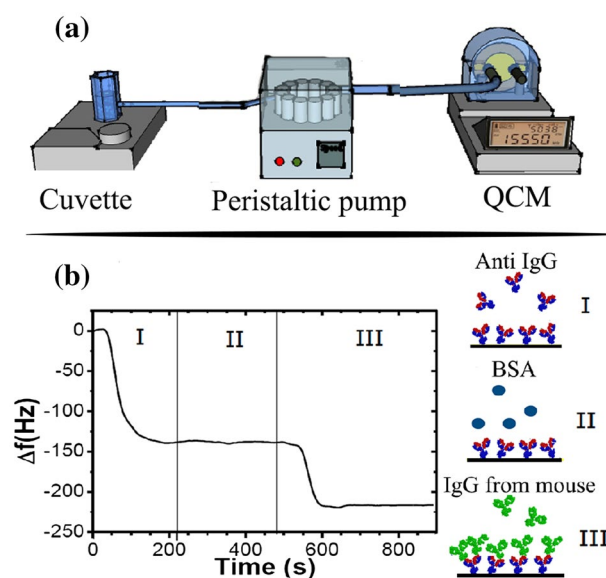
Fig. 1 a Experimental layout for QCM measurements. The antibodies in the cuvette are conveyed through a peristaltic pump to the QCM device. The electronics of the QCM is interfaced with a PC to register the frequency shifts due to the surface changes. **b** QCM-based immune-sensor output signal. The first frequency shift in region I corresponds to the antibody immobilization onto the sensor surface. In the second phase of the measurement (region II), BSA is conveyed to the Nm-QCM in order to fill possible free spaces onto the gold electrode and to avoid non-specific interactions of the analyte with the surface. The lack of any frequency shift in region II demonstrates that the surface is fully covered by antibodies. The frequency drop observed in region III, at about 550 s, is due to the detection of the antigen. The vertical lines highlight the three phases of the measurement protocol described in the text. The cartoon on the *right side* of *panel* (**b**) sketches the phases of the measurement procedure

mouse (25 µg/mL), which is recognized by IgG from goat, flows through the fluidic circuit. This induces the frequency shift observed in region III resulting from the tethering of IgG from mouse to anti-IgG from goat, due to the antigen–antibody interaction.

The QCM gold lamina is modified by deposition of gold NPs produced during fs-LA of an Au bulk target, in high vacuum [3] (see Fig. 2a). LA is induced by irradiating bulk gold sample with ≈300 fs laser pulses at 527 nm from a Nd:glass laser system, at a repetition rate of 33 Hz [4]. The target sample is mounted on a rotating holder in a high vacuum chamber (residual pressure $p \leq 10^{-6}$ mbar). The laser beam is focused on the target sample to a spot size of $\approx 6 \times 10^{-4}$ cm^2, at a fluence of ≈1 J/cm^2. The QCM is mounted on a substrate holder located at 40 mm in front of the target surface (see Fig. 2a). During deposition, the laser beam on the target is rastered over an annulus with a thickness of ≈2 mm to avoid possible consequences on NPs generation due to the formation of deep craters on the target surface after many laser pulses.
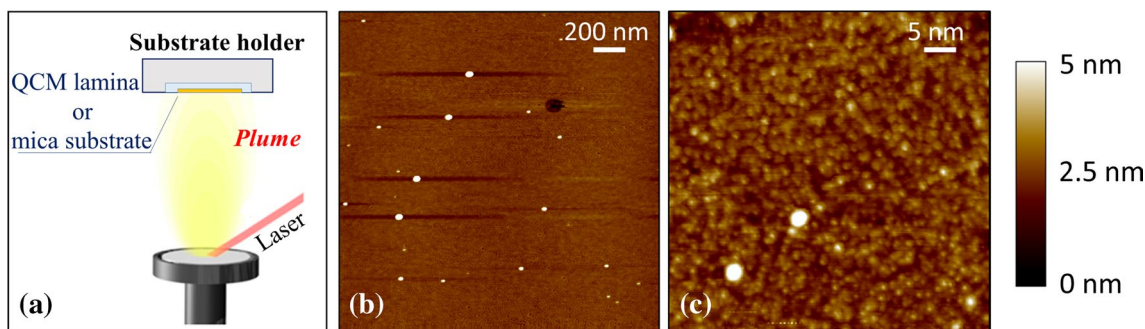
Fig. 2 **a** Schematic of the system for QCM gold lamina modification by deposition of gold NPs produced during fs-LA of an Au bulk target, in high vacuum. The target to QCM lamina distance is 40 mm. Low-density collection of NPs on mica substrates was used to meas-ure Au NPs characteristic size and morphology. **b** AFM image of less than one layer deposit of Au NPs. **c** AFM image of the Au NPs-assembled film. The *color right scale* refers to height, while the *white bars* in *panel* (**c**, **d**) represent in-plane dimensional scales

3 Results and discussion

The size features of the NPs produced during fs-LA of Au bulk target, in high vacuum, are obtained through atomic force microscopy (AFM) analysis. The AFM images are collected in tapping mode by using a sharpened silicon tip with a radius of <5 nm. In particular, less than one layer deposits on freshly cleaved mica substrates are considered to measure the sizes of the Au NPs produced during the fs-LA. As an example, Fig. 2b reports a typical AFM image of the deposit of a low-density collection of NPs. Different AFM images are registered in order to collect the size characteristics of many Au NPs, typically several hundreds. This analysis shows that oblate gold NPs are deposited, characterized by average value of the in-plane diameter and height of ≈15 and ≈5 nm, respectively, in agreement with our previous reports [4]. Moreover, only a fraction of ≈5 % of the NPs shows in-plane diameter and height larger than ≈32 nm and ≈11 nm, respectively.

The main novelty of fs-LA coupled to QCM-based biosensors is represented by the possibility to increase the effective gold surface of the sensor electrode through appropriate nanostructuring obtained by fs-LA NPs depo-sition. The fs-LA is applied directly onto standard QCM electrodes, which are cleaned by piranha treatment. Direct collection of Au NPs produced by fs-LA on the surface of the QCM lamina allows fabricating diverse Nm-QCM samples by varying the deposition time, t_{dep} (see Fig. 2a). Figure 2c reports an example of the typical morphology of the surface when complete Au NPs-assembled film is formed. The density of NPs in the film appears rather large, with most individual NPs sticking to one another, and whose size is similar to that observed in less than one layer deposit. This confirms, also for this case, the basic struc-ture of NPs-assembled films produced by fs-LA in vacuum to be a cauliflower-like, granular agglomerate composed by clusters of NPs sticking to one another, while retaining
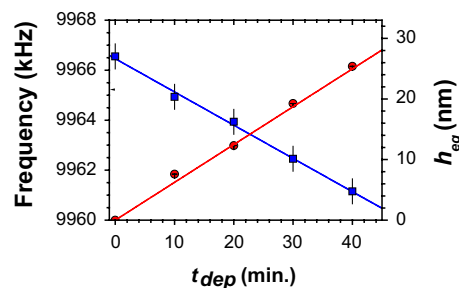
Fig. 3 Frequency of the NP-modified QCMs (*squares*, *left vertical axis*) decorated with different amount of NPs produced by fs-LA. The *horizontal axis* reports the deposition time t_{dep}. Increasing t_{dep} leads to a corresponding decrease of the oscillation frequency of the QCM electrodes as a consequence of gold NPs deposition. The *circles* show the corresponding equivalent thickness, h_{eq}, of the deposited gold NPs (*right vertical axis*)

their own individuality [3, 7]. The different deposition times modify the QCMs surface, thus yielding sensors whose surface changes from a quasi-dispersed coverage of NPs (e.g., see Fig. 1b), with increasing density of NPs, to an assembly of cluster of NPs deposited on the standard QCM gold lamina. This, in turn, permits a direct testing on how the physical modification induced on the QCM lamina influences the effectiveness of antibody attachment. In the following, the diverse modified QCM samples are identi-fied by the corresponding t_{dep} value. In our experiment, t_{dep} varies in the 10–40 min range, while $t_{dep} = 0$ corresponds to standard QCM.

First, the amount of deposited NPs on the Nm-QCM electrodes is estimated by measuring the shift of the work-ing frequency induced by the additional weighting of the gold NPs anchored onto standard electrodes. Figure 3 shows how increasing t_{dep} changes the working frequency of the electrodes; a linear decrease of the frequency indi-cates a linear increase of NPs mass, Δm, deposited onto the lamina by fs-LA, since the response of the QCM is

proportional to the mass tethered to the electrode through the Sauerbrey equation [8]:

$$\Delta f = -\frac{2f_0}{A\sqrt{\rho_q \mu_q}} \Delta m \qquad (1)$$

where Δf is the frequency shift, f_0 the resonance frequency, A the piezoelectric active area, ρ_q the density of quartz, μ_q the shear modulus of AT-cut quartz crystal, and Δm the deposited mass.

In order to test the proposed method and the sensitivity improvements of the QCM device, the different Nm-QCM sensors are used following the measurement procedure already illustrated above and shown in Fig. 1. Figure 4a reports the frequency variation occurring when the anti-IgG from goat flows in the QCM device, i.e., step I of the experimental procedure (see Fig. 1b). We clearly observe that the modification induced to the QCM lamina effectively influences the amount of anti-IgG tethered to the electrode surface. In particular, for $t_{dep} \leq 10$ min, the frequency shift is negligible. As t_{dep} increases above 10 min, the NPs coverage progressively improves the available gold surface for IgG attachment, and a threefold increase of the frequency shift, Δf, is achieved at $t_{dep} = 40$ min, with respect to the value obtained by a standard QCM electrode. Hence, this indicates that four times bigger mass of IgG from goat is attached to the Nm-QCM, which represents a noticeable improvement in the sensor performance due to better functionalization.

Subsequently, the IgG antigen recognition is analyzed (i.e., step III of the procedure in Fig. 1b), and the resulting frequency shift is shown in Fig. 4b. As expected, the improved performance of the sensor consisting in a higher amount of tethered anti-IgG results in a corresponding enhancement of the Δf values, registered by Nm-QCM for $t_{dep} \geq 10$ min. Interestingly, the frequency shift at $t_{dep} = 40$ min is increased by about four times, compared to the standard QCM electrode.

To associate the deposition time to the Nm-QCM characteristics, one can estimate from the corresponding deposited mass, Δm, the related equivalent thickness h_{eq}, i.e., the height of a column that would contain the same mass with a section S equal to the sensitive area of the QCM electrode (as typically done when QCM is used as a thickness monitor) [9]:

$$h_{eq} = \frac{\Delta m}{S \rho_{Au}} \qquad (2)$$

The corresponding values of h_{eq} obtained from Eq. (2) for the different Nm-QCM are reported in Fig. 3 (circles, right scale). We observe that the values of t_{dep} exploited correspond to an equivalent thickness h_{eq} varying from few nm, at low deposition time, up to ≈ 25 nm, for the longest tested deposition time. Then, taking into account the size
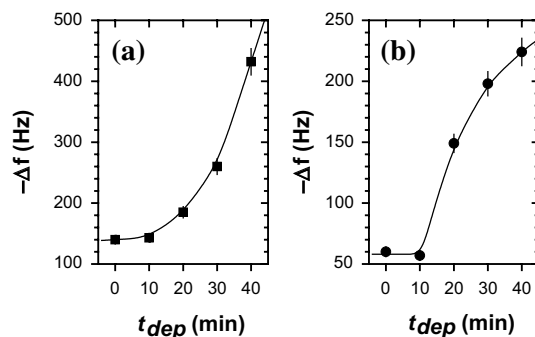
Fig. 4 Frequency shift, Δf, measured for the different Nm-QCM samples. **a** refers to the electrode functionalization with anti-IgG from goat, while **b** corresponds to the recognition of the IgG antigen from mouse. The effects of the different deposition time are visible for t_{dep} larger than ≈ 10 min, indicating that the sensitivity of the Nm-QCM starts increasing when an almost complete layer of NPs begins forming on the gold lamina. The *solid lines* are guides to the eye

characteristics of the gold NPs measured in less than one layer deposit (i.e., an average height of ≈ 5 nm and only 5 % of NPs counted for a height larger than ≈ 11 nm), one can draw out the following two remarks. First, the morphology of the QCM surface is a quasi-dispersed coverage of NPs at $t_{dep} \leq 10$ min and a complete layer with cluster of NPs start forming for 10 nm $< t_{dep} <$ 20 nm. This, in turn, explains the experimental observation of an increased amount of anti-IgG from goat attached to the Nm-QCM during its functionalization with respect to a standard QCM electrode ($t_{dep} = 0$), as shown in Fig. 3a. Second, further increase of t_{dep} leads to the deposition of more than one layer of NPs with correlated formation of cluster of NPs on the surface, which enhances the available surface. Correspondingly, when Nm-QCM is exploited to recognize antigen IgG from mouse, the higher number of anti-IgG from goat tethered to the Nm-QCM surface rises the capturing efficiency as shown in Fig. 3b, eventually resulting in a 4× larger variation of the frequency shift for Nm-QCM elaborated with $t_{dep} = 40$ min with respect to a standard QCM.

Our experimental findings clearly demonstrate that the Nm-QCM can be a suitable route to consistently improve the sensitivity of QCM-based biosensors. However, it is worth noticing the diverse trends of the frequency shift dependence on t_{dep}. In fact, while for anti-IgG functionalization, Δf steadily increases with t_{dep} (see Fig. 4a), for IgG antigens, a progressive reduction of the slope in the dependence of the frequency shift on t_{dep} is observed (see Fig. 4b). This is likely due to the fact that the progressively more nanostructured morphology of the NPs-assembled films produced by fs-LA does not allow complete antigen linkage with the anti-IgG present on the Nm-QCM surface, at large coverage of the electrode. While the complex dynamics of antigen–antibody interaction on the

Nm-QCM surface needs further investigation, our experimental findings effectively prove that fs-LA NPs deposition can provide a useful method to improve the sensitivity of biosensors. We believe that the biosensor sensitivity can be enhanced even further by coupling the Nm-QCM to the photonic immobilization technique (PIT). In fact, as demonstrated by some of the authors [2, 10, 11], when using the PIT technique, the antibody solution is activated by breaking the disulfide bridge in the triad Trp/Cys–Cys through absorption of ultrashort UV laser pulses. The free thiol groups so produced interact with gold lamina making the antibody orients upside, i.e., with its variable parts exposed to the environment, thereby greatly increasing the detection efficiency. Hence, one can guess that combining Nm-QCM and PIT will possibly result in a substantial improvement of QCM-based biosensor sensitivity, which will be the topic of our future experiments.

4 Summary

An application of fs-LA to modify QCM electrodes and improve sensitivity of a biosensor was discussed. Gold NPs produced by fs-LA, in high vacuum, were deposited on a standard QCM electrode, thus enhancing the available surface. We demonstrated that the Nm-QCM offers a viable route to improve the biosensor sensitivity. In particular, the modified biosensor was applied to the anti-IgG from goat that recognized IgG from mouse, achieving a fourfold increase in detection compared to standard QCM electrodes. While this improvement is already sizeable, we foresee a further progress by a combined use of the two technologies Nm-QCM and PIT that will be addressed in future experiments.

References

1. A. Makaraviciute, T. Ruzgas, A. Ramanaviciuscd, A. Ramanaviciene, Anal. Methods **6**, 2134 (2014)
2. B. Della Ventura, L. Schiavo, C. Altucci, R. Esposito, R. Velotta, Biomed. Opt. Express **2**, 3223 (2009)
3. S. Amoruso, G. Ausanio, R. Bruzzese, M. Vitiello, X. Wang, Phys. Rev. B **71**, 033406 (2005)
4. S. Eliezer, N. Eliaz, E. Grossman, D. Fisher, I. Gouzman, Z. Henis, S. Pecker, Y. Horovitz, M. Fraenkel, S. Maman, Y. Lereah, Phys. Rev. B **69**, 144119 (2004)
5. S. Amoruso, N.N. Nedyalkov, X. Wang, G. Ausanio, R. Bruzzese, P.A. Atanasov, Thin Solid Films **550**, 190 (2014)
6. See for instance, for elix water. http://www.emdmillipore.com/US/en/product/Elix-Reference-Water-Purification-system,MM_NF-C84762
7. S. Amoruso, G. Ausanio, R. Bruzzese, L. Lanotte, P. Scardi, M. Vitiello, J. Phys. Condens. Matter **18**, L49 (2006)
8. G.Z. Sauerbrey, Z. Phys. **155**, 206 (1959)
9. M. Ohring, *The Materials Science of Thin Films* (Academic Press, New York, 1992)
10. R. Funari, B. Della, Ventura, L. Schiavo, R. Esposito, C. Altucci, R. Velotta. Anal. Chem. **85**, 6392 (2013)
11. R. Funari, B. Della Ventura, R. Carrieri, L. Morra, E. Lahoz, F. Gesuele, C. Altucci, R. Velotta, Biosens. Bioelectron. **67**, 224–229 (2015)